THE UNIVERSITY OF CHICAGO

PLASTID-TARGETED AZELAIC ACID-INDUCED 1 FAMILY PROTEINS MEDIATE SYSTEMIC DEFENSE PRIMING AND ROOT DEVELOPMENT DURING ARABIDOPSIS STRESS SIGNALING

A DISSERTATION SUBMITTED TO

THE FACULTY OF THE DIVISION OF THE BIOLOGICAL SCIENCES

AND THE PRITZKER SCHOOL OF MEDICINE

IN CANDIDACY FOR THE DEGREE OF

DOCTOR OF PHILOSOPHY

GRADUATE PROGRAM IN CELL AND MOLECULAR BIOLOGY

BY

DEQUANTARIUS JAVON SPEED

CHICAGO, ILLINOIS

JUNE 2022

DEDICATION

To Laquinta, Betty, and Leola for a lifetime of unconditional love.

To my Affiliates at UChicago, for years of mischief, laughter, and support.

To Jean, for her perspective, guidance, and patience.

To Joanna, Nico, Shangchuan, and Suruchi for all of their mentoring and training.

To the Greenberg and Malamy labs for being my home away from home.

To the MGCB and BSD for six and a half of the most formative years of my life.

TABLE OF CONTENTS

List of Figures

List of Tables

ABSTRACT

The lipid transfer protein AZI1 is required for the priming of various systemic defense responses including: SAR (systemic acquired resistance); ISR (induced systemic resistance); and the uptake and mobilization of azelaic acid (AZA). Generated from the oxidation of plastid lipids during infections, AZA primes systemic defenses when applied to leaves or roots and induces striking changes in root development. These changes require the development- and defense-associated kinase MPK3, which is also required for SAR, ISR, and sensitivity to AZA. The AZI1 family also influences root development during salt stress and in response to AZA treatment similar to MPK3, which suggests the AZI1 protein family may serve as downstream coordinators of MPK3-dependent development and stress responses. Furthermore, MPK3 promotes the accumulation of AZI1 at plastids during infections, which suggests a critical role for AZI1's plastid association in defense signaling.

AZI1 is highly dynamic and traffics along the contact sites among the plastid, ER, and plasma membranes. Unlike canonical "signal anchored" proteins that target plastid membranes, AZI1's normal pattern of plastid association requires a bipartite targeting signal that consists of a N-terminal hydrophobic domain and an internal proline-rich region. Including AZI1, the AZI1 gene family consists of seven short genes tandemly aligned on chromosome 4. Except for AZI5/AZI6 and AZI7, which have a shortened or absent PRR, respectively, AZI1 family proteins show a similar localization pattern as AZI1 and contribute to the priming of systemic immunity.

CHAPTER 1

OXYLIPIN SIGNALING COORDINATES PLANT DEVELOPMENT AND SYSTEMIC DEFENSES

1.1 Plants Must Coordinate Growth with Defense when Combatting Stressors

Plant growth is often compromised during stressful or toxic environmental conditions, which results in substantial losses in crop yield. Many abiotic stresses passively inhibit plant growth due to the lack of essential factors like water or phosphorous. In contrast to the passive growth inhibition caused by many abiotic stresses, plant responses to biotic stressors often involves the coordinated repression of growth alongside the induction of immune responses (Bartels et al., 2009; Genot et al., 2017; Lu et al., 2003, 2005; Rate et al., 1999; Su et al., 2018; Vanacker et al., 2001; Zhang et al., 2014; Zhang et al., 2017).

Though much has been revealed regarding the regulation of local and systemic defenses in plants, little is understood about the molecular mechanisms and factors that coordinate plant growth with defense signaling. One such mechanism may be found within the downstream targets of mitogen-activated protein kinase (MAPK/MPK) signaling (Jiang et al., 2022). Arabidopsis MPK3 and the closely related MPK6 are key regulators of plant development and defense signaling (Chai et al., 2014; Sopeña-Torres et al., 2018; Sun and Zhang, 2022). Not only do these kinases regulate multiple root and shoot developmental pathways, MPK3/MPK6 cascades directly inhibit photosynthesis during infections and contribute to developmental responses to pathogens (Gudesblat et al., 2007; Shao et al., 2018; Su et al., 2018; Xu and Zhang, 2015; Zhang et al., 2021). Although several downstream components of MPK3/MPK6 signaling cascades have been identified, few such downstream signals have been identified which

contribute to systemic developmental and immune signaling pathways regulated by MPK3/MPK6. Identification of such a signal could have profound implications for the development of heartier, more stress-tolerant crops that are better capable of growing during nonideal conditions (Egamberdieva et al., 2019).

Herein, I briefly describe *Arabidopsis* root development. I will then present novel findings regarding the roles of phytohormones and a family of lipid transfer proteins (LTPs) in various MPK3/MPK6-dependent stress responses and posit that this protein family coordinates MPK3/MPK6-dependent plant development and defense signaling.

1.2 Root Development is Highly Responsive to Stress and Environmental Cues

As sessile organisms, plants have evolved a high degree of metabolic and developmental plasticity to survive and grow under shifting environmental conditions. Insects, pathogens, droughts, and temperature extremes all pose major threats to plant growth and therefore negatively impact crop yield and global food security. Though photosynthesis requires sufficient sunlight, plant growth is also heavily impacted by soil conditions. Embedded firmly in the soil, roots are the main point of contact between plants and their environment. Thus, plant survival requires that roots be highly responsive to environmental cues and communicate these cues to aerial parts of the plant.

The model plant *Arabidopsis thaliana* has an elegant yet developmentally simple root system that provides structural support for the plants, anchors them in the soil, and serves as the main route of uptake for water and minerals (Fig. 1.1; Petricka et al., 2012). During embryogenesis, the early root, or radicle, protrudes from the seed coat then grows downward in the direction of gravity to establish the primary root. As the primary root grows, secondary (or

Figure 1.1 The Arabidopsis Root System is Highly Responsive to Environmental Conditions

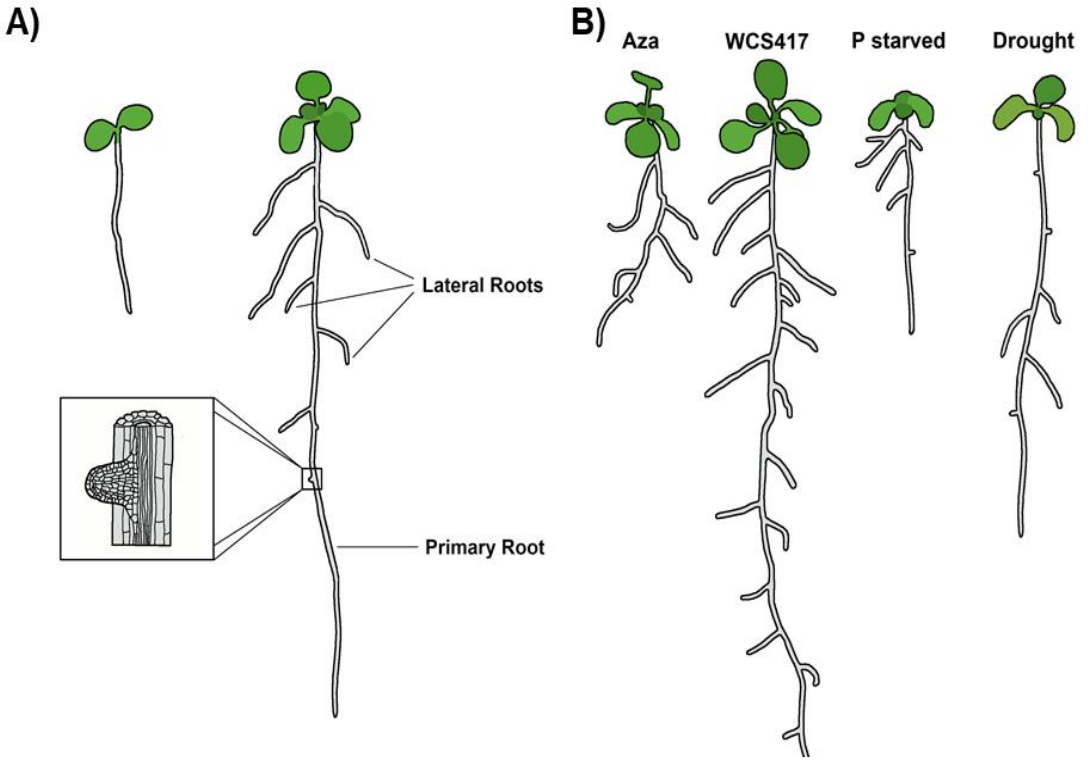

Credit: Riley J, Greenberg Lab,
U. of Chicago

Figure 1.1. The Arabidopsis Root System is Highly Responsive to Environmental Conditions

A) The development of Arabidopsis root systems results from the balance of primary and lateral root growth. Left: a nascent seedling and root 2-4 days after germination. Right: mature seedling and root >7 days after germination. During germination, the early root protrudes gravitropically from the seed coat to establish the primary root. As the primary root grows, lateral roots emerge from primordia cell layers (insert) in response to environmental cues. B) The Arabidopsis root is highly responsive to biotic and abiotic stimuli. Perception of defense-priming compounds like the oxylipin azelaic acid or growth-promoting bacteria alter primary root growth while promoting the development of lateral roots. Similarly, abiotic stresses like drought or nutrient-starvation also induce striking changes in lateral and primary root growth.

lateral) roots of varying length emerge from the sides of the primary and other lateral roots (Fig. 1.1). The length of the primary root along with the number and length of the lateral roots gives mature root systems distinct branching architectures.

Balancing primary and lateral root growth during development is critical for plants to effectively anchor themselves in the soil and acquire water and nutrients under various environmental conditions. Likewise, various root systems have been observed to develop in response to distinct environmental cues. The root responses to phosphate-starvation or drought serve as excellent examples (Comas et al., 2013; Crombez et al., 2019; Li et al., 2012).

Phosphates are core components of many essential cellular factors including nucleic acids, lipids, membranes, and various metabolites. As such, phosphate-deficiency causes a severe arrest of root growth. Due to their high cycling and low soil mobility, phosphates accumulate within the topsoil and become increasingly scarce in deeper soil layers (Koevets et al., 2016). Consistent with this, seedlings grown on phosphate-deficient media develop shallow, wide-ranging root systems that are well-suited for scavenging from the topsoil (Crombez et al., 2019).

Similar to phosphate starvation, drought also slows root growth. However, drought-challenged roots display longer, more narrow root systems, when compared to phosphate-starved plants (Comas et al., 2013). Plants rely on water for photosynthesis, nutrient and mineral transport, and turgor pressure, which is also essential for root elongation (Blatt et al., 2014). Because the topsoil is most exposed to air and drying, soil water increases with depth. Thus, prioritizing root system depth instead of width best promotes survival; such a developmental pattern would require the general suppression of lateral root growth while allowing primary root elongation.

Controlling the balance between primary and lateral root growth is essential for plant adaptability to shifting conditions and requires the complex interplay of signaling cascades involving several major signaling compounds and phytohormones. One such class of phytohormones are the auxins. Well-established as major regulators of root growth and

development, auxins, mostly in the form of indole-3-acetic acid (IAA), control root development through the de-repression of various auxin-responsive genes (Roychoudhry and Kepinski, 2021). The subsequent generation of asymmetric auxin gradients regulates root differentiation and controls the balance between primary and lateral root growth. Recent reviews of auxin signaling and its roles in plant and root development can be found here (Báez and Neumhauser, 2021; McLaughlin et al., 2021). Though auxin is the primary regulator of root growth, root development is highly responsive to other biotic stimuli including other phytohormones and even microbial effectors.

Besides the various abiotic challenges plants encounter in the soil, plants also interact with a large community of soil microbes. In addition to pathogens and pests, roots nurture mutualistic interactions with a variety of commensal rhizobacteria that affect root development (Efthimiadou et al., 2020, Haney et al., 2015). These plant growth-promoting rhizobacteria span several genera of microbiota exist and enhance plant growth and survival under stress conditions. Upon colonizing and forming commensal relationships with plant roots, the growth-promoting rhizobacterium *Pseudomonas simiae* WCS417 stimulates root growth and the formation of new lateral roots in *Arabidopsis* (Pieterse et al., 2014; Banday et al., *in rev*). Not only does colonization of roots with *P. simiae* WCS417 stimulate plant growth and affect root structure, it also primes the activation of broad-spectrum immune responses in a phenomenon termed Induced Systemic Resistance (ISR; Fig. 1.2; Berendsen et al., 2012; Efthimiadou et al., 2020, Haney et al., 2015; Pieterse et al., 2014).

The concurrent stimulation of plant growth and immune signaling implies some degree of crosstalk between rhizobacteria-induced root development and defense signaling. Furthermore, this priming of aerial defenses is root-autonomous which also suggests the existence of some

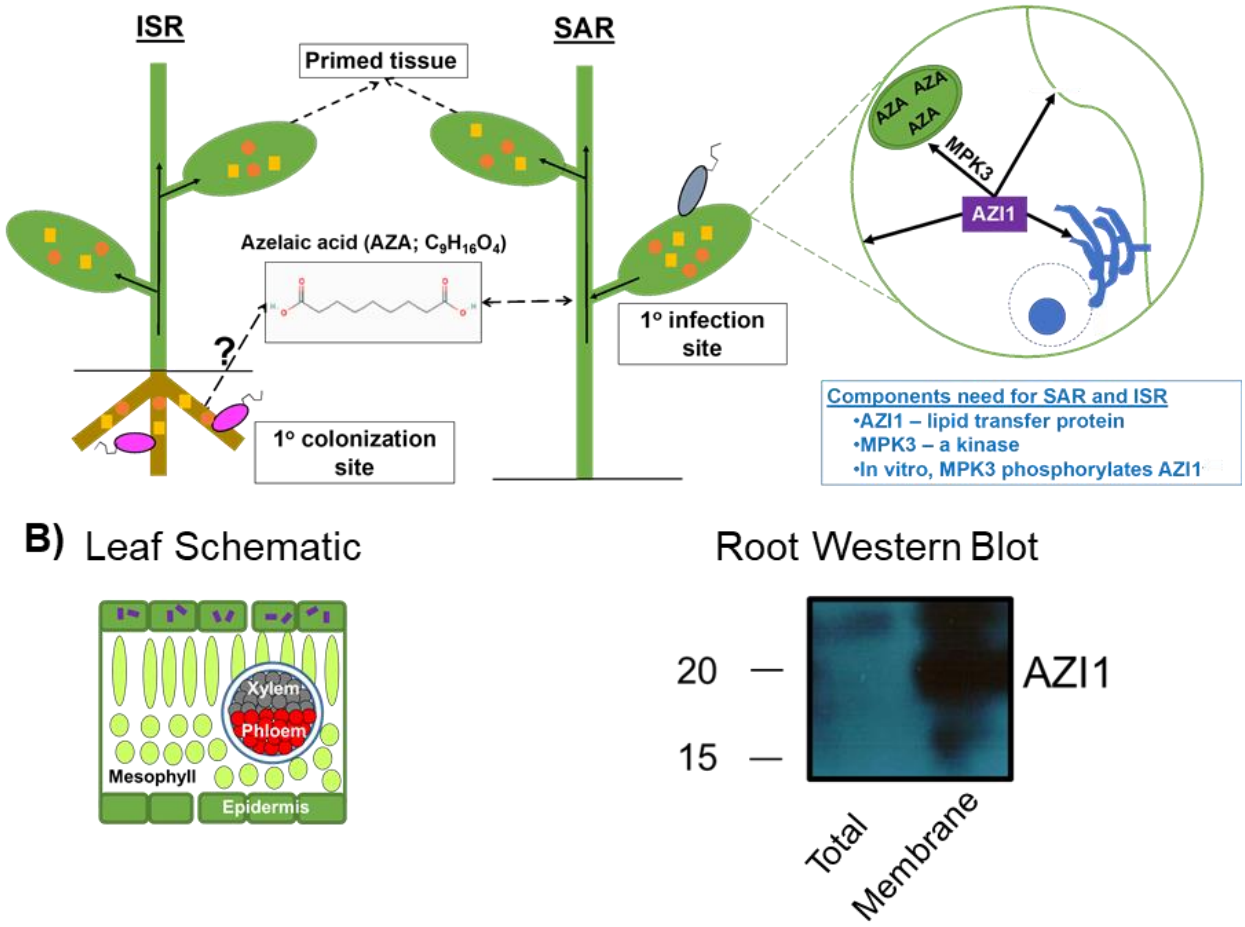

Figure 1.2. Induction of Arabidopsis Systemic Defenses

Recognition of pathogens and microbial products by plant receptors induces signal cascades that prime broad-spectrum defense responses to suppress 2° infections. Successful whole-plant priming requires the long-distance movement of signals produced during a 1° exposure event. Depending on the 1° exposure event, two types of systemic responses that suppress pathogen growth have been described. Induced systemic resistance (ISR) results when roots are exposed to growth-promoting bacteria; when leaves encounter pathogens, systemic acquired resistance (SAR) results. An essential component of SAR and ISR is the lipid transfer protein (LTP) AZI1, which is also needed for mobilization of azelaic acid (AZA), a SAR-priming metabolite. AZA, generated from plastid lipid oxidation, is transported out of plastids to reach its site(s) of action. Functional AZI1-GFP traffics among plastid outer envelope membranes (OEMs), ER, PM, and intercellular channels called plasmodesmata. AZI1's localization pattern is consistent with AZI1 acting in the mobilization of a plastid-derived lipid signal(s) such as AZA. During infections, AZI1 accumulates in plastids in mechanism dependent upon the defense-associated kinase MPK3.

molecular link or mobile signal that connects root-based and shoot-based signaling pathways (Pieterse et al., 2014). Discovery of such a link would have a profound impact on the

understanding of how plants balance defense with development and could aid in the development of heartier, more disease-resistant crops. Thus, it is paramount to identify the mechanisms and pathways that serve to link plant development, especially root development, and systemic defense signaling. Such a mechanism must be active in both immune and developmental signaling pathways and link underground and aerial signaling responses. Potential signals may be found within the oxylipins, a class of phytohormones that are widely present in both the plant and animal kingdoms (de Leon et al., 2015; Fitoussi et al., 2021).

In plants, oxylipins are derived from the oxidation of 18-carbon fatty acids, primarily catalyzed by 9- and 13-lipoxygenases (LOX), α-dioxygenases, or non-enzymatic oxidation within plastids (Grebner et al., 2013; Maynard et al., 2021; Vicente et al., 2012; Zoeller et al. 2012). Enzymes and reactive oxygen species (ROS) active within these oxylipin biosynthesis pathways are induced by biotic and abiotic stressors, prime defenses in response to infections, and regulate plant growth and reproduction, which further suggests that oxylipins connect developmental and immune signaling pathways (Carella, 2020; Christensen and Kolomiets, 2011; Fuessner et al., 2009; Savchenko et al., 2014; Vellosillo et al., 2007).

The biosynthesis of oxylipins is closely tied to root development (Haeggström and Funk, 2011; Martinez and Campos-Gomez, 2016). Expression of *LOX1* and *LOX5*, which encode 9-LOX isoforms, decreases in lateral root primordia just before the nascent lateral root emerges (Liavonchanka and Fuessner, 2006; Vellosillo et al., 2007). Application of the 9-LOX biosynthesis products 9-Hydroxyoctadecatrienoic acid (9-HOT) and 9-keto-10(*E*),12(*Z*),15(*Z*)-octadecatrienoic acid (9-KOT) to plants induces deposition of callose polymers (β-1,3-glucan) in root and leaf cell walls, the production of reactive oxygen species in roots and leaves, and waving in roots. Furthermore, *lox1* and *lox5* knockout mutants show an increased lateral root

density compared to wild-type seedlings and *lox1* mutants are hypersusceptible to SAR-priming pathogens (Vellosillo et al., 2007; Vicente et al., 2012).

Root waving and local defense induction in response to 9-HOT requires the defense-associated gene *NOXY2*. *noxy2* mutants display reduced/no callose deposition, reduced ROS production, and no root waving in response to treatment with 9-HOT. These mutants also show delayed induction of the Pathogenesis-Related 1 and 2 (PR1 and PR2) genes in response to an immunizing infection (Vellosillo et al., 2012). *PR1* and *PR2* are markers for the synthesis of salicylic acid, a critical signal molecule for plant stress and immune signaling (Gao et al., 2015). When viewed with the negative impact that 9-HOT imparts upon lateral root growth, these findings show a clear association between the synthesis of defense-priming compounds and the regulation of root development. However, the root waving response was limited to the area of the root in contact with the oxylipin (Vellosillo et al., 2007). These results suggest that 9-LOX and 9-HOT signaling is only locally transduced. Similarly, 9-HOT has not been reported to prime systemic defenses and is thus unlikely serve as a systemic signal which coordinates development and defense signaling.

Although various oxylipins may have similar effects on plant growth and defense induction, their effects vary and are transmitted via distinct signaling pathways. *noxy2* mutants display wild-type responses to the oxylipins jasmonic acid (a general repression of root elongation and lateral root synthesis) and 9-oxononanoic acid (9-ONA; inhibition of root elongation, increased lateral root density, and loss of root apical dominance; Vellosillo et al., 2007). In contrast to the local defenses induced by 9-HOT and NOXY2 signaling, the oxylipins jasmonic acid and 9-oxononanoic acid (9-ONA), primarily through its derivative azelaic acid

(AZA), prime systemic defense responses in addition to regulating root development (Jung et al., 2009; Vellosillo et al., 2007; Vicente et al., 2012; Bouain et al., 2018).

Although leaf- and root-based immune pathways are marked by the activation of distinct genes and signals, one shared component is the oxylipin AZA, which is derived from further oxidation of 9-ONA (Jung et al., 2009; Niu et al., 2011; Pozo et al., 2008). AZA primes systemic defenses when applied to either roots or leaves, triggers the expression of defense-associated lipid transfer proteins (LTPs), and modifies root morphology similar to 9-ONA (Bouain et al., 2018; Jung et al., 2009; Cecchini et al., 2015; Chapter 2, Cecchini et al., 2019). In the following sections, I explore recent implications regarding the role of AZA in mediating plant development and systemic defense responses.

1.3 The Oxylipin Azelaic Acid Alters Root Growth and Primes Systemic Immunity

Successful whole-plant immune responses require the long-distance movement or transduction of defense priming signals produced during an initial microbial exposure event. Following an initial infection or colonization, various priming signals are produced locally then mobilized to distal, systemic tissues. Once primed, systemic tissues are able to more quickly and strongly mount defenses in response a broad spectrum of secondary pathogens. Two distinct systemic responses, SAR (systemic acquired immunity) and ISR, have been described based on the types and locations of their initial microbial exposure events (Fig. 1.2). Though SAR and ISR both prime broad spectrum bacterial resistance in aerial tissues, they are triggered from the leaves and roots, respectively, and employing overlapping but different signaling compounds.

ISR is induced upon the colonization of roots with certain growth-promoting bacteria like *P. simiae* WCS417 and relies on different signaling components than SAR (Berendsen et al.,

2012; Chini et al., 2009; Pieterse et al., 2014; Li et al., 2021; Yu et al., 2022). As mentioned previously, *P. simiae* WCS417 also promotes primary root growth and enhances lateral root length and density, which further suggests a link between root development and immune responses (Banday et al., in rev; Berendsen et al., 2012; Efthimiadou et al., 2020, Haney et al., 2015; Pieterse et al., 2014) . Jasmonic acid, which induces striking changes in root morphology, also is essential for ISR (Berendsen et al., 2012; Chini et al., 2009; Pieterse et al., 2014; Li et al., 2021; Yu et al., 2022).

The most well-characterized of the oxylipin signals, jasmonic acid and the jasmonate class of compounds are derived from the 13-lipoxygenase (LOX)-driven oxidation of trienoic fatty acids. In contrast to 9-LOX and 9-HOT-driven root development, 13-LOX expression increases just prior to lateral root emergence and jasmonates repress both primary and lateral root growth without inducing root waving (Vellosillo et al., 2007). Jasmonate signaling also plays essential roles in developmental processes such as senescence, fruit ripening, tuberization, and root development (reviewed in Acosta and Farmer, 2010; Berendsen et al., 2012). Jasmonates regulate adaptive responses to various forms of abiotic and biotic stresses, including microbial pathogens, insect herbivory, wounding, and photodamage (Chini et al., 2009; Li et al., 2021; Yu et al., 2022). Although jasmonates are key regulators of ISR and accumulate in leaves infected with SAR-inducing bacteria, jasmonic acid appears dispensable for the leaf-triggered SAR (Truman et al., 2007; Attaran et al. 2009). Deeper reviews of the role of jasmonate signaling in regulating plant defense and development are available (Iqbal et al., 2021; Li et al., 2021).

In contrast to the jasmonate-dependent ISR, SAR involves the chemical inducers salicylic acid and its methylated derivate (SA/MeSA), pipecolic acid, dehydroabietinal, and glycerol-3-phosphate (G3P; Chanda et al., 2011; Durrant and Dong, 2004; Jiang et al., 2021; Návarová et

al., 2012; Park et al., 2007). SAR also involves the phytohormone auxin, which further ties plant development and defense signaling (Truman et al., 2010). Further distinguished from ISR, SAR is triggered by the infection of leaves with certain pathogenic invaders, such as *Pseudomonas cannabina pv. alisalensis* instead of root interactions with growth-promoting rhizobacteria. SAR can also be induced upon inoculation of the microbe-associated molecular pattern (MAMP) flg22 into leaves (Cecchini et al., 2015). Derived from bacterial flagellin, flg22 is recognized by pattern recognition receptors, the output of which triggers MAMP-induced SAR (mSAR; Tateda et al., 2014). Recently, it has been demonstrated that the 9-carbon dicarboxylic acid, AZA, can prime SAR and SAR-like defenses when applied to the leaves or roots, respectively (Jung et al. 2009; Cecchini et al., 2015; Chapter 2, Cecchini et al., 2019).

In addition to priming systemic defenses, root-application of AZA restricts primary root elongation, disrupts apical dominance, and promotes lateral root initiation similar to 9-ONA (Bouain et al., 2018; Chapter 2, Cecchini et al., 2019; Vellosillo et al., 2007). Though 9-ONA serves as an immediate precursor for AZA, any 18-carbon fatty acids which contain a double bond at carbon 9 (18:1, 18:2, and 18:3 fatty acids), can serve as precursors for 9-ONA and AZA (Zoeller et al., 2012). In fact, pathogen infection and exogenous application of 18:1 or 18:2 fatty acids can induce SAR and biosynthesis of AZA in wild-type plants (Jung et al., 2009; Yu et al., 2013).

AZA promotes accumulation of G3P during defense priming and functions in a subsequent positive feedback loop with G3P to promote the more rapid accumulation of salicylic acid during the induction of SAR (Yu et al., 2013). SAR, AZA-induced SAR, and accumulation of G3P requires the unrelated LTPs AZI1 (Azelaic Acid-Induced 1) and DIR1 (Defective in Induced Resistance 1) as well as the Plasmodesmata Localizing Proteins 1 (PDLP1) and PDLP5

(Jung et al., 2009; Cecchini et al., 2015; Lim et al., 2016; Yu et al., 2013). AZI1 forms complexes with itself, its close homolog EARLI1 (EARLY ARABIDOPSIS ALUMINUM INDUCED 1), DIR1, and PDLP1/PDLP5, which suggests these LTPs form may complexes that promote the systemic movement of locally produced defense signals like AZA and G3P (Cecchini et al., 2015; Lim et al., 2016). AZI1 and EARLI1, but not DIR1, accumulates in plastids during defense signaling, the site of production of AZA, and contributes to the systemic movement of AZA, which suggests these defense-associated LTPs may have different functions in priming immunity (Cecchini et al., 2015; Zoeller et al., 2012).

AZI1 and *EARLI1* encode short, ~14 kDa proteins that have been assigned to the Hybrid Proline-Rich Protein superfamily due to their amino acid sequence (Fig. 1.3; Dvořáková et al., 2007, 2012). *azi1* and *earli1* mutants show attenuated root morphology responses to AZA and 9-ONA and do not prime SAR-like defenses in leaves after root-application of AZA like wild-type plants (Bouain et al., 2018; Cecchini et al., 2015). AZI1 and EARLI1 are also essential for the priming of ISR in response to *P. simiae*, which positions the AZI1 protein family as one of the few shared components between SAR, ISR, AZA-induced defense priming, and the systemic mobilization of SAR-priming signals (Cecchini et al., 2015; Jung et al., 2009; Lim et al., 2016; Yu et al., 2013). Therefore, *AZI1* and the AZI1 protein family are prime candidates for key coordinators of plant development and defense.

1.4 The AZI1 Gene Family Promotes Root- and Shoot-based Defense Signaling

Exogenous local application of AZA to leaves induces SAR and the expression of the AZI1 gene family, seven genes that share a high degree of sequence similarity and are tandemly arrayed on chromosome 4 (Fig. 1.3; Cecchini et al., 2015; Jung et al., 2009, Yu et al., 2013). As

Figure 1.3 The AZI1 Gene Family Encodes 7 Highly Similar Proteins

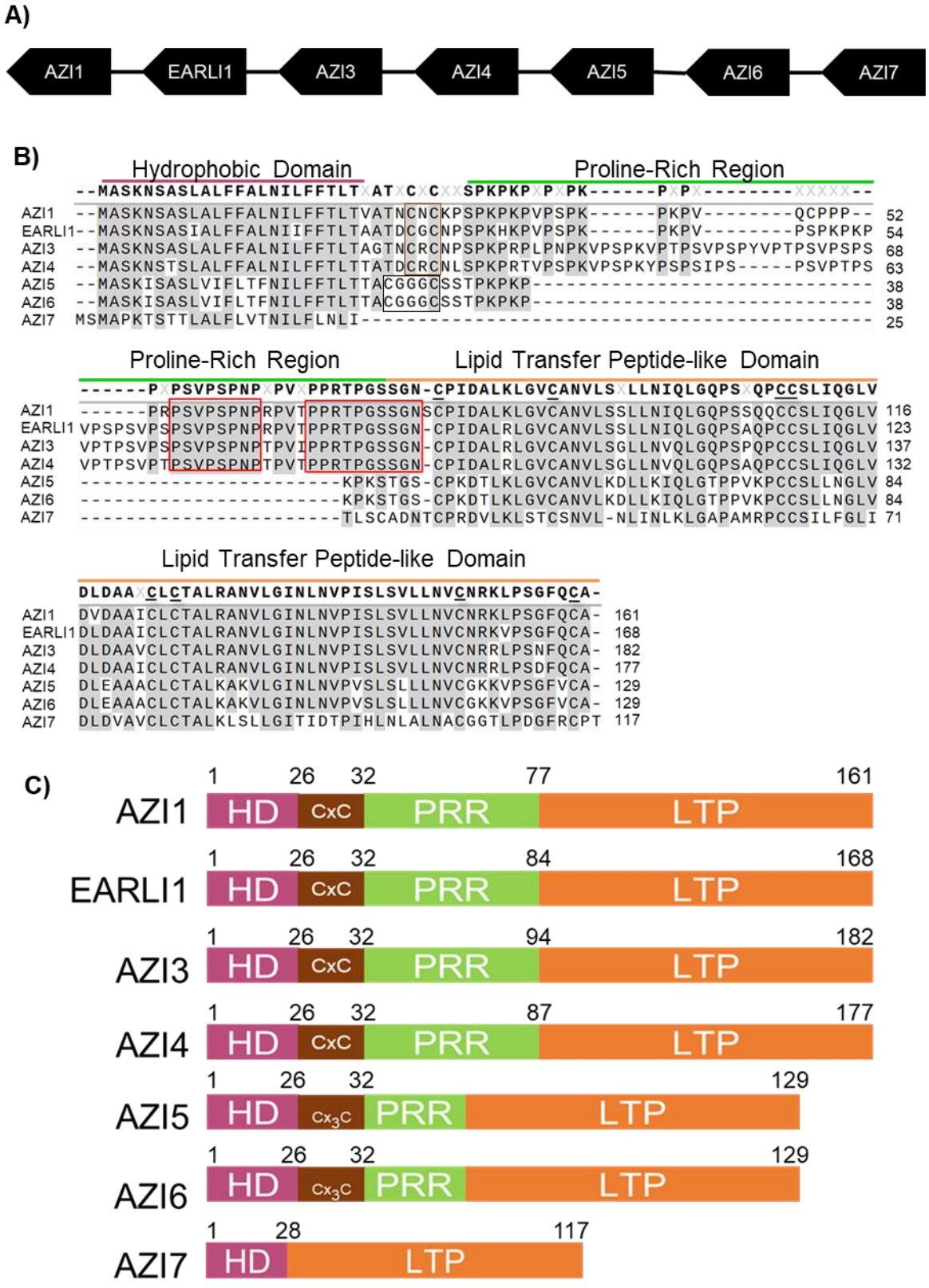

Figure 1.3. The AZI Gene Family Encodes Seven Highly Similar Proteins

A) The AZI1 gene family consists of seven short genes (<650bp) genes that are tandemly arrayed along chromosome 4. B) Alignment and C) diagrams of WT amino acid sequences of the AZI1-family proteins. Except for AZI7, each of the AZI proteins consists of an N-terminal hydrophobic domain (HD), an internal proline-rich region (PRR) of varying length, and a C-terminal lipid transfer protein (LTP) domain that contains a highly conserved 8-cysteine motif (8CM). Amino acids conserved in >50% of AZI1 family proteins are highlighted in grey and represent a consensus depicted in bold above the alignment. "X's" represent less conserved residues. The amino acids corresponding to the SP-like/HD (red line), the PRR (blue line), and the 8CM/LTP domain (black line) are indicated. Cysteines constituting the 8CM are underlined in the consensus sequence. Brown boxes denote the potential palmitoylation CxC motif. Red boxes denote highly conserved amino acid sequences within the plastid targeting signal (PRR) of AZI1, EARLI1, AZI3, and AZI4.

members of the Hybrid Proline-Rich Protein superfamily, the AZI1 family proteins are characterized by a well-conserved structure comprised of an amino (N)-terminal hydrophobic domain (HD), an internal proline-rich region (PRR), and a C-terminal LTP domain which contains a highly conserved 8-cysteine motif (8CM; Fig. 1.2; Dvořáková et al., 2007, 2012). AZI1's N-terminal half recapitulates the trafficking pattern of full-length AZI1 and localizes to plastids in a striking ring-like pattern (Fig. 1.2 and 1.3, Cecchini et al., 2015). The LTP domain is predicted to facilitate protein-protein and protein-lipid interactions (Finkina et al., 2016; José-Estanyol et al., 2002; Malinina et al., 2017). EARLI1, a member of the AZI1 protein family, is highly similar to AZI1 and nearly identical to AZI1 in function (Cecchini et al., 2015). *azi1* and *earli1* mutants are deficient for SAR, mSAR, ISR, AZA-induced defense priming, and AZA uptake and mobilization, which demonstrates a critical role for these proteins in the coordination of multiple systemic signaling pathways (Cecchini et al., 2015).

Confocal microscopy and fractionation of leaf tissue using two-phase partitioning on a Percoll gradient revealed AZI1's plastid association (Cecchini et al., 2015). AZI1-GFP localizes to plastids in a ring-like pattern reminiscent of proteins localized to the plastid outer envelope membrane. Unlike proteins embedded in the inner envelope membrane, outer envelope proteins are exposed to the cytosol and are therefore susceptible to protease digestion after plastid purification. AZI1 is largely degraded in thermolysin-treated plastids, which confirms its outer envelope localization (Cecchini et al., 2015).

The systemic movement of radiolabeled AZA away from the local application site is significantly reduced in *azi1* and *earli1* mutants compared to wild-type plants (Cecchini et al., 2015). Membrane contact sites between organelles and ER, which is continuous with plasmodesmata, serve as points of lipid exchange between juxtaposed membranes (Pérez-Sancho et al., 2016). Functional AZI1-GFP traffics among the plastid, ER, and plasma membranes including plasmodesmata (Cecchini et al., 2015). During infections, both AZI1 and AZA accumulate within plastids (Cecchini et al., 2015; Zoeller et al., 2012). AZI1's dynamic subcellular localization and interactions with plasmodesmal transport proteins (PDLP1/PDLP5) suggests a pathway by which AZI1 might facilitate the intercellular movement of defense priming signals like AZA and proposes an important role for AZI1/EARLI1's plastid targeting (Cecchini et al., 2015; Lim et al., 2016; Yu et al., 2013). Consistent with this hypothesis, the defense-associated kinases MPK3 and MPK6 are essential for the priming of systemic defenses and may modify AZI1's plastid targeting region (Fig. 1.2 and 1.3; Beckers et al., 2009; Cecchini et al., 2015; Pitzschke et al., 2014). Additionally, *mpk3*, *azi1,* and *earli1* mutants show reduced seedling germination, survival, and root growth when exposed to media containing high

concentrations of NaCl, which further suggests a role for the plastid pool of AZI1/EARLI1 in defense signaling (Pitzschke et al., 2014; Scott, 2019; Yan et al., 2021).

Though our lab previously reported on the necessity of the PRR for AZI1's plastid targeting, we did not assess what functions, if any, the other domains of AZI1 might hold. AZI1's architecture differs from known "signal-anchored" plastid envelope proteins, which use only a hydrophobic N-terminal HD and positively charged protein region (CPR) to target plastid envelopes (Cecchini et al., 2015; Kim et al., 2011; Lee et al., 2014). AZI1's N-terminal half recapitulates the trafficking pattern of full length AZI1 and therefore forms a functional plastid envelope targeting signal (Fig. 1.2 and 1.3; Cecchini et al., 2015). Except for AZI5, AZI6, and AZI7, which have a shortened or absent PRRs, AZI1 family proteins show a similar localization pattern as AZI1 and EARLI1 (Cecchini et al., 2015). Interestingly, AZI1, EARLI1, AZI3, and AZI4 share two completely conserved regions near the distal ends of their PRRs (Fig. 1.3).

1.5 Project Aims and Overview of Findings

Given the roles of AZI1 and EARLI1 in mediating SAR, ISR, and sensitivity to AZA, I set out to determine how AZI1 and the AZI1 gene family regulate plant defense signaling and development during AZA signaling.

In the following chapters, I present published work describing the role of AZI1, EARLI1, MPK3, and MPK6 in mediating root-based defense priming and developmental responses to AZA (Chapter 2, Cecchini et al., 2019), published work describing the role of MPK3/MPK6 and conserved protein motifs in AZI1's normal localization pattern during defense induction (Chapter 3, Cecchini, Speed et al., 2021), and new data describing the roles of additional plastid and non-plastid-targeted AZI1 family proteins in mediating SAR and root responses to AZA

(Chapter 4). I also describe new findings regarding the role of the AZI1 family in mediating leaf developmental responses to root-applied AZA and the role of the AZI1 family in regulating root development in response to salt stress (Chapter 4). Finally, I propose that the AZI1 gene family and the kinases that regulate them are essential components of LTP signaling complexes that mediate the systemic movement and perception of AZA, regulate root and shoot development in response to biotic and abiotic stress signals, and mediate the priming of systemic immune signaling (Chapter 5).

CHAPTER 2

UNDERGROUND AZELAIC ACID-CONFERRED RESISTANCE TO *PSEUDOMONAS SYRINGAE* IN *ARABIDOPSIS*

Preface

This chapter includes a paper published from collaborative work completed under the supervision of Professor Jean Greenberg (DOI: 10.1094/MPMI-07-18-0185-R). The article is included with permission from the publishers. My contributions to the project are as follows:

During my rotation in Jean Greenberg's laboratory, I identified the relationship between AZI1/EARLI1's accumulation in plastids during infection and active MPK3 signaling (Chapter 4; Cecchini et al., 2021). Based on these findings and a literature review, hypothesized that if AZI1's infection-driven plastid accumulation was critical for defense signaling, then MPK3 and MPK6 should contribute to similar defense responses as AZI1 and EARLI1.

In the following study, I collaborated with Dr. Nicolas Cecchini to treat roots with AZA or *Pseudomonas simiae* WCS417 and stimulate root-based defenses before challenging leaves with *Pseudomonas cannabina pv. alisalensis* to assess defense priming (Fig. 2.3B; Fig. 4D). I also collaborated with Dr. Suruchi Roychoudhry to determine the subcellular localization of AZI1 in roots (Fig. 2.5C and D); I also confirmed biochemically that AZI1/EARLI1 localizes to plastid membranes similar to as seen in leaves (unpublished; see: Chapter 1, Fig. 1.2).

In collaboration with lead authors Dr. Nicolas Cecchini and Dr. Suruchi Roychoudhry, I edited and revised the manuscript, cover letter, and responses to reviewers.

Title: Underground azelaic acid-conferred resistance to *Pseudomonas syringae* in *Arabidopsis*

Running title: Underground AZA-immunity against pathogens

Nicolás M. Cecchini[1,2#], Suruchi Roychoudhry[1,3#], DeQuantarius J. Speed[1], Kevin Steffes[1], Arjun Tambe[1], Kristin Zodrow[1], Katerina Konstantinoff[1], Ho Won Jung[4], Nancy L. Engle[5], Timothy J. Tschaplinski[5], Jean T. Greenberg[1*]

[1]Department of Molecular Genetics and Cell Biology, The University of Chicago, 929 East 57th Street GCIS 524W, Chicago, IL 60637, USA. [2]Current address: Centro de Investigaciones en Química Biológica de Córdoba, CIQUIBIC, CONICET, Departamento de Química Biológica-Ranwel Caputto, Facultad de Ciencias Químicas, Universidad Nacional de Córdoba, Haya de la Torre y Medina Allende, Ciudad Universitaria, Córdoba, X5000HUA, Argentina. [3]Current address: Centre for Plant Sciences, University of Leeds, Leeds LS2 9JT, UK. [4]Department of Molecular Genetics, Dong-A University, 37 Nakdong-Daero 550beon-gil, Saha-gu, Busan 49315, Korea. [5]Oak Ridge National Lab, PO Box 2008, Oak Ridge, TN 37831, U.S.A.

[#] These authors contributed equally to this work

* To whom correspondence should be addressed.

E-mail: jgreenbe@uchicago.edu

SUMMARY

Local interactions between individual plant organs and diverse microorganisms can lead to whole plant immunity via the mobilization of defense signals. One such signal is the plastid lipid-derived oxylipin azelaic acid (AZA). Arabidopsis lacking AZI1 or EARLI1, related lipid transfer family proteins, exhibit reduced AZA transport among leaves and cannot mount systemic immunity. AZA has been detected in roots as well as leaves. Therefore, the present study addresses the effects on plants of AZA application to roots. AZA, but not the structurally related suberic acid, inhibits root growth when directly in contact with roots. Treatment of roots with AZA also induces resistance to *Pseudomonas syringae* in aerial tissues. These effects of AZA on root growth and disease resistance depend at least partially on AZI1 and EARLI1. AZI1 in roots localizes to plastids, similar to its known location in leaves. Interestingly, kinases previously shown to modify AZI1 *in vitro*, MPK3/6, are also needed for AZA-induced root growth inhibition and above ground immunity. Finally, [^{2}H]-AZA applied to the roots does not move to aerial tissues. Thus, AZA application to roots triggers systemic immunity through an AZI1/EARLI1/MPK3/MPK6-dependent pathway and AZA's effects may involve an additional mobile signal(s).

INTRODUCTION

Plants are capable of inducing systemic resistance programs after local recognition of microbes effectors or molecular patterns associated with them (Fu and Dong 2013; Spoel and Dong 2012). Systemic responses usually include the establishment of a long-lasting alert state or "priming" of the defenses, which allows the plant to mount faster/stronger defense responses upon encountering new pathogens (Hilker et al. 2016; Martinez-Medina et al. 2016; Parker 2009). This recognition can happen in various plant tissues or organs such as leaves or roots and triggers different systemic defense programs (Pieterse et al. 2014). Infection of leaves with pathogens induces systemic acquired resistance (SAR) in distal aerial tissues (Cecchini et al. 2015; Fu and Dong 2013; Mishina and Zeier 2007), whereas root colonization by beneficial microbes promotes induced systemic resistance (ISR) in shoots (Pieterse et al. 1996). While SAR is dependent on the hormone salicylic acid (SA) defense pathway, ISR often relies on the jasmonic acid/ethylene (JA/ETs) signaling pathway (Pieterse et al. 2014). Although these defense programs do not share many components, the primed immunity triggered in aerial tissues is effective against an overlapping spectrum of invaders (Pieterse et al. 2014).

During the induction of systemic resistance, plants generate signals locally that are capable of moving to induce defenses in distal tissues (Chanda et al. 2011; Chaturvedi et al. 2012; Chen et al. 2018; Jung et al. 2009; Návarová et al. 2012; Park et al. 2007; Truman et al. 2007; Wittek et al. 2014). Among those signals, several are hydrophobic or lipid-related molecules, such as the oxylipin azelaic acid (AZA) (Chanda et al. 2011; Chaturvedi et al. 2012; Jung et al. 2009; Riedlmeier et al. 2017; Truman et al. 2007; Wittek et al. 2014). The exogenous application of AZA to aerial tissues induces a "primed" state comparable to that seen after SAR induced by pathogen infection (Jung et al. 2009). AZI1 and EARLI1, two key proteins related to lipid transfer proteins

(LTPs), are known components of the AZA signaling pathway (Cecchini et al. 2015; Jung et al. 2009). They are both needed for AZA priming induction and for the establishment of SAR. Furthermore, *azi1-1* and *earli1-1* mutant plants have reduced movement of AZA from local to distal leaves. AZI1 is also needed for the action of the proposed systemic and/or inter-plant defense signals glycerol-3-phosphate, dehydroabietinal and pinene-monoterpenes (Chaturvedi et al. 2012; Riedlmeier et al. 2017; Yu et al. 2013). In leaves, AZI1 and EARLI1 localize in endoplasmic reticulum (ER), plasma membrane (PM), plasmodesmata (PD) and in the plastid outer envelope membrane (OEM; (Cecchini et al. 2015)), the site of generation of AZA and other signals (Chanda et al. 2011; Chaturvedi et al. 2012; Jung et al. 2009; Nandi et al. 2004; Park et al. 2007; Zoeller et al. 2012). It was suggested that these LTP family proteins could form part of membrane contact site (MCS) complexes, allowing the movement of lipidic molecules through non-vesicular transport. MCSs between plastids, ER and PD membranes play key roles in moving non-polar priming signals to systemic tissues (Cecchini et al. 2015).

Several signals implicated in systemic resistance were proposed to be generated in leaves, but intriguingly, signals for systemic defense programs have yet to be identified in roots (Pieterse et al. 2014; Shah 2009). Among possible root signals that are related to various biotic or abiotic stresses are oxylipins or molecules related to oxylipin metabolism (Constantino et al. 2013; Fragoso et al. 2014; Ghanem et al. 2012; Grebner et al. 2013; León Morcillo et al. 2012; Nalam et al. 2013). Interestingly, many oxylipins are known to be generated in roots and several are related directly to defense against pathogens (Mukhtarova et al. 2011; Nalam et al. 2012; Vicente et al. 2012). In addition, some of these same oxylipins induce root developmental growth arrest and/or morphological changes when applied to seedlings (Vellosillo et al. 2007). This suggests that oxylipins mediate a mechanistic link between root development and root defenses. Among the

oxylipins that induce root architectural changes are AZA and the 9-oxo nonanoic acid (ONA) (Bouain et al. 2018; Vellosillo et al. 2007). Exogenous ONA induces systemic resistance and can generate AZA by oxidation (Wittek et al. 2014; Zoeller et al. 2012). Moreover, like AZA, ONA treatment of leaves induces disease resistance that depends on AZI1 (Wittek et al. 2014).

Although roots can produce AZA (Mukhtarova et al. 2011), it is not known whether AZA can move from roots-to-shoot or if the AZI1/EARLI1 LTP family proteins affect AZA-induced signaling after root application, as was observed in leaves (Cecchini et al. 2015). *AZI1* and *EARLI1* are expressed in roots (Bouain et al. 2018; Hruz et al. 2008). Furthermore, both LTP family proteins are required for ISR (Cecchini et al. 2015). One possibility is that AZI1 and EARLI1 are needed for normal AZA movement and/or for systemic signaling triggered from roots as in leaves. Similarly, factors that modify these proteins may also be needed for root-mediated signaling. Candidate proteins for modifying AZI1 and EARLI1 are the regulatory kinases MPK3/6, which can phosphorylate AZI1 *in vitro* (Pitzschke et al. 2014). Moreover, MPK3 is also required for SAR development and, together with MPK6, for defense priming triggered by SA (Beckers et al. 2009).

Here, we analyzed if root-applied AZA can induce systemic disease resistance in *Arabidopsis* aerial tissues. Moreover, we also studied if AZA can move shootward from the root and if its action/signaling requires AZI1 and EARLI1 and their potential regulatory kinases. We show that AZA applied to roots induces both root morphological changes and systemic resistance; these phenotypes depend on AZI1 and EARLI1 as well as on MPK3 and MPK6. Furthermore, we show that AZI1 localization in roots resembles that seen in leaves. Interestingly, we did not see a detectable shootward movement of AZA from roots. Thus, although similar in its effect on disease resistance, AZA signaling from roots might have important differences compared to its mode of action in aerial tissues.

RESULTS

AZA inhibition of root growth depends on both AZI1 and EARLI1

AZA can inhibit root growth in an AZI-dependent manner (Bouain et al. 2018). Other oxylipins associated with defense against pathogens can also induce root growth arrest and/or developmental changes (Vellosillo et al. 2007; Vicente et al. 2012). Therefore, we analyzed if AZA's effect on the roots is specific and root-autonomous. To do this, aseptic wild-type Columbia-0 (WT Col-0) plants were grown on solid media supplemented with 40 µM of AZA or corresponding mock conditions. As a control for specificity, we treated plants with 40 µM suberic acid (C8), a molecule closely related in structure to AZA that cannot induce disease resistance (Jung et al. 2009). As shown in Figure 2.1A, seedlings grown on AZA plates showed a drastic inhibition of primary root growth, accompanied by increased lateral root density compared with control plants. Developmental defects were not observed in aerial tissues (Fig. 2.1D). Importantly, AZA induced the same effects on plants in which shoot tissue was isolated from contact with AZA by using a glass cover slip (see methods section; Fig. 2.2A and B). This indicates that AZA's effect is root-autonomous. C8 treatment did not induce any change in root architecture (Fig. 2.1A). Thus, specifically AZA (and not a related molecule) is able to induce developmental changes in roots.

Since both LTP family proteins AZI1 and EARLI1 are needed for AZA-mediated systemic signaling (Cecchini et al. 2015; Jung et al. 2009; Yu et al. 2013), we next analyzed the effect of AZA on the roots of mutants lacking these factors. *azi1-1* and *earli1-1* mutant plants showed reduced responses to AZA in terms of root growth inhibition as well as increase in lateral root density when compared to WT Col-0 plants (Fig. 2.1B and C). This differential AZA response is well illustrated in Figure 2.1D. The results indicate that both AZI1 and EARLI1 are required for full AZA-mediated developmental responses in plant roots.

Figure 2.1 Effect of azelaic acid (AZA) on seedling root growth.

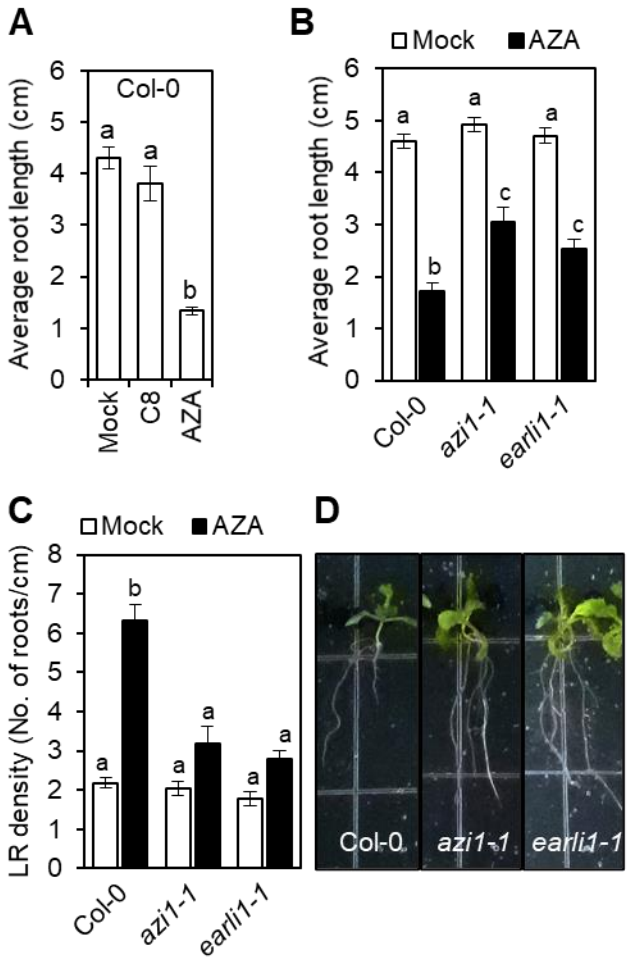

Figure. 2.1**.** Effect of azelaic acid (AZA) on seedling root growth

Average root length (**A** and **B**) and lateral root (LR) density (**C**) of 12-day-old seedlings grown on solid ½ MS agar media supplemented with 40 µm AZA or suberic acid (C8) (in 5mM MES buffer pH 5.7) and control MES (mock) in WT Col-0, *azi1-1* and *earli1-1* plants. The average of root length or LR density plus/minus standard error from two (**A**) and four (**B** and **C**) independent experiments (with 10-12 biological replicates each) is shown. Different letters indicate statistically significant differences ($P<0.01$, analysis of variance (ANOVA), post hoc Tukey's HSD test). **D,** Representative pictures of the seedlings analyzed for (**B** and **C**) grown on the same plate.

Figure 2.2 AZA's effect on root growth is root autonomous.

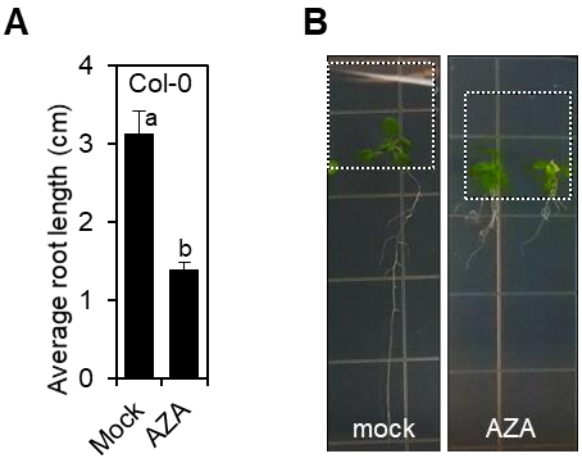

Figure 2.2. AZA's effect on root growth is root autonomous
A, Average root length of 10-day-old Col-0 seedlings grown on solid ½ MS agar media supplemented with 40 µm AZA (in 5mM MES buffer pH 5.7) or control MES (mock). Seedling aerial tissue was isolated from contact with media using a sterile glass cover slip (shown in white-dashed lines in **B**). The average of root length plus/minus standard error from three independent experiments (each with 10-12 biological replicates) is shown. Different letters indicate statistically significant differences ($P<0.01$, Student's *t*-test). **B,** Representative pictures of the seedlings analyzed for (**A**).

Root-supplied AZA induces systemic resistance to P. syringae

AZA treatment of a few lower leaves induces disease resistance in distal (systemic) leaves (Jung et al. 2009). Considering this, we examined if application of AZA to roots is also able to increase disease resistance in aerial tissues. To do this, adult WT Col-0 plant roots were treated with 1 mM AZA (or mock) solution and leaves were infected with *Pseudomonas cannabina* pv *alisalensis* (formerly called *P. syringae* pv *maculicula* (Bull et al. 2010)) strain *Pma*DG3 one day later. The growth of *Pma*DG3 was quantified three days post-infection. We also treated plants with 1 mM C8 as control. As shown in Fig. 2.3A, plants treated with AZA showed increased resistance to *Pma*DG3 compared to mock- or C8- treated plants. This indicates that AZA can induce systemic resistance when applied to the roots. Interestingly, root AZA treatment did not

trigger systemic resistance to *Pma*DG3 in *earli1-1* mutant plants compared to the mock treatment or WT Col-0 (Fig. 2.3B). However, *azi1-1* plants were still able to induce aerial defenses, albeit at a lower level than WT plants (Fig. 2.3B). These results indicate that EARLI1 is an essential factor for root-AZA systemic resistance establishment, while AZI1 is partially needed for full resistance.

Figure 2.3 Root-applied AZA specifically confers systemic disease resistance to Pseudomonas syringae.

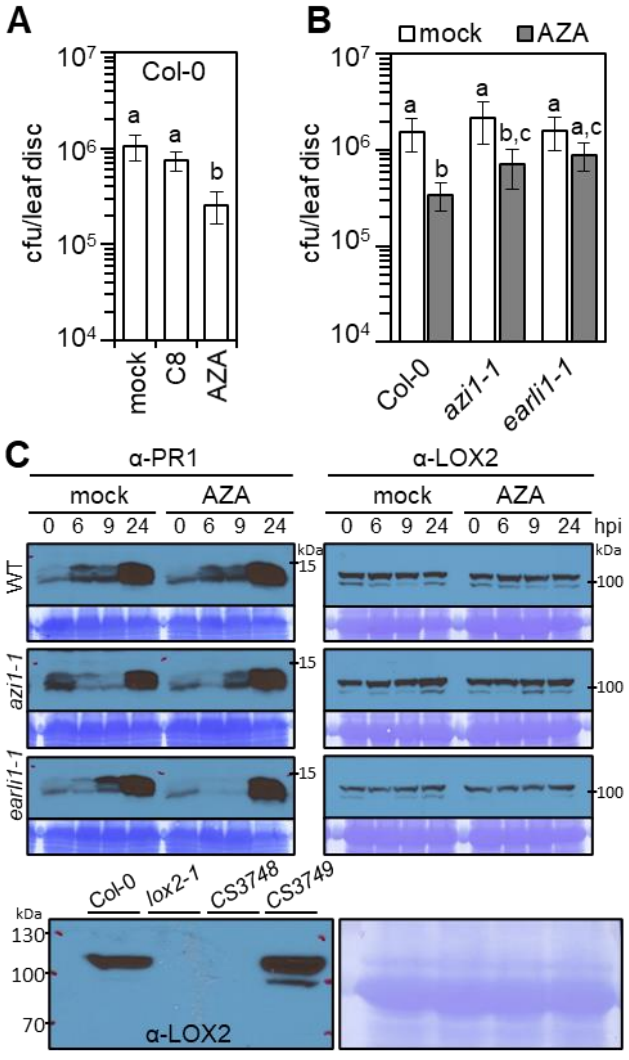

Figure 2.3. Root-applied AZA specifically confers systemic disease resistance to *Pseudomonas syringae*

A, Growth of virulent bacteria PmaDG3 on WT Col-0 plants 3 days post infection (OD600=0.0003). PmaDG3 was infiltrated in leaves 1 day after roots were treated with control

Figure 2.3. Root-applied AZA specifically confers systemic disease resistance to *Pseudomonas syringae* (cont)
Col-0, *azi1-1* and *earli1-1* treated as in (A). The average of CFU per leaf disc plus/minus standard error from two independent experiments in (A) and four in (B) (each one with 8 biological replicates) is shown. Graph Y-axes are in $\log_{10}$ scale. C, PR1 and LOX2 protein levels in WT Col-0 and *azi1-1* and *earli1-1* total extracts at different times post infiltration of *Pma*DG3 (OD_{600}=0.01) to test priming in plants previously treated as in (B). The blots stained with Coomassie blue are presented to show loading. Similar results were observed in four independent experiments. Lower panel shows LOX2 (*Arabidopsis* LOX-C; Agrisera AS07 258) antibody validation. LOX2 protein level in WT Col-0, *lox2-1* (*LOX2* mutant plant), CS3748 (*LOX2* silenced line) and CS3749 (CS3748 control line) total protein extracts. Antibody was used at 1:25,000 dilution. The blots stained with Coomassie blue are presented to show loading. D, PR1 and LOX2 levels in (C) relative to the total protein content in each Coomassie blue membrane lane as quantified by densitometry. The average plus/minus standard error from four independent experiments are shown.

Root-supplied AZA does not prime PR1 or LOX2 in leaves

To determine if AZA treatment of roots can induce priming in leaf tissue through a similar signaling pathway as that in aerial tissue (Cecchini et al. 2015; Jung et al. 2009), we analyzed the levels and kinetics of the pathogenesis-related protein 1 (PR1) accumulation in leaves. After roots were treated with AZA or a mock treatment, PR1 priming in leaves was analyzed at different times post infection with *Pma*DG3 infection. AZA-treated WT plants did not show faster and/or higher induction of PR1 compared with mock treatment (Fig. 2.3C and D). Additionally, because previous studies found that *LOX2* in leaves is a priming target during ISR (Conrath et al. 2006; Pozo et al. 2008), we analyzed the induction kinetics of LOX2 after AZA root treatment and leaf infections. We used an antibody specific for LOX2 for these experiments (Fig. 2.3C, lower panel). As observed in Figure 2.3C and D, we did not detect priming of LOX2. In agreement with these data, *azi1-1* and *earli1-1* mutant plants did not show PR1 or LOX2 priming (Fig. 2.3C and D).

These results indicate that root application of AZA induces systemic disease resistance without priming PR1 or LOX2 production in aerial tissues.

MPK3/6 are needed for root responses to AZA and induced systemic resistance.

MPK3 and possibly MPK6 can phosphorylate AZI1 *in vitro* (Pitzschke et al. 2014). Therefore, we analyzed if MPK3 and MPK6 have roles in the AZA-induced root developmental phenotype and/or systemic resistance induction. As shown in Fig. 2.4A and B, AZA-induced root growth inhibition was reduced in the mutants compared with WT Col-0 plants, while the increase in lateral root density disappeared. Moreover, both *mpk3* and *mpk6* single mutants were unresponsive to AZA root treatment when analyzed for systemic resistance to *Pma*DG3 infection (Fig. 2.4C). These results indicate that MPK3 and MPK6 are required for AZA-mediated systemic defense induction from roots.

Since AZA signaling components AZI1 and EARLI1 are needed for normal ISR establishment (Cecchini et al. 2015), we also tested if MPK3/6 are implicated in this important systemic defense response. For this, we inoculated WT Col-0, *mpk3* and *mpk6* roots with *P. fluorescence* and after two weeks, analyzed the growth of *Pma*DG3 after challenging distal leaves. Compared to WT plants, both mutants were completely ISR defective (Fig. 2.4D).

Taken together, these results indicate that MPK3 and MPK6 are important components for root-mediated systemic disease resistance induced by different stimuli.

AZI1 likely localizes to the plastid outer envelope and other membranes in roots

In leaf tissue, AZI1 localizes to endoplasmic reticulum, plasma membrane, plasmodesmata and the plastid outer envelope, the site where AZA and other oxylipins are produced (Cecchini et al. 2015; Lim et al. 2016). To discern AZI1's possible site(s) of action in roots, we examined its subcellular localization in this tissue in plants previously shown to express functional dexamethasone (dex)-inducible AZI1:GFP (Cecchini et al. 2015). Roots expressing AZI1:GFP and

Figure 2.4 *mpk* mutants are compromised in root-mediated responses to AZA

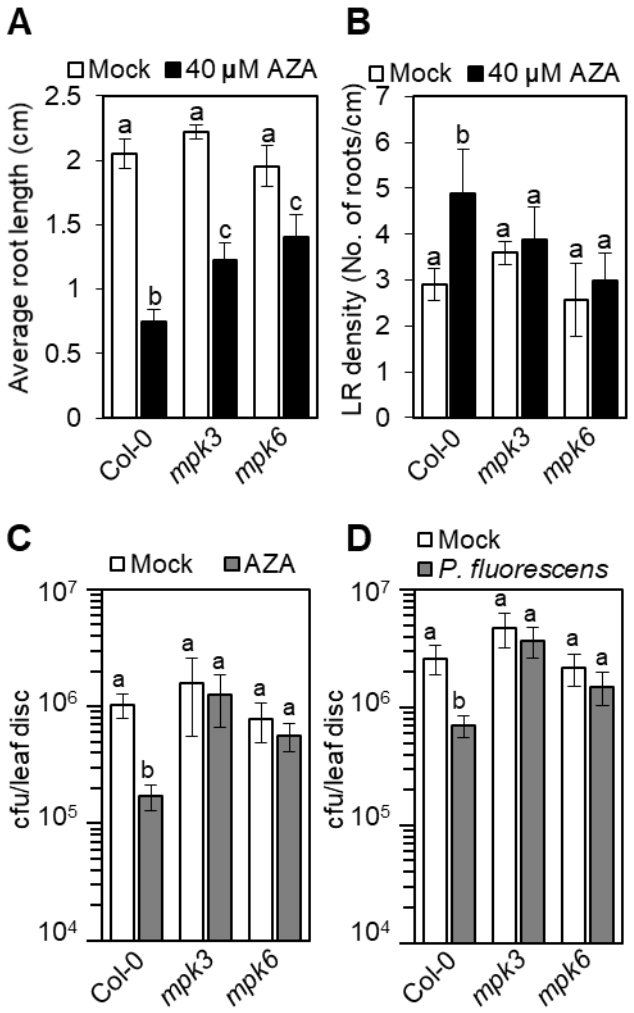

Figure 2.4 *mpk* mutants are compromised in root-mediated responses to AZA

Average root length (**A**) and lateral root density (**B**) of 10-day-old seedlings grown on solid ½ MS agar media supplemented with 40 µm AZA (in 5mM MES buffer pH 5.7) or control MES (mock) in WT Col-0, *mpk3* and *mpk6* plants. The average of root length or lateral root density plus/minus standard error from three independent experiments (each one with 8-10 biological replicates) is shown. **C** and **D,** Growth of the virulent bacteria *Pma*DG3 on WT Col-0, *mpk3* and *mpk6* plants 3 days post infection (OD_{600}=0.0003). *Pma*DG3 was infiltrated in leaves 1 day after root treatment with control H_2O (mock), or AZA (in H_2O) (**C**); or after 15 days of mock (10mM $MgSO_4$) or *P. fluorescence* root inoculation (**D**). The average of CFU per leaf disc plus/minus standard error from three independent experiments in (**C**) and (**D**) (each one with 8 biological replicates) is shown. Graph Y-axes are in $\log_{10}$ scale. Plants were grown in peat pellets. Different letters indicate statistically significant differences ($P<0.01$, analysis of variance (ANOVA), post hoc Tukey's HSD test).

stained with propidium iodine (PI) to visualize cell borders were analyzed by laser scanning confocal microscopy (Fig. 5A). GFP signals were evident at cell peripheries (near PI signals, likely at the plasma membrane and/or ER) and at autofluorescent structures inferred to be small plastids. Close-up imaging revealed AZI1:GFP ring patterns that surrounded the small autofluorescent plastids (Fig. 5B). This fluorescence pattern resembles the AZI1 plastid outer envelope localization in leaves (Cecchini et al. 2015). To validate the plastid localization, roots of F1 plants resulting from a cross of the AZI1:GFP line to a line with the root-plastid marker RecAred (Haswell and Meyerowitz, 2006) were analysed. A pool of AZI1:GFP protein co-localized to plastids marked by RecAred (Fig. 5C and D). In the RecAred-expressing line, no GFP signals were detected, indicating there was no bleed-through of the RecAred signal to the GFP channel (Fig. 5E).

These results suggest that AZI1 has similar subcellular sites of action in roots and leaves.

Figure 2.5 AZI1 root-subcellular localization in Arabidopsis

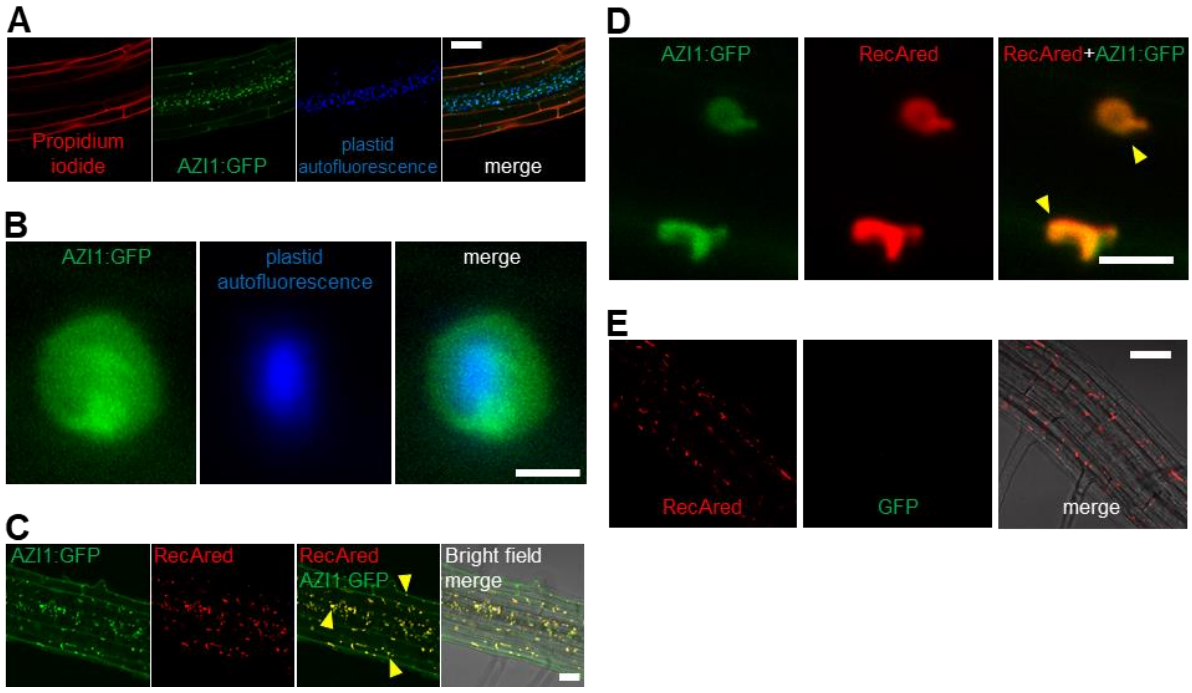

Figure 2.5 AZI1 root-subcellular localization in Arabidopsis
Average root length (**A**) and lateral root density (**B**) of 10-day-old seedlings grown on solid ½ MS agar media supplemented with 40 µm AZA (in 5mM MES buffer pH 5.7) or control MES (mock) in WT Col-0, *mpk3* and *mpk6* plants. The average of root length or lateral root density plus/minus standard error from three independent experiments (each one with 8-10 biological replicates) is shown. **C** and **D,** Growth of the virulent bacteria *Pma*DG3 on WT Col-0, *mpk3* and *mpk6* plants 3 days post infection (OD_{600}=0.0003). *Pma*DG3 was infiltrated in leaves 1 day after root treatment with control H_2O (mock), or AZA (in H_2O) (**C**); or after 15 days of mock (10mM $MgSO_4$) or *P. fluorescence* root inoculation (**D**). The average of CFU per leaf disc plus/minus standard error from three independent experiments in (**C**) and (**D**) (each one with 8 biological replicates) is shown. Graph Y-axes are in $\log_{10}$ scale. Plants were grown in peat pellets. Different letters indicate statistically significant differences (P<0.01, analysis of variance (ANOVA), post hoc Tukey's HSD test).

AZA is not transported from root to shoot

AZA moves from local leaves to systemic tissues in a manner that partially requires AZI1 and EARLI1 (Cecchini et al. 2015; Jung et al. 2009). One possibility is that AZA also moves from the roots to the shoot with AZI1 and EARLI1 playing roles in this movement. To test this hypothesis, we applied 1 mM of deuterium-labeled AZA (^{2}H-AZA) to WT, *azi1-1* and *earli1-1* seedling roots and quantified the amount of ^{2}H-AZA in treated root and untreated leaf tissue after 24 hrs. Although ^{2}H-AZA was taken up, the ^{2}H-AZA was not detectable in aerial tissues (Table 1). Compared to WT Col-0 plants, *azi1-1* and *earli1-1* mutant plants did not show differences in the root uptake of ^{2}H-AZA. We also quantified the amount of unlabeled AZA present in the same samples. Table 1 shows that internal AZA was measured in roots and shoots, indicating that we were able to detect it in both tissues. We considered the possibility that AZA might cause increased ONA accumulation in leaves. While we were able to obtain a spectrum for synthetic ONA after derivatization (Supplementary Fig. 2.1), we were unable to detect ONA in our biological samples. Possibly ONA levels are below the limit of detection.

These data suggest that AZA is either unable to move from roots to distal aerial tissue when exogenously applied (or that the movement is very low) or AZA was transformed to an AZA-derivative. This contrasts with the high mobility of AZA applied to leaves, which moved both to other leaves and roots (Cecchini et al. 2015).

DISCUSSION

Signals acting in plant underground tissues and capable of inducing above ground systemic resistance are scarce. Intriguingly, the SAR signal AZA can be produced in stressed roots (Jung et al. 2009; Mukhtarova et al. 2011). We showed here that application of AZA to roots effectively triggers systemic disease resistance in leaves. The effects of root-applied AZA depend on AZI1 and EARLI1, which are also needed for other systemic defense programs (e.g. SAR and ISR). Additionally, the possible regulators of AZI1, MPK3 and MPK6, are required for the root-mediated response to AZA and *P. fluorescens* (a potent inducer of ISR). Although common factors are needed for AZA's disease resistance induction after application to leaves or roots, AZA's effects on signaling may be tissue-specific. In particular, AZA applied to roots did not cause priming of defense markers usually associated with systemic resistance programs and priming establishment. We also observed that AZA applied to roots does not move upward to aerial tissue. One idea is that AZA applied to roots might induce the generation or facilitate the movement of related molecules capable of translocating from roots and triggering systemic resistance. Considering these and our previous results, we propose that the oxylipin AZA, and AZA-signaling, is an important and general factor functioning in multiple systemic plant immunity programs.

AZA can induce systemic resistance and priming of the SAR-associated PR1 defense protein when applied to leaves (Balmer et al. 2015; Conrath et al. 2015; Jung et al. 2009). However,

when root-applied, AZA is capable of inducing systemic resistance independently of PR1 priming. Moreover, LOX2, an ISR priming target protein (Conrath et al. 2006; Pozo et al. 2008), is not primed either. These findings indicate that additional systemic defense/priming target(s) in leaves may exist for root-applied AZA. A different primed factor is probably explained by the finding that AZA does not accumulate systemically when applied to roots compared to what was described in leaves (Jung et al. 2009). As discussed above, there may be a "new" AZA-derived systemic signal(s) generated in roots. Since pathogen resistance resulting from AZA application to roots requires the LTP-family proteins AZI1 and EARLI1, it is probable that such a putative systemic root signal(s) is lipidic in nature. If this is the case, its movement to and/or generation in aerial tissues might also depend on AZI1/EARLI1 LTPs, as was observed for AZA in leaves (Cecchini et al. 2015). Because a pool of AZI1 is plastid localized, it is possible that this signal(s) could be related to AZA or precursors of oxylipins that are generated in plastid envelopes (Mukhtarova et al. 2011; Zoeller et al. 2012). An alternative possibility is that AZA applied to roots causes induction of a directly antimicrobial product that is translocated to leaves.

Diverse oxylipins can induce defenses (Blée 2002; Prost et al. 2005). Interestingly, many of these molecules can also induce root developmental changes (Vellosillo et al. 2007). This suggests that the oxylipins' developmental effects on roots could be related to defense signaling. ISR-inducing and other plant-growth promoting rhizobacteria (PGPR) and fungi usually induce root architectural changes upon colonization. Moreover, these developmental changes are very similar to those generated by AZA root-treatment: loss of apical dominance and/or abundant lateral root formation (Contreras-Cornejo et al. 2009; Ortiz-Castro et al. 2011; Spaepen et al. 2014; Zamioudis et al. 2013). Although this root phenotype induced by beneficial microbes is believed to be related to the promotion of plant growth, it is not known how root architecture changes relate

to the induction of systemic resistance to pathogens (Pieterse et al. 2014). One possibility is that auxin-signaling balances growth and systemic immunity (Stringlis et al. 2017). Here we found that the same signaling molecule (AZA) activates both phenotypes. It is possible that oxylipins that act via AZI1/EARLI1 are implicated in PGPR responses, connecting growth and systemic defense. Consistent with this, inoculation with the PGPR *Azospirillum brasilense* up-regulates the root expression of *AZI1* and induces growth inhibition (Spaepen et al. 2014). Moreover, this root arrest is diminished in *azi1* mutant plants (Bouain et al. 2018). Future experiments in which oxylipin profiles are compared during ISR and other root-biotic interactions may shed light on this hypothesis. We also note that distinct AZA concentrations confer the growth and defense phenotypes, respectively. It is possible that although the developmental and resistance signaling pathways share components (i.e. AZI1 and EARLI1), they can have differential sensitivities/threshold responses to AZA. However, the higher concentration needed for disease resistance may be due to the technical limitation of adding AZA to peat pots that may make some of the AZA unavailable to be taken up by the roots.

MPK3 and MPK6 are important components that contribute to SAR in leaves (Beckers et al. 2009). These kinases contribute to AZA-induced root architecture changes, and they are also needed for aerial tissue disease resistance induced by treatment of roots with *P. fluorescens*. Notably, MPK3 and MPK6 have important defense roles in roots (Fujimoto et al. 2015; Sidonskaya et al. 2016). Because MPK3 regulates the abundance of AZI1 under abiotic stress conditions (Pitzschke et al. 2014), one possibility is that the requirement of these MPKs for systemic resistance induction is explained by their regulation of AZI1 and/or AZI1 LTP-family proteins such as EARLI1. In support of this, both *azi1-1* and *mpk3* mutant plants show slight intolerance to salt stress. Moreover, the salt stress phenotype of *mpk3* is partially rescued by

overexpression of AZI1, suggesting these proteins may act in the same process(es) (Pitzschke et al. 2014). MPK3 and MPK6 become activated in response to reactive oxygen species (ROS) (Asai et al. 2002; Jalmi and Sinha 2015; Kovtun et al. 2000) and upon plastid calcium release during basal defenses (Guo et al. 2016). Because AZA is generated by plastidic ROS increases (Zoeller et al. 2012), this raises the possibility that MPKs, AZI1-family LTPs and AZA (or other plastid oxylipins) are regulated and act in concert when root defense responses are triggered.

Although we did not find AZA accumulating in leaves after root application, AZA can move to the roots when applied to leaves (Cecchini et al. 2015). Thus, it is possible that the AZA produced in aerial tissue when systemic resistance is triggered, moves to the underground tissues. AZA in roots may induce other signal(s), which in turn reinforce the aerial systemic immunity. This shoot–root–shoot loop in plant defense was previously suggested for other oxylipins (Agut et al. 2016; Erb et al. 2009; Groen 2016; Nalam et al. 2012). Furthermore, root stresses might control the activation state of MPK3/6, resulting in AZI1/oxylipin signaling regulation. If this is true, depending on root conditions, systemic defenses could be more or less reinforced depending on an integration of the environment. Remarkably, this idea is in agreement with the so-called Darwin 'root-brain' hypothesis (Baluška et al. 2009; Fragoso et al. 2014; Kutschera and Niklas 2009), which postulates that roots are the sensorial regulatory place where plants make "decisions" that orchestrate above-ground processes.

METHODS

Plants

Arabidopsis thaliana mutant plants *azi1-1*, *earli1-1*, *mpk3-1*, *mpk6-2* and *lox2-1* were previously described (Glauser et al. 2009; Jung et al. 2009; Liu and Zhang 2004; Wang et al. 2007;

Xu et al. 2011). The silenced *LOX2* SALK-line CS3748 and its control line CS3749 (Bell et al. 1995) were obtained from the Arabidopsis Biological Resources Center (Ohio State University, Columbus, OH, USA). *azi1-1*, *earli1-1*, *mpk3-1*, *mpk6-2* and *lox2-1* plants were in the Columbia-0 (Col-0) background while CS3748 and CS3749 lines in Col gl1. Transgenic plants expressing AZI1:GFP fusion protein under the control of dexamethasone (dex)-inducible promoter (in the *azi1-1* background) (dex-AZI1:GFP) was previously described (Cecchini et al. 2015). F1 plants from a cross of RecAred background (Col-0 plants expressing red fluorescence protein targeted to root plastids (Haswell and Meyerowitz 2006)) with dex-AZI1:GFP were used for co-localization analysis. For ISR and AZA-induced disease resistance assays, sterile seeds were stratified for 3 days at 4°C, grown in Jiffy-7 pellets (Jiffy Products International, Canada) under 12 h day and 12 h night conditions at 20-21°C, 200-230 μmol sec^{-1} m^{-2} light at rosette level, 50-70% relative humidity and bottom watered with sterile water two times per week (Cecchini et al. 2015; Haney et al. 2015). For localization and AZA effects on root architecture, sterile seeds were stratified for 2 days at 4°C, germinated and grown in ½ MS (Murashige and Skoog media; Sigma-Aldrich, St. Louis, MO) (1% sucrose) agar plates in a growth chamber with 16h light (120 μmol sec^{-1} m^{-2}) and 8 h dark cycles at 21°C.

Azelaic acid treatment of seedlings on plate assays

Seeds were germinated and grown on ½ MS (1% sucrose) agar plates supplemented with 40 μM of azelaic acid (AZA; $C_9H_{16}O_4$, MW 188.22, Sigma-Aldrich, St. Louis, MO), 40 μM of suberic acid (C8; $C_8H_{14}O_4$, MW 174.2, Sigma-Aldrich) prepared in 5 mM 2-[N-morpholino]ethane-sulfonic acid (MES) buffer, pH 5.7) or an appropriate volume of MES as mock-control. 10 mM stock solution of AZA and C8 were prepared in 5mM MES buffer, pH 5.7.

The plates were placed vertically into a plant growth chamber. Ten to twelve days after germination, the plates were photographed using a Canon Power Shot A590 digital camera. Root lengths and lateral root numbers were analyzed using ImageJ.

For the assays where the contact between aerial tissues and the agar media was avoided, two-day-old seedlings were transferred to new MS plates with 18 x 18 mm sterile glass cover slips placed on the media. Seedling cotyledons and hypocotyl were then isolated from the agar by being gently placed on top of the cover slips with only the roots in contact with the media.

^{2}H-Azelaic acid root uptake and movement quantification

Arabidopsis seeds were germinated and grown for 14 days on a ~60 mm diameter disk mesh (0.375 mm mesh, McMaster-Carr #93185T22, Chicago, IL) placed onto 0.4 % agarose ½ MS (1% sucrose) in 80 ml beakers in sterile conditions. The mesh was then transferred, together with the seedlings, to 50 x 9 mm plates containing a solution of 1mM deuterium-labeled azelaic acid (^{2}H-azelaic acid; MW 202.31, Medical Isotopes Inc., Pelham, NH) prepared in 5 mM MES buffer (pH 5.6). The mesh affixed to the plate borders permitted the roots, but not the aerial tissues to be in contact with the solution. The plates were put inside a humid chamber and after 24 hours, roots and aerial tissues were separately collected, weighed and frozen for the metabolite extraction (Lisec et al. 2006). Extracts were derivatized and subjected to GC/MS analysis to determine the concentration of labeled ^{2}H-azelaic acid and unlabeled azelaic acid (Jung et al. 2009; Li et al. 2012; Tschaplinski et al. 2012). A synthetic sample of ONA (a kind gift of Dr. Carmen Castresana, Centro Nacional de Biotecnología-Consejo Superior de Investigaciones Científicas) was used as standard. For the ONA fragmentation patterns generation, approx. 1 mg was dissolved in 500 µL of silylation–grade acetonitrile followed by the addition of 500 µL N-methyl-N-

trimethylsilyltrifluoroacetamide (MSTFA) with 1% trimethylchlorosilane (TMCS) (Pierce Chemical Co., Rockford, IL) and heated for 1 h at 70 ºC to generate trimethylsilyl (TMS) derivatives. After 2 hours, 0.1 µL of derivatized ONA was injected into an Agilent Technologies Inc. (Santa Clara, CA) 5975C inert XL gas chromatograph-mass spectrometer fitted with an Rtx-5MS with Integra-guard (5% diphenyl/95% dimethyl polysiloxane) 30 m x 250 µm x 0.25 µm film thickness capillary column, with the operating conditions as previously described (Li et al. 2012; Tschaplinski et al. 2012).

Systemic resistance assays by root application of dicarboxylic acids

Roots of 25~28-day-old plants in Jiffy-7 pellets were submerged for ~30 seconds in 1mM azelaic acid, 1mM suberic acid or mock (0.13% methanol) solutions. This procedure allows the treatment of the entire root system without the aerial tissues coming into contact with the solutions. Azelaic acid and suberic acid stock solutions (750 mM) were prepared in methanol and then diluted to a final concentration in sterile water. For these assays, a higher concentration of AZA used compared with plate assays to ensure that sufficient AZA was available to be absorbed by the roots in case the Jiffy-7 pellet matrix absorbed some of the AZA.

To evaluate systemic resistance, leaves were syringe-inoculated with virulent *Pseudomonas cannabina* pv *alisalensis* (formerly called *P. syringae* pv. *maculicola* ES4326 (Bull et al. 2010)) carrying an empty vector (*Pma*DG3) (OD_{600}=0.0003) (Guttman and Greenberg 2001) one day after root-treatments. Growth was quantified by dilution plating using 8 leaves from 8 different plants 3 days after *Pma*DG3 inoculation.

To analyze possible priming of PR1 and LOX2 induction, leaves were inoculated with *Pma*DG3 (OD_{600}=0.01) one day after root treatments and protein samples were obtained at

different times post infection. At least 3 leaves from 3 different plants were used per time point. The same amount (weight) of each sample was extracted in loading buffer (125 mM Tris (pH 6.8), 20 % glycerol, 4 % SDS, 5 M urea, 0.01 % bromophenol Blue). For immunoblots, equal amounts of total proteins were separated by SDS-PAGE. Primary antibodies used herein were against PR1 (Agrisera AS10 687, 1:2,500, validated by Agrisera, Sweden), LOX-C (*Arabidopsis* LOX2; Agrisera AS07 258, 1:25,000, validated herein). Secondary anti-rabbit antibody conjugated to horseradish peroxidase (Thermo Scientific, Waltham, MA) was used at 1:1000. Band signals were detected by using SuperSignal West Stable Peroxidase (Thermo Scientific).

Induced systemic resistance (ISR)

ISR assays were done as previously described (Haney et al. 2015) with some modifications. Ten-day old seedlings were first inoculated (on the top surface of the Jiffy pot) with 6 mL solution of *P. fluorescens* WCS417r to a final density OD_{600} of 0.01 (10^5 CFU/mL). Then, the entire pots were submerged for ~30 seconds in the same solution without allowing contact of bacteria with the leaves. To evaluate the systemic resistance, 15 days after root system inoculations, leaves five and six were syringe-infiltrated with *Pma*DG3 (OD_{600}=0.0003). Growth was quantified by dilution plating using eight leaves from different plants 3 days after *PmaDG3* inoculation.

Confocal microscopy

Five day old transgenic *Arabidopsis* seedlings expressing AZI1:GFP under the dex-inducible promoter (Cecchini et al. 2015) or expressing both AZI1:GFP and RecAred were transferred to new plates containing 30 μM dexamethasone. After 24 hours, seedlings were mounted in water or 40 μg/ml propidium iodide solution (to stain cell walls) and imaged using an

upright Zeiss LSM710 laser-scanning confocal microscope (Zeiss, Germany). The 488 nm laser was used for GFP fluorescence (emission: 505 to 530 nm), while the 535 nm laser was used for propidium iodide and RFP fluorescence (emission: 570 to 620 nm) and the 633 nm laser for plastid autofluorescence (emission: 650-750 nm). Images were taken using a LD C-Apochromat 40x/1.1 W Korr objective. Sequential acquisition mode was used for acquisition of fluorescence. Images were processed using ImageJ (http://rsb.info.nih.gov/ij), ZEN 2012 (Zeiss) and Adobe Photoshop software.

ACKNOWLEDGMENTS

This research was supported by NSF grant IOS1456904 to JTG. This research was also supported, in part, by the Genomic Science Program (Science Focus Area 'Plant:Microbe Interfaces'), U.S. Department of Energy, Office of Science, Biological and Environmental Research to Oak Ridge National Laboratory, which is managed by UT-Battelle, LLC, for the US Department of Energy under Contract no DE-AC05-00OR22725. DJ Speed was supported by T32 GM007183 and a predoctoral fellowship award from the Ford Foundation. NMC is a Career Investigator of CONICET (Argentina). We thank SC Jiang and J Jelenska for helpful discussions. We thank Carmen Castresana for the gift of synthetic ONA.

AUTHOR CONTRIBUTIONS

JTG, NMC and SR conceived and designed the experiments. NMC, SR, DJS, KS, AT, KZ, KK, HWJ, NLE and TJT performed the experiments. JTG, NMC, SR, HWJ, NLE and TJT analyzed and interpreted data. JTG and NMC wrote the paper.

REFERENCES

- Agut, B., Gamir, J., Jaques, J. A., and Flors, V. 2016. Systemic resistance in citrus to Tetranychus urticae induced by conspecifics is transmitted by grafting and mediated by mobile amino acids. J. Exp. Bot. 67:5711–5723.
- Asai, T., Tena, G., Plotnikova, J., Willmann, M. R., Chiu, W.-L., Gomez-Gomez, L., Boller, T., Ausubel, F. M., and Sheen, J. 2002. MAP kinase signalling cascade in Arabidopsis innate immunity. Nature. 415:977–983.
- Balmer, A., Pastor, V., Gamir, J., Flors, V., and Mauch-Mani, B. 2015. The "prime-ome": towards a holistic approach to priming. Trends Plant Sci. 20:443–452.
- Baluška, F., Mancuso, S., Volkmann, D., and Barlow, P. 2009. The "root-brain" hypothesis of Charles and Francis Darwin. Plant Signal. Behav. 4:1121–1127.
- Beckers, G. J. M., Jaskiewicz, M., Liu, Y., Underwood, W. R., He, S. Y., Zhang, S., and Conrath, U. 2009. Mitogen-activated protein kinases 3 and 6 are required for full priming of stress responses in Arabidopsis thaliana. Plant Cell. 21:944–953.
- Bell, E., Creelman, R. a, and Mullet, J. E. 1995. A chloroplast lipoxygenase is required for wound-induced jasmonic acid accumulation in Arabidopsis. Proc. Natl. Acad. Sci. U. S. A. 92:8675–8679.
- Blée, E. 2002. Impact of phyto-oxylipins in plant defense. Trends Plant Sci. 7:315–321.
- Bouain, N., Satbhai, S. B., Korte, A., Saenchai, C., Desbrosses, G., Berthomieu, P., Busch, W., and Rouached, H. 2018. Natural allelic variation of the AZI1 gene controls root growth under zinc-limiting condition. PLoS Genet. 14:e1007304.
- Bull, C. T., Manceau, C., Lydon, J., Kong, H., Vinatzer, B. A., and Fischer-Le Saux, M. 2010. Pseudomonas cannabina pv. cannabina pv. nov., and Pseudomonas cannabina pv. alisalensis (Cintas Koike and Bull, 2000) comb. nov., are members of the emended species Pseudomonas cannabina (ex Sutic & Dowson 1959) Gardan, Shafik, Belouin, Brosch, Grimont & Grimont 1999. Syst. Appl. Microbiol. 33:105–15.
- Cecchini, N. M., Steffes, K., Schläppi, M. R., Gifford, A. N., and Greenberg, J. T. 2015. Arabidopsis AZI1 family proteins mediate signal mobilization for systemic defence priming. Nat. Commun. 6:7658.
- Chanda, B., Xia, Y., Mandal, M. K., Yu, K., Sekine, K.-T., Gao, Q., Selote, D., Hu, Y., Stromberg, A., Navarre, D., Kachroo, A., and Kachroo, P. 2011. Glycerol-3-phosphate is a critical mobile inducer of systemic immunity in plants. Nat. Genet. 43:421–427.
- Chaturvedi, R., Venables, B., Petros, R. a, Nalam, V., Li, M., Wang, X., Takemoto, L. J., and Shah, J. 2012. An abietane diterpenoid is a potent activator of systemic acquired resistance. Plant J. 71:161–172.
- Champigny, M. J., Isaacs, M., Carella, P., Faubert, J., Fobert, P. R., and Cameron, R. K. 2013. Long distance movement of DIR1 and investigation of the role of DIR1-like during systemic acquired resistance in Arabidopsis. Front. Plant Sci. 4:230.
- Chen, Y.-C., Holmes, E. C., Rajniak, J., Kim, J., Tang, S., Fischer, C. R., Mudgett, M. B., and

Sattely, E. S. 2018. N-hydroxy-pipecolic acid is a mobile metabolite that induces systemic disease resistance in Arabidopsis. Proc. Natl. Acad. Sci. U. S. A. 115:E4920–E4929.

- Conrath, U., Beckers, G. J. M., Flors, V., García-Agustín, P., Jakab, G., Mauch, F., Newman, M., Pieterse, C. M. J., Poinssot, B., Pozo, M. J., Pugin, A., Schaffrath, U., Ton, J., Wendehenne, D., Zimmerli, L., and Mauch-Mani, B. 2006. Priming: getting ready for battle. Mol. Plant. Microbe. Interact. 19:1062–1071.
- Conrath, U., Beckers, G. J. M., Langenbach, C. J. G., and Jaskiewicz, M. R. 2015. Priming for enhanced defense. Annu. Rev. Phytopathol. 53:97–119.
- Constantino, N. N., Mastouri, F., Damarwinasis, R., Borrego, E. J., Moran-Diez, M. E., Kenerley, C. M., Gao, X., and Kolomiets, M. V. 2013. Root-expressed maize lipoxygenase 3 negatively regulates induced systemic resistance to Colletotrichum graminicola in shoots. Front. Plant Sci. 4:510.
- Contreras-Cornejo, H. A., Macías-Rodríguez, L., Cortés-Penagos, C., and López-Bucio, J. 2009. Trichoderma virens, a plant beneficial fungus, enhances biomass production and promotes lateral root growth through an auxin-dependent mechanism in Arabidopsis. Plant Physiol. 149:1579–1592.
- Erb, M., Lenk, C., Degenhardt, J., and Turlings, T. C. J. 2009. The underestimated role of roots in defense against leaf attackers. Trends Plant Sci. 14:653–659.
- Fragoso, V., Rothe, E., Baldwin, I. T., and Kim, S.-G. 2014. Root jasmonic acid synthesis and perception regulate folivore-induced shoot metabolites and increase Nicotiana attenuata resistance. New Phytol. 202:1335–1345.
- Fu, Z. Q., and Dong, X. 2013. Systemic acquired resistance: turning local infection into global defense. Annu. Rev. Plant Biol. 64:839–863.
- Fujimoto, T., Mizukubo, T., Abe, H., and Seo, S. 2015. Sclareol induces plant resistance to root-knot nematode partially through ethylene-dependent enhancement of lignin accumulation. Mol.Plant Microbe Interact. 28:398–407.
- Ghanem, M. E., Ghars, M. A., Frettinger, P., Pérez-Alfocea, F., Lutts, S., Wathelet, J. P., du Jardin, P., and Fauconnier, M. L. 2012. Organ-dependent oxylipin signature in leaves and roots of salinized tomato plants (Solanum lycopersicum). J. Plant Physiol. 169:1090–1101.
- Glauser, G., Dubugnon, L., Mousavi, S. A. R., Rudaz, S., Wolfender, J.-L., and Farmer, E. E. 2009. Velocity estimates for signal propagation leading to systemic jasmonic acid accumulation in wounded Arabidopsis. J. Biol. Chem. 284:34506–34513.
- Grebner, W., Stingl, N. E., Oenel, A., Mueller, M. J., and Berger, S. 2013. Lipoxygenase6-dependent oxylipin synthesis in roots is required for abiotic and biotic stress resistance of Arabidopsis. Plant Physiol. 161:2159–2170.
- Groen, S. C. 2016. Signalling in systemic plant defence - roots put in hard graft. J. Exp. Bot. 67:5585–5587.
- Guo, H., Feng, P., Chi, W., Sun, X., Xu, X., Li, Y., Ren, D., Lu, C., Rochaix, J. D., Leister, D., and Zhang, L. 2016. Plastid-nucleus communication involves calcium-modulated MAPK signalling. Nat. Publ. Gr. 7:1–15.

- Guttman, D. S., and Greenberg, J. T. 2001. Functional analysis of the type III effectors AvrRpt2 and AvrRpm1 of Pseudomonas syringae with the use of a single-copy genomic integration system. Mol. Plant. Microbe. Interact. 14:145–155.
- Haney, C. H., Samuel, B. S., Bush, J., and Ausubel, F. M. 2015. Associations with rhizosphere bacteria can confer an adaptive advantage to plants. Nat. Plants. 1:15051.
- Haswell, E. S., and Meyerowitz, E. M. 2006. MscS-like proteins control plastid size and shape in Arabidopsis thaliana. Curr. Biol. 16:1–11.
- Hilker, M., Schwachtje, J., Baier, M., Balazadeh, S., Bäurle, I., Geiselhardt, S., Hincha, D. K., Kunze, R., Mueller-Roeber, B., Rillig, M. C., Rolff, J., Romeis, T., Schmülling, T., Steppuhn, A., van Dongen, J., Whitcomb, S. J., Wurst, S., Zuther, E., and Kopka, J. 2016. Priming and memory of stress responses in organisms lacking a nervous system. Biol. Rev. Camb. Philos. Soc. 91:1118–1133.
- Hruz, T., Laule, O., Szabo, G., Wessendorp, F., Bleuler, S., Oertle, L., Widmayer, P., Gruissem, W., and Zimmermann, P. 2008. Genevestigator v3: a reference expression database for the meta-analysis of transcriptomes. Adv. Bioinformatics. 2008:420747.
- Jalmi, S. K., and Sinha, A. K. 2015. ROS mediated MAPK signaling in abiotic and biotic stress- striking similarities and differences. Front. Plant Sci. 6:769.
- Jia, W., Li, B., Li, S., Liang, Y., Wu, X., Ma, M., Wang, J., Gao, J., Cai, Y., Zhang, Y., Wang, Y. Y., Li, J., and Wang, Y. Y. 2016. Mitogen-Activated Protein Kinase Cascade MKK7-MPK6 Plays Important Roles in Plant Development and Regulates Shoot Branching by Phosphorylating PIN1 in Arabidopsis. PLoS Biol. 14:e1002550.
- Jung, H. W., Tschaplinski, T. J., Wang, L., Glazebrook, J., and Greenberg, J. T. 2009. Priming in systemic plant immunity. Science. 324:89–91.
- Kovtun, Y., Chiu, W. L., Tena, G., and Sheen, J. 2000. Functional analysis of oxidative stress-activated mitogen-activated protein kinase cascade in plants. Proc Natl Acad Sci U S A. 97:2940–2945.
- Kutschera, U., and Niklas, K. J. 2009. Evolutionary plant physiology: Charles Darwin's forgotten synthesis. Naturwissenschaften. 96:1339–1354.
- León Morcillo, R. J., Ocampo, J. a, and García Garrido, J. M. 2012. Plant 9-lox oxylipin metabolism in response to arbuscular mycorrhiza. Plant Signal. Behav. 7:1584–1588.
- Li, Y., Tschaplinski, T. J., Engle, N. L., Hamilton, C. Y., Rodriguez, M., Liao, J. C., Schadt, C. W., Guss, A. M., Yang, Y., and Graham, D. E. 2012. Combined inactivation of the Clostridium cellulolyticum lactate and malate dehydrogenase genes substantially increases ethanol yield from cellulose and switchgrass fermentations. Biotechnol. Biofuels. 5:2.
- Lim, G.-H., Shine, M. B., de Lorenzo, L., Yu, K., Cui, W., Navarre, D., Hunt, A. G., Lee, J.-Y., Kachroo, A., and Kachroo, P. 2016. Plasmodesmata Localizing Proteins Regulate Transport and Signaling during Systemic Acquired Immunity in Plants. Cell Host Microbe. 19:541–549.
- Lisec, J., Schauer, N., Kopka, J., Willmitzer, L., and Fernie, A. R. 2006. Gas chromatography mass spectrometry-based metabolite profiling in plants. Nat. Protoc. 1:387–396.

- Liu, Y., and Zhang, S. 2004. Phosphorylation of 1-aminocyclopropane-1-carboxylic acid synthase by MPK6, a stress-responsive mitogen-activated protein kinase, induces ethylene biosynthesis in Arabidopsis. Plant Cell. 16:3386–3399.
- Martinez-Medina, A., Flors, V., Heil, M., Mauch-Mani, B., Pieterse, C. M. J., Pozo, M. J., Ton, J., van Dam, N. M., and Conrath, U. 2016. Recognizing Plant Defense Priming. Trends Plant Sci. 21:818–822.
- Mishina, T. E., and Zeier, J. 2007. Pathogen-associated molecular pattern recognition rather than development of tissue necrosis contributes to bacterial induction of systemic acquired resistance in Arabidopsis. Plant J. 50:500–513.
- Mukhtarova, L. S., Mukhitova, F. K., Gogolev, Y. V, and Grechkin, A. N. 2011. Hydroperoxide lyase cascade in pea seedlings: Non-volatile oxylipins and their age and stress dependent alterations. Phytochemistry. 72:356–364.
- Müller, J., Beck, M., Mettbach, U., Komis, G., Hause, G., Menzel, D., and Šamaj, J. 2010. Arabidopsis MPK6 is involved in cell division plane control during early root development, and localizes to the pre-prophase band, phragmoplast, trans-Golgi network and plasma membrane. Plant J. 61:234–248.
- Nalam, V. J., Keereetaweep, J., and Shah, J. 2013. The green peach aphid, Myzus persicae, acquires a LIPOXYGENASE5-derived oxylipin from Arabidopsis thaliana, which promotes colonization of the host plant. Plant Signal. Behav. 8:e22735.
- Nalam, V. J., Keeretaweep, J., Sarowar, S., and Shah, J. 2012. Root-derived oxylipins promote green peach aphid performance on Arabidopsis foliage. Plant Cell. 24:1643–1653.
- Nandi, A., Welti, R., and Shah, J. 2004. The Arabidopsis thaliana dihydroxyacetone phosphate reductase gene SUPPRESSOR OF FATTY ACID DESATURASE DEFICIENCY1 is required for glycerolipid metabolism and for the activation of systemic acquired resistance. Plant Cell Online. 16:465–477.
- Návarová, H., Bernsdorff, F., Döring, A.-C., and Zeier, J. 2012. Pipecolic acid, an endogenous mediator of defense amplification and priming, is a critical regulator of inducible plant immunity. Plant Cell. 24:5123–141.
- Ortiz-Castro, R., Díaz-Pérez, C., Martínez-Trujillo, M., del Río, R. E., Campos-García, J., and López-Bucio, J. 2011. Transkingdom signaling based on bacterial cyclodipeptides with auxin activity in plants. Proc. Natl. Acad. Sci. U. S. A. 108:7253–7258.
- Park, S.-W. S.-W., Kaimoyo, E., Kumar, D., Mosher, S., and Klessig, D. F. 2007. Methyl Salicylate Is a Critical Mobile Signal for Plant Systemic Acquired Resistance. Science. 318:113–116
- Parker, J. E. 2009. The quest for long-distance signals in plant systemic immunity. Sci. Signal. 2:pe31.
- Pieterse, C. M. J., Zamioudis, C., Berendsen, R. L., Weller, D. M., van Wees, S. C. M., and Bakker, P. a H. M. 2014. Induced Systemic Resistance by Beneficial Microbes. Annu. Rev. Phytopathol. 52:347–375.
- Pieterse, C. M., van Wees, S. C., Hoffland, E., van Pelt, J. A., and van Loon, L. C. 1996.

Systemic resistance in Arabidopsis induced by biocontrol bacteria is independent of salicylic acid accumulation and pathogenesis-related gene expression. Plant Cell. 8:1225–1237.

- Pitzschke, A., Datta, S., and Persak, H. 2014. Salt stress in Arabidopsis: lipid transfer protein AZI1 and its control by mitogen-activated protein kinase MPK3. Mol. Plant. 7:722–738.
- Pozo, M. J., Van Der Ent, S., Van Loon, L. C., and Pieterse, C. M. J. 2008. Transcription factor MYC2 is involved in priming for enhanced defense during rhizobacteria-induced systemic resistance in Arabidopsis thaliana. New Phytol. 180:511–523.
- Prost, I., Dhondt, S., Rothe, G., Vicente, J., Rodriguez, M. J., Kift, N., Carbonne, F., Griffiths, G., Esquerré-Tugayé, M.-T., Rosahl, S., Castresana, C., Hamberg, M., and Fournier, J. 2005. Evaluation of the antimicrobial activities of plant oxylipins supports their involvement in defense against pathogens. Plant Physiol. 139:1902–1913.
- Riedlmeier, M., Ghirardo, A., Wenig, M., Knappe, C., Koch, K., Georgii, E., Dey, S., Parker, J. E., Schnitzler, J.-P., and Vlot, A. C. 2017. Monoterpenes support systemic acquired resistance within and between plants. Plant Cell. 29:1440–1459.
- Shah, J. 2009. Plants under attack: systemic signals in defence. Curr. Opin. Plant Biol. 12:459–464.
- Sidonskaya, E., Schweighofer, A., Shubchynskyy, V., Kammerhofer, N., Hofmann, J., Wieczorek, K., and Meskiene, I. 2016. Plant resistance against the parasitic nematode Heterodera schachtii is mediated by MPK3 and MPK6 kinases, which are controlled by the MAPK phosphatase AP2C1 in Arabidopsis. J. Exp. Bot. 67:107–118.
- Spaepen, S., Bossuyt, S., Engelen, K., Marchal, K., and Vanderleyden, J. 2014. Phenotypical and molecular responses of Arabidopsis thaliana roots as a result of inoculation with the auxin-producing bacterium Azospirillum brasilense. New Phytol. 201:850–861.
- Spoel, S. H., and Dong, X. 2012. How do plants achieve immunity? Defence without specialized immune cells. Nat. Rev. Immunol. 12:89–100.
- Stringlis, I. A., Proietti, S., Hickman, R., Van Verk, M. C., Zamioudis, C., and Pieterse, C. M. J. 2017. Root transcriptional dynamics induced by beneficial rhizobacteria and microbial immune elicitors reveal signatures of adaptation to mutualists. Plant J. 140:874–888.
- Tschaplinski, T. J., Standaert, R. F., Engle, N. L., Martin, M. Z., Sangha, A. K., Parks, J. M., Smith, J. C., Samuel, R., Jiang, N., Pu, Y., Ragauskas, A. J., Hamilton, C. Y., Fu, C., Wang, Z.-Y., Davison, B. H., Dixon, R. A., and Mielenz, J. R. 2012. Down-regulation of the caffeic acid O-methyltransferase gene in switchgrass reveals a novel monolignol analog. Biotechnol. Biofuels. 5:71.
- Truman, W., Bennett, M. H., Kubigsteltig, I., Turnbull, C., and Grant, M. 2007. Arabidopsis systemic immunity uses conserved defense signaling pathways and is mediated by jasmonates. Proc. Natl. Acad. Sci. U. S. A. 104:1075–1080.
- Vellosillo, T., Martínez, M., López, M. A., Vicente, J., Cascón, T., Dolan, L., Hamberg, M., and Castresana, C. 2007. Oxylipins produced by the 9-lipoxygenase pathway in Arabidopsis regulate lateral root development and defense responses through a specific signaling cascade. Plant Cell. 19:831–846.

- Vicente, J., Cascón, T., Vicedo, B., García-Agustín, P., Hamberg, M., and Castresana, C. 2012. Role of 9-lipoxygenase and α-dioxygenase oxylipin pathways as modulators of local and systemic defense. Mol. Plant. 5:914–928.
- Wang, H., Ngwenyama, N., Liu, Y., Walker, J. C., and Zhang, S. 2007. Stomatal development and patterning are regulated by environmentally responsive mitogen-activated protein kinases in Arabidopsis. Plant Cell. 19:63–73.
- Wittek, F., Hoffmann, T., Kanawati, B., Bichlmeier, M., Knappe, C., Wenig, M., Schmitt-Kopplin, P., Parker, J. E., Schwab, W., and Corina Vlot, A. 2014. Arabidopsis ENHANCED DISEASE SUSCEPTIBILITY1 promotes systemic acquired resistance via azelaic acid and its precursor 9-oxo nonanoic acid. J. Exp. Bot. 65:5919–5931.
- Xu, D., Huang, X., Xu, Z.-Q., and Schläppi, M. 2011. The HyPRP gene EARLI1 has an auxiliary role for germinability and early seedling development under low temperature and salt stress conditions in Arabidopsis thaliana. Planta. 234:565–577.
- Yu, K., Soares, J. M., Mandal, M. K., Wang, C., Chanda, B., Gifford, A. N., Fowler, J. S., Navarre, D., Kachroo, A., and Kachroo, P. 2013. A Feedback Regulatory Loop between G3P and Lipid Transfer Proteins DIR1 and AZI1 Mediates Azelaic-Acid-Induced Systemic Immunity. Cell Rep. 3:1266–1278.
- Zamioudis, C., Mastranesti, P., Dhonukshe, P., Blilou, I., and Pieterse, C. M. J. 2013. Unraveling root developmental programs initiated by beneficial Pseudomonas spp. bacteria. Plant Physiol. 162:304–318.
- Zhang, Y., and Schläppi, M. 2007. Cold responsive EARLI1 type HyPRPs improve freezing survival of yeast cells and form higher order complexes in plants. Planta. 227:233–43.
- Zoeller, M., Stingl, N., Krischke, M., Fekete, A., Waller, F., Berger, S., and Mueller, M. J. 2012. Lipid profiling of the Arabidopsis hypersensitive response reveals specific lipid peroxidation and fragmentation processes: biogenesis of pimelic and azelaic acid. Plant Physiol. 160:365–378.

Table 1. Root uptake and transport of [^{2}H]azelaic acid in WT (Col-0), *azi1-1* and *earli1-1* plants.

		AZA (mean ± SD)	**[^{2}H]-AZA** (mean ± SD)
shoot	Col-0	0.21^a ± 0.027	ND
	azi1-1	0.21^a ± 0.028	ND
	earli1-1	0.16^a ± 0.011	ND
root	Col-0	6.96^b ± 2.68	24.31^c ± 8.60
	azi1-1	7.14^b ± 2.23	23.4^c ± 5.62
	earli1-1	7.69^b ± 1.71	20.11^c ± 4.24

Amount (µg/g fresh weight) of azelaic acid (AZA) or [^{2}H]azelaic acid ([^{2}H]-AZA) in shoot or root tissues 1 d after application of 1 mM of [^{2}H]-AZA to roots of 14 day old plants.

Different superscript letters indicate statistically significant differences ($P<0.01$, analysis of variance (ANOVA), post hoc Tukey's HSD test).

SD = standard error from six biological replicates (each one with ~20 seedlings).

ND = not detected.

Supplementary Figure 2.1 AZI1 root-subcellular localization in Arabidopsis

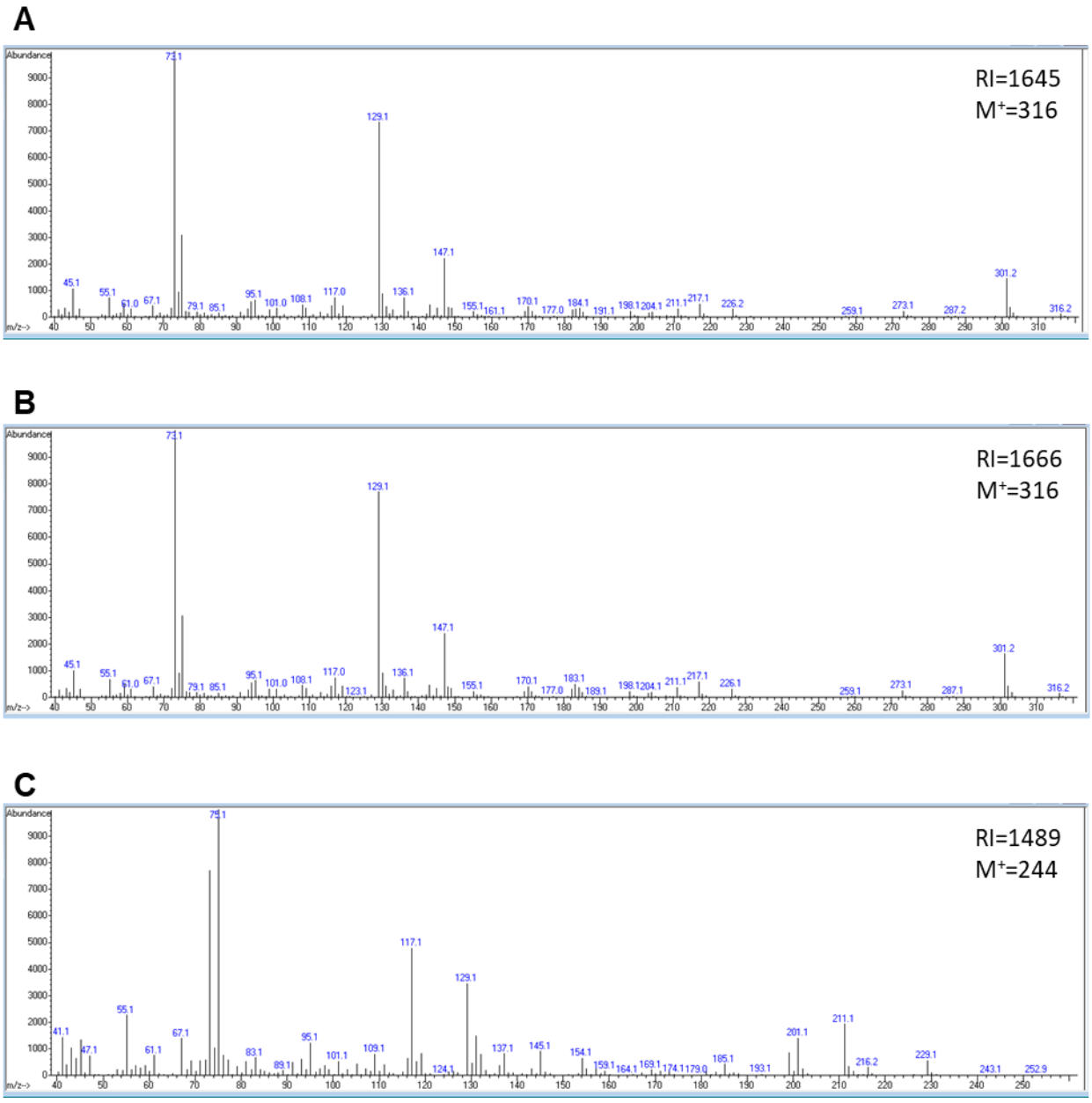

Supplementary Figure 2.1. AZI1 root-subcellular localization in Arabidopsis
Electron impact ionization (70 eV) fragmentation patterns of trimethylsilyl (TMS) derivatized 9-oxononanoic acid (ONA), including (**A**) 2 TMS peak A, (**B**) 2 TMS peak B, and (**C**) 1 TMS peak (silylated only on the carboxyl group). The Kovats retention index (RI) and the molecular ion (M^+) are included for each peak.

CHAPTER 3

KINASES AND PROTEIN MOTIFS REQUIRED FOR AZI1 PLASTID LOCALIZATION AND TRAFFICKING DURING PLANT DEFENSE INDUCTION

Preface

This chapter includes a paper published from collaborative work completed under the supervision of Professor Jean Greenberg (DOI: 10.1111/tpj.15137). The article is included as-published with permission from the publishers. I co-authored this work with Dr. Nicolas Cecchini. My contributions to the project are as follows:

Prior to my rotation with Jean Greenberg as a 1st year PhD student, I performed a literature review and discovered a potential relationship between the kinase MPK3 and AZI1. During my rotation, I used two-phase partitioning on a percoll gradient to fractionate leaf tissues into plastid and total leaf extracts. Upon probing these extracts, I confirmed a relationship between active MPK3 and the accumulation of AZI1 at plastids and hypothesized that MPK3 might regulate AZI1's subcellular targeting during defense signaling (Fig. 4e).

Based on its degree of hydrophobicity and similarity to signal anchor transmembrane peptides, I hypothesized that AZI1's N-terminal hydrophobic domain was essential for plastid targeting similar to the PRR (Chapter 1, 1.2). I optimized a two-phase total leaf partitioning protocol to characterize the contribution of various regions of AZI1's N-terminal targeting signal in driving plastid association (Fig. 2D and E). I also optimized protocols for the assessment of plastid enrichment and contamination (Fig. 2D-F). Finally, I identified the association with non-signal anchor variants of AZI1 with plastid membranes (Fig. 2E).

Although the results were preliminary and unpublished, I troubleshot new methods of treating leaves with pathogen molecular patterns to induce the accumulation of AZI1/EARLI1 in plastids as in Fig. 4A and B.

To help determine if MPK3/MPK6 co-localized with AZI1/EARLI1 *in vivo* transiently expressed RFP fusion constructs of each protein in tobacco leaves, I then performed an anti-RFP western blot to confirm the fusion proteins were still largely intact (Fig. 6C and D).

Dr. Cecchini wrote the first draft of the manuscript. I revised and edited the manuscript in collaboration with Dr. Cecchini and Dr. Greenberg. After receiving the reviewer's comments, I regularly communicated with Dr. Cecchini and I wrote the first draft of the response to the reviewers. I also revised the manuscript and cover letter in collaboration with Dr. Cecchini and Dr. Greenberg.

TITLE

"Kinases and protein motifs required for AZI1 plastid localization and trafficking during plant defense induction"

Nicolás M. Cecchini[1,2#], DeQuantarius J. Speed[1#], Suruchi Roychoudhry[1,3], Jean T. Greenberg[1]*

[1]Department of Molecular Genetics and Cell Biology, The University of Chicago, 929 East 57th Street GCIS 524W, Chicago, IL 60637, USA. [2]Current address: Centro de Investigaciones en Química Biológica de Córdoba (CIQUIBIC-CONICET) and Departamento de Química Biológica Ranwel Caputto, Facultad de Ciencias Químicas, Universidad Nacional de Córdoba, Haya de la Torre y Medina Allende - Ciudad Universitaria, Córdoba, X5000HUA, Argentina. [3]Current address: Centre for Plant Sciences, University of Leeds, Leeds LS2 9JT, UK.

* To whom correspondence should be addressed.

e-mail: jgreenbe@uchicago.edu

[#] These authors contributed equally to this work.

RUNNING TITLE

Signal-anchored AZI1 targets plastids via PRR/MPK

SIGNIFICANCE STATEMENT

In this work, we studied how AZI1, a key factor for plant systemic immunity, localizes to plastids. We show that AZI1 belongs to a unique class of signal-anchored proteins and that the defense-associated kinases MPK3/6 affect its targeting/trafficking, which in turn might determine the magnitude of systemic movement of defense signal(s) for resistance and priming induction.

SUMMARY

The proper subcellular localization of defense factors is an important part of the plant immune system. A key component for systemic resistance, lipid transfer protein (LTP)-like AZI1, is needed for the systemic movement of the priming signal azelaic acid (AZA) and a pool of AZI1 exists at the site of AZA production, the plastid envelope. Moreover, after systemic defense-triggering infections, the proportion of AZI1 localized to plastids increases. However, AZI1 does not possess a classical plastid transit peptide that can explain its localization. Instead, AZI1 uses a bipartite N-terminal signature that allows for its plastid targeting. Furthermore, the kinases MPK3 and MPK6, associated with systemic immunity, promote the accumulation of AZI1 at plastids during priming induction. Our results indicate the existence of a mode of plastid targeting possibly related to defense responses.

INTRODUCTION

Plants have an innate, non-adaptive, immune system based on the ability to recognize non-self-molecules (Spoel and Dong, 2012). Pathogen recognition depends largely on two types of proteins: pattern recognition receptors that reside on the plasma membrane and perceive microbe-

associated molecular patterns (MAMPs; e.g. flg22 peptide, derived from bacterial flagellin) (Macho and Zipfel, 2014), and intracellular resistance proteins (R proteins), receptors that recognize specific effector proteins, or the effector-induced alterations on their targets, that are injected by pathogenic microbes to promote virulence (Jones and Dangl, 2006; Cesari, 2018). After pathogen recognition, plants trigger local defense responses, such as reactive oxygen species accumulation, callose depositions and the activation of key signaling kinases, including MPK3 and MPK6 (MPK3/6) (Gómez-Gómez and Boller, 2000; Chinchilla *et al.*, 2006; Boller and Felix, 2009; Schwessinger *et al.*, 2011). Additionally, pathogen infections can also induce long-lasting and broad-spectrum systemic resistance (Fu and Dong, 2013; Pieterse *et al.*, 2014). Depending on the plant tissue involved in the initial recognition, different types of systemic resistance programs are established. Aerial tissues induce systemic acquired resistance (SAR) (Fu and Dong, 2013), whereas roots trigger the so-called induced systemic resistance (ISR) that extends to the aerial tissue (Pieterse *et al.*, 2014). In addition, when a MAMP(s) is/are perceived, it can also induce systemic resistance termed MAMP-triggered SAR (mSAR) (Mishina and Zeier, 2007; Cecchini *et al.*, 2015b).

Systemic immunity programs are typically characterized by an alert or "primed" state, which allows the plant to efficiently reactivate its defenses (more rapidly and/or strongly) against a subsequent pathogen attack (Jung *et al.*, 2009; Parker, 2009; Conrath *et al.*, 2015; Martinez-Medina *et al.*, 2016). For the establishment of systemic immunity after microbial recognition, the local production of one or more signal molecules capable of moving to distal tissues and priming defenses is needed. Several systemic signals have been described and many appear to be acting together during different systemic resistance programs (Park *et al.*, 2007; Truman *et al.*, 2007; Jung *et al.*, 2009; Chanda *et al.*, 2011; Chaturvedi *et al.*, 2012; Návarová *et al.*, 2012;; Wittek *et*

al., 2014; Chen et al. 2018). One of those signals is the lipid-derived azelaic acid (AZA). AZA is locally generated in plastid envelopes and possibly thylakoid membranes and moves from local leaves to the systemic tissues (Ren et al., 2008; Jung *et al.*, 2009; Zoeller *et al.*, 2012; Yu *et al.*, 2013; Gao *et al.*, 2014; Cecchini *et al.*, 2015b). AZA can induce a primed state when exogenously applied to aerial tissues (Jung *et al.*, 2009; Cecchini *et al.*, 2015b). A key component shared between SAR, ISR and mSAR programs and the associated priming, is the lipid transfer protein (LTP)-like AZI1 (AZELAIC ACID INDUCED 1), and its close paralog EARLI1 (EARLY ARABIDOPSIS ALUMINUM INDUCED 1) (Jung *et al.*, 2009; Cecchini *et al.*, 2015b). AZI1 is required for the systemic movement of AZA specifically affecting systemic, but not local disease resistance (Cecchini *et al.*, 2015b). Remarkably, AZI1 is also needed for the action of other proposed systemic defense signals glycerol-3-phosphate, dehydroabietinal and pinene-monoterpenes (Chaturvedi *et al.*, 2012; Yu *et al.*, 2013; Riedlmeier *et al.*, 2017). Proteins proposed to posttranslationally alter AZI1 are MPK3/6, which can phosphorylate AZI1 *in vitro* (Pitzschke *et al.*, 2014); these kinases have prominent roles in SAR, ISR and defense priming induced by AZA (Beckers *et al.*, 2009; Cecchini *et al.*, 2019).

AZI1 is a membrane protein and a pool of it, together with EARLI1, exists near the site of AZA production, the plastid outer envelope membrane (Zoeller *et al.*, 2012; Cecchini *et al.*, 2015b). AZI1 also localizes to the endoplasmic reticulum (ER), plasma membrane (PM) and plasmodesmata (Cecchini *et al.*, 2015b; Lim *et al.*, 2016). It was proposed that AZI1 forms part of membrane contact site complexes between plastids and ER membranes, allowing the non-vesicular transport of AZA and possibly other non-polar signals to systemic tissues (Cecchini *et al.*, 2015b). After SAR-triggering infections, AZI1/EARLI1 becomes highly enriched at plastid envelopes, which suggests that plastid targeting is critical for AZI1/EARLI1's role in signaling (Cecchini *et*

al., 2015b). However, AZI1 and EARLI1 do not possess a "classical" predicted or known signal sequence/motif that can explain their localization. AZI1 motifs can be divided into an amino terminal hydrophobic domain (HD, which is also a putative signal peptide (SP)), a central proline-rich region (PRR) with unknown function, and a C-terminal LTP domain (8 cysteine motif; 8CM) predicted to bind lipids (Figure 3.1a). Proteins like AZI1 that have a PRR plus an 8CM domain are considered "Hybrid Proline Rich Proteins" (HyPRPs) (Dvoráková *et al.*, 2007). Previously, it was suggested that AZI1 employs an undescribed N-terminal bipartite signal (SP+PRR) that drives its plastid targeting (Cecchini *et al.*, 2015b).

Although many proteins that are localized to plastids show no recognizable signals, plastid targeting mechanisms for nuclear-encoded proteins have been defined to some extent and can be divided into three groups: 1) targeted proteins with cleavable transit peptides or pre-sequences that are recognized in the plastid envelope and then imported to the stroma, thylakoids or move back to inner or outer envelopes (Lee *et al.*, 2017); 2) proteins with no cleavable signal where a transmembrane domain (TMD) acts as a targeting signal and anchors them to outer envelope membrane (Kim and Hwang, 2013); 3) and the (less understood) plastidic β-barrel proteins in which the secondary/tertiary structures constitute the organelle targeting region (Lee *et al.*, 2014). In addition, TMD-driven plastid proteins can be separated into tail-anchored (C-terminal region TMD) or signal anchored (N-terminal region TMD) (Kim and Hwang, 2013). Signal-anchored proteins are flanked by a charged positive region (CPR), usually containing at least three basic residues, important for the targeting as an ER import evading signal (Waizenegger *et al.*, 2003; Lee *et al.*, 2011). It was proposed that the degree of hydrophobicity of the TMD determines whether the region will anchor to plastid, mitochondria or ER membranes. Although there is a degree of overlap, signal-anchored proteins in which the TMDs show a Wimley and White

Figure 3.1 Membrane association of AZI1's N-terminal region

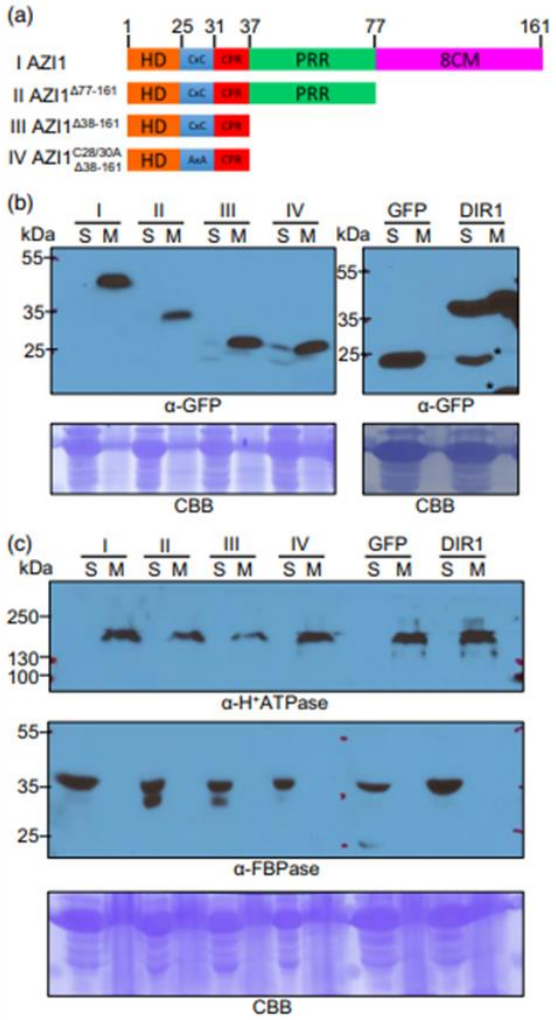

Figure 3.1. Membrane association of AZI1's N-terminal region
(a) Scheme of AZI1 deletion variants used in (b). Amino acid positions delimiting different AZI1 domains are shown in the upper part. Different variants are identified with roman numerals (left side). In AZI1 variant IV, both acylation sites were replaced by alanine (C28/30A). HD: hydrophobic domain / predicted signal peptide, similar to signal peptide, possible transmembrane domain; CxC: possible acylation sites; CPR: positively charged region; PRR: proline-rich region; 8CM: lipid transfer domain (8-cysteine motif). (b) Western blots of microsomal membrane (M) and soluble (S) protein fractions from N. benthamiana expressing GFP alone or fused to AZI1 variants (a) or DIR1:GFP. Bands were revealed using anti-GFP antibody. Similar results were observed in three independent experiments. (c) Western blots of microsomal membrane (M) and soluble (S) protein fractions samples used in (b). Bands were revealed using anti-H+ATPase and anti-FBP antibodies as an integral membrane protein and cytosolic markers, respectively. The blots in (b) and (c) stained with Coomassie blue (CBB) are presented to show loading. The asterisks indicate possible cleavage products.

hydrophobicity score >0.4 mainly target the ER, whereas those with lower values mainly target plastids and/or mitochondria (Lee *et al.*, 2011; Lee *et al.*, 2014).

Here, we characterized AZI1 motifs in relation to their impact on subcellular targeting (with a focus on plastids) and identified pathogen defense components that modulate AZI1 localization. We report that specific features of the AZI1 amino terminus and the defense-associated kinases MPK3/6 mediate AZI1-plastid targeting and/or intracellular trafficking. Our results suggest the existence of a mechanism of plastid targeting and trafficking that is active during defense responses against pathogens.

RESULTS

AZI1 is a signal-anchored protein

The TargetP algorithm (Emanuelsson *et al.*, 2007) predicts that AZI1's hydrophobic amino terminus is a signal peptide. However, since AZI1 strongly associates with membranes (Cecchini *et al.*, 2015b), this domain might be a non-cleavable TMD anchor, as has been shown for many signal-anchored proteins (Figure 3.1a I) (Jayasinghe *et al.*, 2001; Kim and Hwang, 2013). In support of this idea, amino acids 31 to 37 (KPSPKPK) in AZI1's amino terminus constitute a charged protein region (CPR) that is characteristic of signal-anchored proteins (Figure 3.1a I).

To further analyze the possibility that AZI1's N-terminal region (AZI1$^{\Delta 38\text{-}161}$ containing the HD+CPR) functions as a signal anchor, we tested if it was sufficient to confer membrane association. We generated a construct where AZI1$^{\Delta 38\text{-}161}$ was fused to a GFP construct (Figure 3.1a III) and analyzed its localization by fractionation. AZI1 fused to GFP was previously shown to retain function (Cecchini *et al.*, 2015b). Microsomal and soluble fractions were obtained from

agroinfiltrated *Nicotiana benthamiana* leaves and examined by immunoblot. A large pool of the AZI1$^{\Delta 38\text{-}161}$:GFP fusion protein was found in the microsomal fraction (M), with only traces present in the soluble fraction (S) (Figure 3.1b III). Because AZI1 also possesses two possible acylation sites after the HD (C28/C30; CSS-Palm 2.0; (Ren *et al.*, 2008)) that could relate to its microsomal localization, we repeated the analysis using a second construct with these residues mutated (cysteines to alanines, CxC→AxA) (Figure 3.1a IV). Figure 3.1b IV shows that this variant also largely partitioned with the microsomal fraction, indicating that these sites do not significantly affect membrane localization. As previously shown, full length AZI1 or AZI1 without the LTP domain (8CM) also localized to microsomal fractions (Figure 3.1b I and II) (Cecchini *et al.*, 2015b). As controls, the soluble GFP and the soluble/microsomal DIR1:GFP constructs showed the expected fractionation patterns indicating that we can detect transiently expressed proteins located to the soluble and membrane fractions of *N. benthamiana* (Figure 3.1b, right panel) (Cecchini *et al.*, 2015b). In addition, the distribution of markers for microsomal and soluble fractions, H^+ATPase and FBPase, respectively, indicated that the fractionation worked as anticipated (Figure 3.1c).

Together, these results strongly suggest that the N-terminal 37 amino acids that include AZI1's putative SP (the HD region in Figure 3.1) are sufficient to confer membrane anchoring, indicating that AZI1 is a signal-anchored protein.

The PRR and TMD are required for the normal pattern of AZI1 plastid envelope targeting

Most signal-anchored proteins targeted to plastid envelopes (or mitochondria) have an N-terminal TMD Wimley and White hydrophobicity score below 0.4 (Lee *et al.*, 2011). In contrast, AZI1's HD displays a 0.58 score, indicative of an ER membrane resident signal-anchored protein

(MPEx software 3.2, amino acids 8 to 26, http://blanco.biomol.uci.edu/mpex/index.html; (Jayasinghe *et al.*, 2001; Kim and Hwang, 2013)). Thus, to determine whether other domain/motifs are required for AZI1 plastid outer envelope membrane targeting, we generated AZI1 variants for each one (Figure 3.2a) and fused them to GFP or an HA tag.

To test the subcellular localization of AZI1-GFP variants, we imaged agrotransformed *N. benthamiana* leaves by confocal microscopy. The deletions of the PRR motif (AAs 38-77), or CPR+PRR (AAs 32-77) and CxC+CPR+PRR (AAs 26-77) regions, abolished AZI1's plastid targeting (Figure 3.2b, compare I and II to V, VI and VII). Quantitation of the GFP fluorescence showed a significant decrease in GFP signal localized to plastid upon deletion of these regions (Figure 3.2c I, II, V, VI, and VII). Consistent with our previous work (Cecchini et al, 2015b), fractionation confirmed the loss of plastid targeting for PRR deletion variants V and VI; quantitation of chlorophyll and immunoblot analysis of BiP2 indicates that chloroplast enrichment was successful without significant ER contamination (Figure 3.2d). In contrast, plastid location was largely retained in AZI1 variants upon the loss of the CPR region or putative acylation sites (Figure 3.2b-d I, VIII, and IX). Though non-essential, the CPR may weakly affect plastid targeting (Figure 3.2c VIII). We also performed microscopy on two AZI1 versions fused to GFP where the HD or the HD plus the following acylation sites were deleted (Figure 3.2a, X and XI). Neither variant displayed AZI1's characteristic ring-like localization around plastids or clear ER or plasma membrane localization sites (Figure 3.2b X and XI). Instead, both the AZI1$^{\Delta 2\text{-}25}$:GFP (X) and AZI1$^{\Delta 2\text{-}30}$:GFP (XI) fluorescence signal displayed a filamentous pattern as if associated with actin filaments or microtubules (Figure 3.2b, X and XI). Surprisingly, even though neither variant displayed AZI1's ring-like localization around plastids, fractionation revealed that both variants X

Figure 3.2 Membrane association of AZI1's N-terminal region

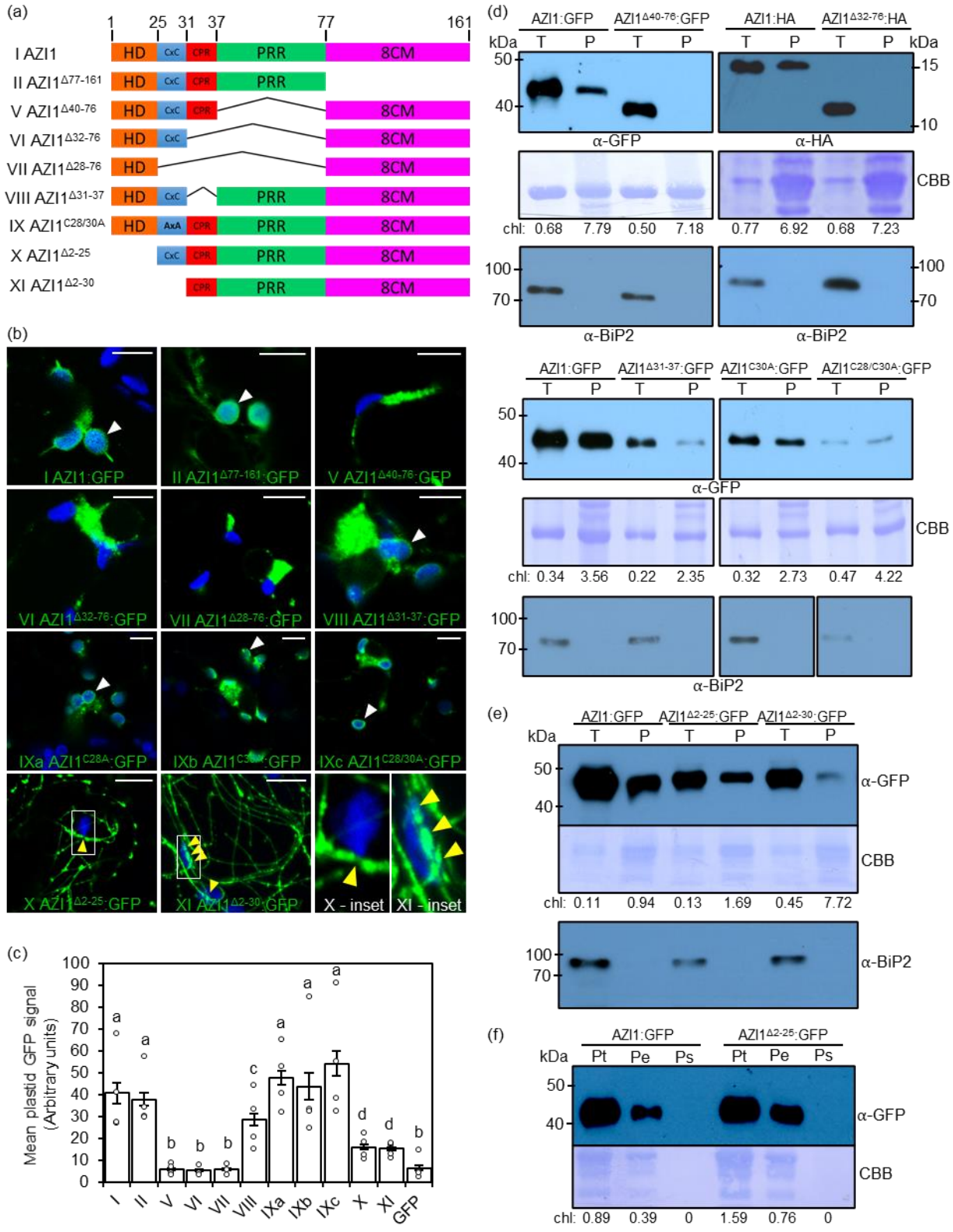

Figure 3.2. AZI1 protein regions required for its plastid targeting
(a) Scheme of AZI1 deletion and mutant variants used for the localization pattern analysis in (b) and subcellular fractionation in (d). Amino acids positions delimiting AZI1 domains are shown in the upper part. Different variants are identified with roman numerals (left). See Figure 1a for the definitions of each region. (b) Laser scanning confocal microscopy micrographs showing localization of GFP-tagged AZI1 variants (a) expressed in N. benthamiana. AZI1 variant IX includes different AZI1 versions where acylation sites were replaced by alanine (version IXa:C28A, IXb:C30A, IXc: C28/30A). AZI1 variants X and XI inset panel (at bottom-right position) shows a close up of the filamentous signal overlapping ("touching") with plastid autofluorescence. White arrowheads indicate GFP fluorescence in plastid envelopes (note the rings of GFP signal in green that surround autofluorescent plastids in blue in the micrographs). Yellow arrowheads indicate filamentous GFP signal overlapping plastid autofluorescence. Bar = 10 μm. (c) Quantification of mean GFP signal intensity of AZI1 and its variant constructs within the plastids. The GFP signal intensity from 20-25 plastids was quantified for each construct, from 4-5 independent imaging experiments. The bars represent standard errors of means of these values. Individual data points are shown on the bar chart as scatter-dots. (d-f) Western blots of plastid (P) and total (T) fractions and total (Pt), envelope (Pe) and soluble (Ps) plastid subfractions from N. benthamiana expressing GFP- or HA-tagged AZI1 or AZI1 deletion and mutation variants. Bands were revealed using anti-GFP or anti-HA antibody as indicated. Asterisks indicate unspecific bands. The blot stained with Coomassie blue (CBB) is presented to show loading. 7-10 ug of protein were loaded on blots probed with anti-GFP antibody and 30 ug of protein were loaded on the blot probed with anti-HA antibody. Chlorophyll amount (μg) is shown for each fraction to indicate the plastid enrichment. Similar results were observed in two or more independent experiments. Western blots of the same total and plastid extracts were also probed with anti-BiP2 to assess the level of ER contamination in plastid fractions. For the blots containing variants VIII, IXb, and IXc, the lanes containing the size marker between variants were cropped from the images. For the panels displaying variants VIII, IXb, and IXc, the anti-GFP and anti-BiP2 blots were yielded from separate SDS-PAGE gels.

and XI associate with plastids (Figure 3.2e). Further partitioning of plastids into membrane and soluble fractions indicates that variant X is plastid-membrane associated (Figure 3.2f). Close inspection of the confocal micrographs supports the fractionation results, as there were points of contact between GFP filaments and plastids (Figure 3.2b, X and XI yellow arrowheads, and X and XI insets at bottom-right panel). This was also observed in the GFP fluorescence quantitation when compared to control GFP (Figure 3.2c X and XI). We noted that variants X and XI were similar in apparent mass to AZI1 (Figure 3.2e). It is possible that the higher percentage of proline residues in AZI1 variants relative to AZI1 causes anomalous migration patterns during SDS-PAGE similar to what has been previously described for other proline-rich proteins (Hames, 1998). Alternatively,

higher than expected migration may be due to extra posttranslational modifications related to the formation into filaments of variants X and XI.

These results corroborate our earlier observations about the importance of the PRR for plastid targeting (Cecchini *et al.*, 2015b). Furthermore, they show that the HD/TMD is required for the normal ring-like pattern of plastid membrane association. Together, they indicate that the motifs required for full AZI1 plastid outer envelope membrane targeting are the HD/TMD plus the PRR (Table S3.1), suggesting a bipartite signal-anchored protein targeting mechanism.

Loss of the TMD causes AZI1 to stably associate with microtubules

The fluorescence patterns of AZI1-GFP variants that lack the TMD showed strong similarities to microtubules (MTs) and/or actin filaments (AFs) (Figure 3.2b X and XI; Kang *et al.*, 2014; Kumar *et al.*, 2018). Therefore, we investigated the effects of Oryzalin (Ozn) and Latrunculin B (LatB), MT and AF inhibitors, respectively, on the AZI1$^{\Delta 2\text{-}30}$:GFP filamentous pattern. As Figure 3.3a (left panel) shows, Ozn but not LatB treatment vastly reduced AZI1$^{\Delta 2\text{-}30}$:GFP filaments compared with mock treatment. The effectiveness controls for the inhibitors, on MT-targeted (RFP-TUB6) and actin-targeted (LifeAct) markers, showed the expected results (Figure 3.3a, middle and right panels). Moreover, when we co-expressed AZI1$^{\Delta 2\text{-}30}$:GFP together with RFP-TUB6, we observed a robust co-localization between GFP and RFP signals (Figure 3.3b, upper panels). No obvious co-localization was observed between RFP-TUB6 and LifeAct markers (Figure 3.3b, bottom panels). Importantly, live imaging of AZI1:GFP together with RFP-TUB6 showed that full length AZI1 in vesicle-like structures moved in close association with MT bundles (Figure 3.3c and Movie S3.1). The proportion of AZI1:GFP colocalizing with RFP-TUB6

Figure 3.3 Co-localization of AZI1 variants with the microtubule network

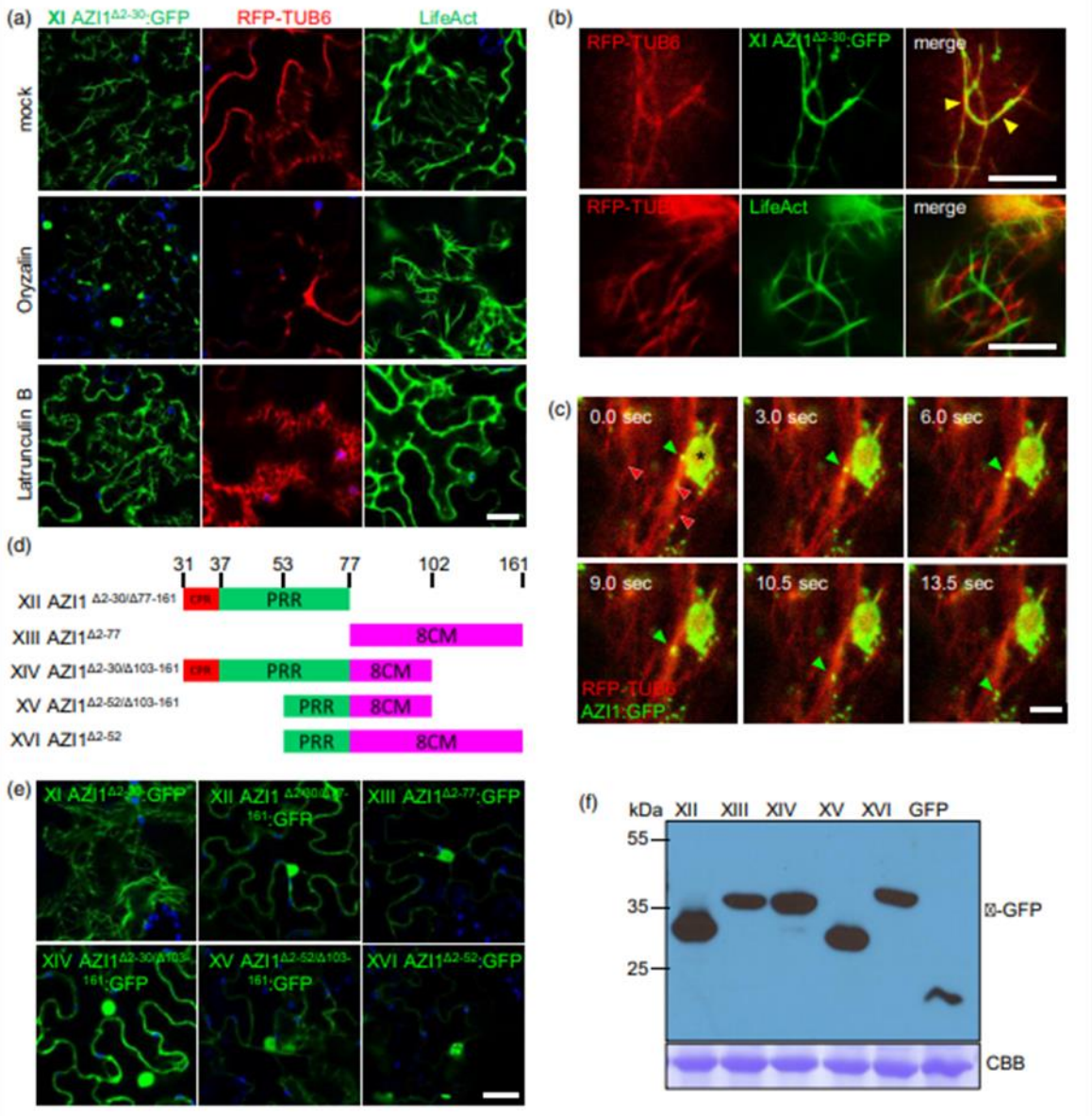

Figure 3.3. Co-localization of AZI1 variants with the microtubule network
(a) to (c) and (e) Laser scanning confocal microscopy micrographs showing localization of GFP-tagged AZI1 variants, microtubule marker (RFP:TUB6) and filamentous actin marker (LifeAct:GFP) in N. benthamiana. (a) Micrographs showing the effect of actin (Latrunculine B, LatB) and microtubule (oryzalin, Ozn) inhibitors or mock treatments on AZI1 variant XI:GFP, RFP:TUB6 or LifeAct:GFP localization patterns. (b) RFP:TUB6 is co-expressed with AZI1 variant XI:GFP or LifeAct. (c) Time series micrographs showing dynamic localization of AZI1:GFP in vesicle-like structures (green arrowhead) moving on microtubule bundle (red arrowhead; microtubule marker; RFP:TUB6). Asterisk indicates a plastid. sec, seconds. Micrographs show GFP (green), RFP (red) and plastid autofluorescence (blue). In (a) and (e)

Figure 3.3. Co-localization of AZI1 variants with the microtubule network *(cont)*
Bar = 20 µm, (c) Bar = 5 µm, and (b) upper panel Bar = 50 µm and middle and bottom panel Bar = 10 µm. (d) Scheme of AZI1 variants used in (e) and (f). Amino acid positions delimiting AZI1 domains are shown in the upper part. Different variants are identified with roman numerals (left). (f) Western blots of total protein from N. benthamiana expressing GFP alone or fused to AZI1 variants used in (e). Bands were revealed using anti-GFP antibody. The blot stained with Coomassie blue (CBB) is presented to show loading.

represents ~16 % of the total signal compared with a ~3 % found in control GFP (Figure S3.1a). Thus, loss of the TMD anchor induced AZI1 to (more) stably associate with MTs network, suggesting that there is a close relationship between AZI1 and cell cytoskeleton. We considered the possibility that the association of AZI1$^{\Delta 2\text{-}25}$:GFP and AZI1$^{\Delta 2\text{-}30}$:GFP with discrete contact points on plastids (Figure 3.3.2b,e) might be due to the accumulation of these AZI1 variants along the MTs. However, tubulin was absent from plastid fractions, suggesting that these variants associate with plastids without stable/strong MTs associations (Figure S3.1b).

Next, to analyze which of the AZI1 motifs/regions are required for AZI1$^{\Delta 2\text{-}25/2\text{-}30}$:GFP association with MTs, we generated several deletion constructs for AZI1. Partial deletions fused to GFP were transiently expressed in *N. benthamiana* to assess the localization patterns (Figure 3.3d). Interestingly, none of the deletions generated showed a filamentous pattern comparable with AZI1$^{\Delta 2\text{-}30}$:GFP (Figure 3.3e), and instead, the constructs localized to the ER/cytoplasm and nuclei. Western blot analysis indicated that the GFP was not cleaved from the expressed fusion proteins (Figure 3.3f).

These results suggest that AZI1's PRR and 8CM regions are required together for the direct or indirect association with MTs.

Microtubules are dispensable for flg22-induced enrichment of AZI1 to plastids

To dissect which cellular components are needed for AZI1 targeting, we began by identifying a defined, strong defense-inducing stimulus other than pathogen infection (Cecchini *et al.*, 2015b) that might cause enrichment of AZI1 to plastids. Since AZI1 and its paralogue EARLI1 are also needed for mSAR induction, we measured AZI1/EARLI1 levels in total and plastid extracts after flg22 treatment.

We infiltrated *Arabidopsis* WT plants with flg22 or H_2O (mock) and analyzed the native AZI1/EARLI1 levels in total extracts at different times post-treatment by Western blot. Figure 3.4a shows that between 3-6 hours post treatment (hpt), the total amount of AZI1 greatly increased in response to flg22 (+) compared to mock (-). Local AZI1/EARLI1 induction by flg22 treatment was also pronounced at 12 hpt (Figure 3.4b, total - WT plants). To determine if this AZI1 increase translated to higher levels in plastids, we treated *Arabidopsis* with flg22 and analyzed the levels of AZI1/EARLI1 in total and plastid fractions at 6 and 12hpt (Figure 3.4b and S2a, WT plants). The amount of plastid-localized AZI1/EARLI1 increased in flg22-treated samples compared to mock; at 12 hpt there was a greater fold increase in the amount of AZI1/EARLI1 targeted to plastids (~10x) relative to the fold increase in the total extract (~3x). Thus, flg22 MAMP treatment strongly induces AZI1/EARLI1 protein levels and increases their relative enrichment in the plastid fraction.

Considering the above results and the role of cytoskeletal dynamics for protein trafficking, we next studied the importance of the cytoskeleton for AZI1 targeting to plastids during MAMP stimulation. We quantified AZI1/EARLI1 protein levels in *Arabidopsis* WT Col-0 total and plastid fractions 6 hpt with flg22 and 3 h post-infiltration with or without inhibitors for microtubules (Ozn) and actin filaments (LatB), respectively. This set up allowed us to make the inhibitor treatments

Figure 3.4. Impact of MAP kinase mutations and cytoskeleton inhibitors on AZI1/EARLI plastid targeting during defense signaling.

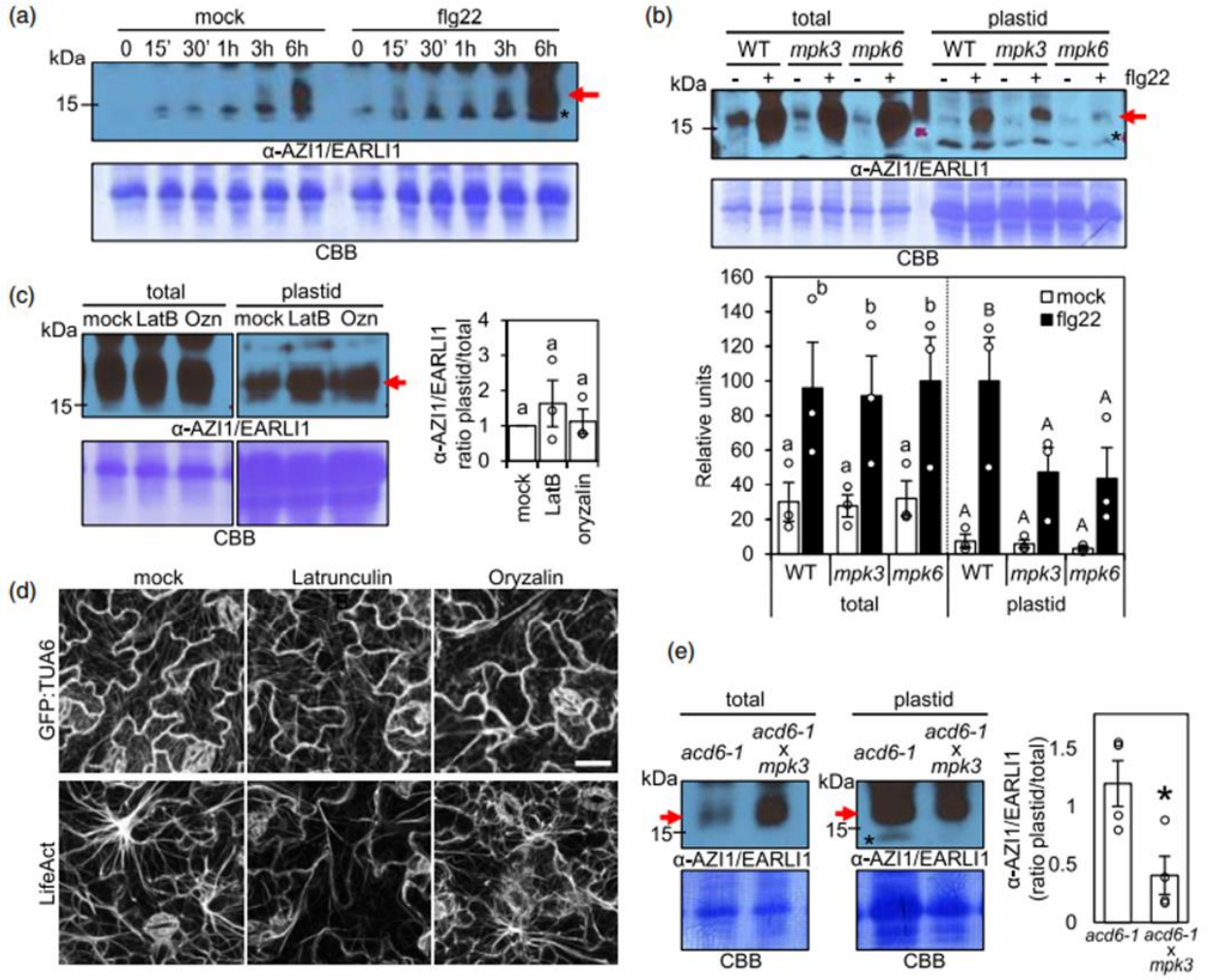

Figure 3.4. Impact of MAP kinase mutations and cytoskeleton inhibitors on AZI1/EARLI plastid targeting during defense signaling

(a) Western blot of total extracts from WT Col-0 Arabidopsis leaves to test AZI1–EARLI1 protein levels at different times post infiltration with 1 µM flg22 or water (mock). **(b)** AZI1–EARLI1 levels in total and plastid fractions from *Arabidopsis* leaves of WT Col-0, *mpk3*, and *mpk6* plants 12h post treatment with 1 µM flg22 (+) or water (mock, -). Shown in the graph is quantitation of AZI1–EARLI1 levels relative to the total protein content in each Coomassie blue membrane lane, as quantified by densitometry. The highest value in total or plastid fractions was set to 100 in the relative units. **(c)** AZI1–EARLI1 protein levels in total and plastid fraction from Arabidopsis WT Col-0 leaves 6h post treatment with 1 µM flg22 and 3h post-infiltration with inhibitors of actin filaments (Latrunculine B, LatB), microtubules (oryzalin, Ozn) or mock. Right graph: ratio of AZI1/EARLI1 in plastids vs total in different treatments, as quantified by densitometry. Western blot panels separated with vertical line belong to the same blot. **(d)** Actin and microtubule cytoskeleton changes in *Arabidopsis* after inhibitor treatments. Col/Lifeact-GFP and Col-*gl1*/GFP-TAU6 transgenic plants expressing actin or

Figure 3.4. Impact of MAP kinase mutations and cytoskeleton inhibitors on AZI1/EARLI plastid targeting during defense signaling (cont)

microtubule markers, respectively, were imaged by laser-scanning confocal microscopy at 6h post treatment with 1 µM flg22 and 3h post-infiltration with inhibitors of actin filaments (Latrunculine B), microtubules (oryzalin) or mock. The representative micrographs shown are Z-series maximum intensity projections. Micrographs show GFP signal (greyscale). Bar = 20µm. **(e)** AZI1–EARLI1 protein levels in total and plastid fractions from untreated *Arabidopsis* leaves of *acd6-1* and *acd6-1mpk3-1* mutant plants. Right graph: plastid to total ratio of AZI1–EARLI1 levels relative to the total protein content in each Coomassie blue membrane lane, as quantified by densitometry.

The averages +/- standard error from three (b and c) or four (e) independent experiments are shown. In (b and c), different letters (lower or uppercase) indicate statistically significant differences ($P<0.01$, analysis of variance (ANOVA), SNK test (b) or Tukey test (c)). The dotted line indicates that the total and plastid fractions were analyzed independently in (c). In the graph in (e), the asterisk indicates statistically significant differences determined by *t*-test (*$P<0.05$, n=4). In (b), (c) and (d) the individual data points are shown on the bar chart as scatter-dots. In (a), (b), (c) and (e) the blots stained with Coomassie blue (CBB) are presented to show loading. Bands were revealed using anti-AZI1/EARLI1 polyclonal serum. Red arrow indicates the AZI1/EARLI1 monomer band. Asterisks indicate unspecific bands.

before the earliest robust increase of AZI1 in plastids (Figure S2a; Figure 3.4a). As shown in Figure 3.4c, Ozn or LatB treatments did not affect the plastid AZI1 levels compared to mock. As efficacy controls for the inhibitor treatments, we used the same treatment conditions to study transgenic plants expressing Col/Lifeact-GFP and Col-*gl1*/GFP-TUA6, actin or microtubules markers, respectively. Both inhibitor treatments strongly disrupted the respective AF and MT cytoskeletons (Figure 3.4d).

These results suggest that although AZI1 can traffic in close association with MTs, disruption of the cytoskeleton does not significantly impact AZI1 targeting to plastids.

MPK3 and MPK6 enhance AZI1/EARLI1 plastid targeting during defense induction

AZI1's PRR is a proposed phosphorylation target for MPK3 and possibly MPK6 (Pitzschke *et al.*, 2014), two key signaling factors associated with biotic and abiotic stress (Rodriguez *et al.*, 2010). Moreover, we recently showed that these kinases are also needed for

underground AZA-induced priming (Cecchini *et al.*, 2019). Since the PRR is required for plastid targeting (Figure 3.2), we analyzed if MPK3/6 affect plastid localization of AZI1/EARLI1 proteins.

We treated WT Col-0, *mpk3* and *mpk6* mutant plants with flg22 or H_2O (mock) and analyzed the levels of native AZI1/EARLI1 in plastids fractions compared to total extracts (Figure 3.4b; Figure S3.2a). Compared to WT, the *mpk3* and *mpk6* plants displayed decreased levels of AZI1/EARLI1 specifically in plastid fractions 12h after flg22 treatment, but not in mock-treated plastid fractions or any total extracts (Figure 3.4b). In addition, we also observed a reduction of AZI1/EARLI1 in *mpk6* plastids fraction at 6 hpt (Figure S3.2a). Immunoblots with phospho-antibody show that MPK3/4/6 were still active at both 6 and 12 hrs post flg22 treatment compared with mock treated plants (Figure S3.2b).

Together, these results strongly suggest that both MPK3 and MPK6 are required for robust AZI1 plastid enrichment during flg22-MAMP defense induction. Supporting this idea, *acd6-1*, a plant with constitutively active MPK3 and pattern receptor-mediated immunity (Tateda *et al.*, 2014), showed a reduced proportion of AZI1/EARLI1 in the plastid fraction relative to the total extract when an *mpk3* mutation was present (Figure 3.4e). The lower total levels of AZI1 in *acd6-1* versus *acd6-1mpk3* may be due to an altered balance of signaling molecules/hormones including salicylic acid, which is affected by both mutations (Vanacker et al 2001; Zhang et al., 2014).

MPK3 and MPK6 are required for mSAR induction in Arabidopsis

Considering the requirement of AZI1 and EARLI1 for mSAR (Cecchini *et al.*, 2015b), we next analyzed if MPK3 and MPK6 are also needed for this systemic defense program. We pretreated by infiltrating three lower leaves of WT Col-0, *mpk3* and *mpk6* plants with flg22 or H_2O

(mock), and 2d later infected plants with virulent *Pseudomonas* strain *Pma*DG3 in the same (local) or systemic leaves. Both MPK3 and MPK6 were required for systemic resistance induced by flg22, as judged by the growth of *Pma*DG3 (Figure 3.5, right graph). *mpk3* was completely mSAR defective and *mpk6* displayed a weak and statistically insignificant induction. As previously reported, local resistance after flg22 treatment was not affected in either *mkp3* or *mpk6* single mutant plants compared to WT plants (Figure 3.5, left graph) (Su *et al.*, 2017). However, mock-treated *mpk6* plants showed modestly increased resistance to *Pma*DG3 relative to the other genotypes tested.

Figure 3.5. flg22 local and systemic disease resistance induction in Arabidopsis WT Col-0, mpk3 and mpk6 plants.

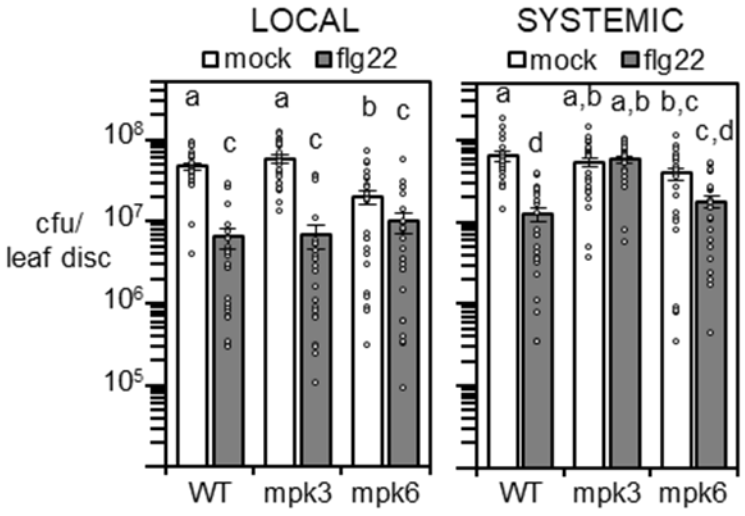

Figure 3.5. flg22 local and systemic disease resistance induction in Arabidopsis WT Col-0, mpk3 and mpk6 plants

Growth of the virulent bacteria *Pma*DG3 on plants 3 days post infection (OD_{600}=0.0003). *Pma*DG3 was infiltrated in local or distal leaves after 2 days of the local leaf treatment with water (mock) or 200 ηM flg22. The average of cfu per leaf disc +/- standard error from three independent experiments (each one with eight biological replicates) is shown. Graph *y* axes are in $\log_{10}$ scale. Different letters show significant differences between treatments and/or mutants ($P<0.01$, analysis of variance (ANOVA), Tukey test). Individual data points are shown on the bar chart as scatter-dots.

These data indicate MPK3/6 are required for mSAR induction, possibly related to their effect on AZI1/EARLI's plastid targeting. Because MPK3 and MPK6 are also required for SAR and ISR (Beckers *et al.*, 2009; Cecchini *et al.*, 2019), our data strongly indicates a key role for these kinases in plant systemic resistance programs.

AZI1, MPK3 and MPK6 co-localize at sites of plastid–ER contacts

It was previously suggested that MPK3 interacts with AZI1 and forms protein complexes near the cell boundary (Pitzschke *et al.*, 2014). To get deeper insight into the subcellular localization and possible complex formation between AZI1 and MPK3/6, we analyzed their co-localization by confocal microscopy.

We co-expressed MPK3:RFP or MPK6:RFP together with AZI1:GFP by agro-transformation of *N. benthamiana* leaves. As shown in Figure 6.1a, both MPK3:RFP and MPK6:RFP localized to the nucleus in a spherical pattern and partially co-localized with AZI1:GFP at perinuclear ER and plastid/stromule–ER contact sites. Some co-localization signals are likely to be plastid–ER and/or stromule–ER contact sites (Figure 6.1a; bottom panels) (Cecchini *et al.*, 2015b). No co-localization was found between control soluble GFP and MPK3:RFP or MPK6:RFP at those places (Figure 6.1b). As expected, control GFP and MPKs co-localize at nuclei and cytoplasm. Immunoblots to detect MPK3 and MPK6 fusion proteins established that free RFP was not detectable (Figures 6c and 6d).

Next, we assessed putative interactions between AZI1 and MPK3 during defense induction. Immunoprecipitation (IP) assays were implemented by using *Arabidopsis* that expressed functional HA-tagged AZI1 previously shown to complement *azi1* (Cecchini *et al.*, 2015b). AZI1:HA-expressing plants treated with flg22 or H_2O (mock) for 6 hpt were used for

Figure 3.6. AZI1 and MPK3/6 co-localization and complexes.

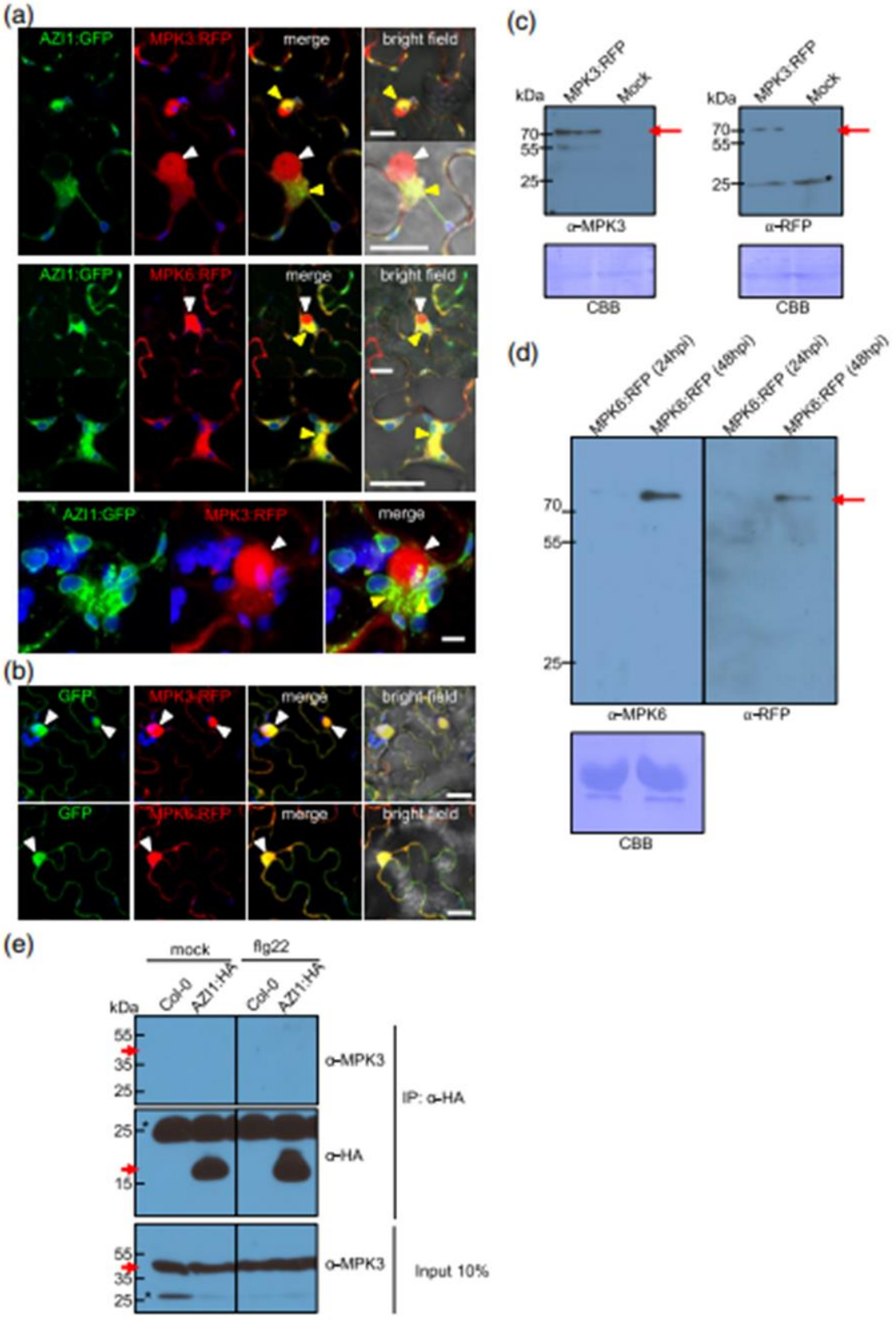

Figure 3.6. AZI1 and MPK3/6 co-localization and complexes
Growth of the virulent bacteria *Pma*DG3 on plants 3 days post infection (OD_{600}=0.0003). *Pma*DG3 was infiltrated in local or distal leaves after 2 days of the local leaf treatment with water (mock) or 200 ηM flg22. The average of cfu per leaf disc +/- standard error from three independent experiments (each one with eight biological replicates) is shown. Graph *y* axes are in $\log_{10}$ scale. Different letters show significant differences between treatments and/or mutants (P<0.01, analysis of variance (ANOVA), Tukey test). Individual data points are shown on the bar chart as scatter-dots.

immunoprecipitation with an anti-HA matrix. MPK3 did not co-precipitate with AZI1:HA in either mock- or flg22-treated samples (Figure 6.1e).

Altogether, these results indicate that although they partially co-localize, AZI1 does not form stable complexes with MPK3 in *Arabidopsis* under our assay conditions.

DISCUSSION

Not much information exists about the subcellular targeting/trafficking regulation of immune components (Ben Khaled *et al.*, 2015; Wang *et al.*, 2016; Gu *et al.*, 2017). AZI1, a key factor for the plant systemic defenses, shows dynamic levels in plastid envelopes (Jung *et al.*, 2009; Cecchini *et al.*, 2015b). Interestingly, AZI1 does not have a recognizable "classic" plastid targeting signal. Here, we discovered and characterized a N-terminal bipartite signature that explains AZI1's subcellular location: a predicted signal peptide followed by a PRR (Cecchini *et al.*, 2015b). AZI1's putative signal peptide is a non-cleavable TMD that anchors the protein to membranes, placing this LTP-like protein as a signal-anchored protein. In addition, unlike what was found for other signal-anchored proteins, the presence of a PRR after the TMD (and not the TMD hydrophobicity (Kim and Hwang, 2013)) is required for plastid targeting. Together, our data establishes AZI1 as belonging to a previously undescribed class of signal-anchored proteins. Remarkably, the defense-associated kinases MPK3 and MPK6 are required for the increased targeting of AZI1 to plastids

in response to flg22. Moreover, our results suggest that AZI1 utilizes the MT network for intracellular trafficking. Therefore, we propose that after pathogen or MAMP recognition, MPK3/6 are locally stimulated and, by acting on its N-terminal bipartite signal, enhance AZI1 plastid targeting. This in turn could determine how much systemic defense priming ensues.

AZI1 is a variant of signal-anchored proteins

AZI1 is a signal-anchored protein targeted to plastids. This finding explains our previous work showing that AZI1 is present in microsomal fractions (Cecchini *et al.*, 2015b). Supporting this, other reports showed no cleavage of the AZI1 putative signal peptide (Zhang and Schläppi, 2007; Pitzschke *et al.*, 2016). Because traces of AZI1 TMD:GFP were detected in the soluble fraction ($AZI1^{\Delta 38\text{-}161}$ and $AZI1^{C28/30A\ \Delta 38\text{-}161}$), we cannot completely rule out that a very small amount of AZI1 is capable of entering the secretory pathway. In agreement with this possibility, using protoplasts and root exudates, the localization of a small proportion of AZI1 was consistent with its being secreted to plant cell walls (Zhang and Schläppi, 2007; Pitzschke *et al.*, 2016). Alternatively, soluble traces of AZI1 TMD:GFP in our experiments might be contamination from the microsomal extraction fractionation.

Most signal-anchored proteins targeted to plastids have relatively low TMD hydrophobicity indices (Lee *et al.*, 2011). In contrast, AZI1's TMD hydrophobicity index is higher and its targeting to/co-fractionation with plastids depends on the presence of the PRR (Cecchini *et al.*, 2015b; this work). It seems possible that the PRR substitutes for the requirement for a low degree of hydrophobicity within the TMD as the factor for plastid targeting. Interestingly, the PRR has features that are shared with bona fide chloroplastic transit peptides (cTPs). These include a

large number of serine, arginine and proline residues, and overall low peptide complexity (targetP, (Emanuelsson *et al.*, 2000); (Bruce, 2000; Lee *et al.*, 2018)). Thus, AZI1 may use a chimeric targeting mechanism with components shared by signal anchor- and cTP-containing proteins. In this scenario, proteins required for both signal anchor and cTP targeting may also be involved in AZI1 targeting.

Interestingly, an algorithm trained to find apicoplast (plastid analogue in apicomplexan organisms) protein targeting signals, a putative SP + cTP (Zuegge *et al.*, 2001), correctly predicts AZI1's plastid localization (Cecchini *et al.*, 2015b). In addition, because transit peptides/presequences and the AZI1 PRR exhibit a high content of positively charged residues (Mackenzie, 2005), the PRR may act as a CPR region (albeit the PRR is longer than the CPRs in signal-anchored proteins). This would explain our findings that deletion of the AZI1 CPR does not strongly affect AZI1's targeting.

AZI1's predicted S-acylation sites (Ren *et al.*, 2008) are conserved in most HyPRP members, suggesting an important role for these residues. However, mutation of these sites did not affect AZI1's plastid localization. S-acylation often acts as a mechanism to fine-tune proteins (re)localization and/or stability (Hemsley, 2015; Daniotti *et al.*, 2017). Thus, small differences in AZI1 trafficking dynamics may have been missed in our experiments. Alternatively, the predicted acylation sites (cysteine residues) may be involved in the formation of disulphide bonds and the formation of AZI1-complexes, as previously suggested (Zhang and Schläppi, 2007; Cecchini *et al.*, 2015b).

MPK3/6 are needed for defense-related AZI1 plastid targeting and mSAR

As observed after stimulation of R protein-mediated defenses, MAMP treatment greatly induces the fraction of AZI1 localized to plastids, probably reflecting shared signals and/or components between the SAR and mSAR programs (Mishina and Zeier, 2007; Cecchini *et al.*, 2015b). The kinases MPK3 and MPK6 are known shared factors between R- and PRR-induced systemic responses and priming (Beckers *et al.*, 2009; Rodriguez *et al.*, 2010; Cecchini *et al.*, 2019). Remarkably, MPK3 and MPK6 specifically impact AZI1 targeting and are required for the increased accumulation of AZI1 at plastids. Thus, it is possible that MPK3/6 act in systemic defense programs, at least in part, by regulating AZI1's increased levels in plastids, which in turn may affect the movement of systemic defense priming signals such as AZA or glycerol-3-phosphate (Yu *et al.*, 2013; Cecchini *et al.*, 2019; Cecchini *et al.*, 2015b). Moreover, MPK3 and MPK6 can promote plastid-associated ROS production (Su *et al.*, 2018), which play an important role in SAR and could facilitate the generation of AZA in this organelle (Wang *et al.*, 2014; Zoeller *et al.*, 2012). Considering that MPK3 and MPK6 are activated in response to diverse abiotic stresses (Rodriguez *et al.*, 2010; Jalmi and Sinha, 2015), it is also possible that AZI1 is required in plastids during other environmental conditions. We speculate that in these situations, AZI1 could facilitate the movement of other signals, like other plastid oxylipins related to stress resistance (Blée, 2002; Prost *et al.*, 2005; Breuers *et al.*, 2011).

How might MPK3/6 regulate AZI1's abundance in plastids? Phosphorylation of cTP residues by STY kinases regulates chloroplast import rate (Martin *et al.*, 2006; Lamberti *et al.*, 2011). Thus, one idea is that MPK3/6 might impact AZI1 targeting by directly phosphorylating the PRR. In support of this, AZI1's PRR has several predicted MAPK-phosphorylation sites and

MPK3 can phosphorylate the PRR *in vitro* (Pitzschke *et al.*, 2014). Previous work indicated that AZI1 might interact with MPK3 in an *in planta* heterologous system (Pitzschke *et al.*, 2014). However, although AZI1 and MPK3/6 partially co-localized, stable complexes containing AZI1 and MPK3 in *Arabidopsis* were not detectable by co-immunoprecipitation. Labile and/or short-lived interactions between AZI1-MPK3/MPK6 may not permit co-immunoprecipitation in our conditions. Since MPKs are thought to have many substrates, it is not surprising that stable complexes were not detectable (Bigeard and Hirt, 2018; Rayapuram *et al.*, 2018).

MTs and AZI1 trafficking

Surprisingly, the loss of the N-terminal TMD causes AZI1 to stably co-localize with microtubules. AZI1's PRR and 8CM domain together may directly or indirectly interact with MT filaments, suggesting that AZI1 uses them for intracellular trafficking. Supporting this idea, full length AZI1-GFP moves along (or very close to) MT bundles. It is unlikely that AZI1-MT interactions guide AZI1 to plastids, since MT inhibitor treatment did not affect the abundance of AZI1 in plastids. MTs play a key role for the extension of stromules (Erickson *et al.*, 2017; Erickson *et al.*, 2018; Kumar *et al.*, 2018), plastid structures where AZI1 also resides (Cecchini *et al.*, 2015b). Both stromules and AZI1 enrichment in plastids are highly induced with similar kinetics by flg22 ((Caplan *et al.*, 2015) and this work). One possibility is that plastid-anchored AZI1 in close proximity to MTs might help stromules extend to and/or make contact with other structures in cells. It is also possible that the MT network is required for AZI1 to target non-plastid subcellular sites like plasmodesmata (PD), which was suggested to be required for AZA transport and ultimately systemic resistance (Cecchini *et al.*, 2015b). The localization of AZI1 to PD during

defense signaling may indicate the importance of AZI1's trafficking among distinct subcellular compartments for SAR and priming establishment (Lim *et al.*, 2016). Since AZI1 is also required for the action of other systemic signals generated in plastids like glycerol-3-phosphate, dehydroabietinal and pinene-monoterpenes (Chaturvedi *et al.*, 2012; Yu *et al.*, 2013; Riedlmeier *et al.*, 2017), it is possible that it also allows small metabolites to reach PDs for simplastic movement. Future work will address these possibilities.

In summary, AZI1 uses a previously undescribed variant of the signal anchor proteins mechanism to target plastids. This targeting and/or stability in the plastid pool of AZI1 is impacted by two key defense associated kinases, MPK3 and MPK6, probably for a tight modulation during defense induction against pathogens and possible other stresses. This could be especially important considering how fundamental plastids are for many types of defense responses (Caplan *et al.*, 2008; Grant and Jones, 2009; Nomura *et al.*, 2012; Zeier, 2013; Cecchini *et al.*, 2015a; de Torres Zabala *et al.*, 2015; Medina-Puche *et al.*, 2020). In particular, a timely regulation of the AZI1 pool in plastids could grant an efficient movement of AZA for the establishment of systemic defenses. Additionally, since several HyPRPs contain an N-terminal bipartite signal, this targeting mechanism could also be functional for all of them. It is also conceivable that other non-HyPRP plant proteins also use a similar N-terminal targeting signal. Supporting this idea, several signal-anchored proteins with high TMD hydrophobicity and predicted to be retained in the ER, were reported to be plastid-localized (Lee *et al.*, 2011).

Collectively, this work strengthens the idea that subcellular re-localization of defense components is a key aspect of plant immune signaling, especially with regards to the phenomena of priming, in which a well-placed ambush can be the difference between disease and death.

EXPERIMENTAL PROCEDURES

Plants

All *Arabidopsis thaliana* plants were 25~28-day-old Columbia (Col) ecotype. *mpk3-1*, *mpk6-2* and *acd6-1* were previously described (Lu *et al.*, 2003; Liu and Zhang, 2004; Wang *et al.*, 2007). *acd6-1mpk3* double mutant and the Col/Lifeact-GFP were generated previously (Smertenko *et al.*, 2010; Tateda *et al.*, 2014). The transgenic plant Col-*gl1*/GFP-TUA6 was obtained from ABRC (CS6551) (Ueda *et al.*, 1999). *Arabidopsis* plants expressing HA-tagged AZI1 under dexamethasone (Dex)-inducible promoter where previously generated (pBAV154:AZI1; (Cecchini *et al.*, 2015b)). Plants were grown under 12 h day (8:00 am to 8:00 pm) and 12 h night conditions at 20°C, 200-230 µmol sec^{-1} m^{-2} light at rosette level and 50-70% relative humidity (Jung *et al.*, 2009). *Nicotiana benthamiana* were grown at 24°C and with 16 h day light. Plants were grown for 4 weeks before *Agrobacterium tumefaciens*-mediated transient transformation.

Vectors and constructs

All primers and vectors used in this study are described in Supplementary table 1. The vectors and constructs carrying full length AZI1 as well as the deletion AZI1-variants II. and VI. were previously described (Cecchini *et al.*, 2015b). The AZI1 deletion and point mutation variants as well as the *MPK3* and *MPK6* full coding region were cloned from *A. thaliana* cDNA using PCR primers linked to specific sequences compatible with the TOPO pENTR® and GATEWAY® cloning procedure, and introduced into the plant expression vector pBAV150 (Vinatzer *et al.*,

2006). *MPK3* and MPK6 were also introduced into pSITE-4NA (CD3-1642/ABRC (Nelson *et al.*, 2007)). To generate internal deletion and point mutation constructs the proper primers were used to amplified the fragments to be linked by PCR. When required, a start codon was added in the forward primers. All these constructs permitted the expression of the transgenes with C-terminal GFP or HA-tag (pBAV150/pBAV154; (Vinatzer *et al.*, 2006)) controlled by the Dex-inducible promoter or with C-terminal mRFP1 driven by the 35S promoter (pSITE-4NA). The vector used for the expression of the actin cytoskeleton marker Lifeact-GFP was previously described (Smertenko *et al.*, 2010). The microtubule marker RFP-TUB6 construct was kindly provided by Dr. Wasteneys (Ambrose *et al.*, 2011).

Subcellular localization

For localization studies, 4-week-old *N. benthamiana* leaves were infiltrated with *Agrobacterium tumefaciens* C58C1 or GV3101 strains carrying the different constructs. In order to express fusion proteins from the Dex-inducible vectors, 20 μM or 30 μM Dexamethasone (D4902; Sigma-Aldrich, USA) was infiltrated into leaves 1 d after agroinfiltration. Fractionation and confocal microscopy studies were done 21 h after Dex. *Agrobacterium* harboring different constructs were infiltrated together for co-expression analysis. *N. benthamiana* leaves were prepared for microscopy as described (Littlejohn *et al.*, 2010). A Zeiss LSM710 laser-scanning confocal microscope (Zeiss, Germany) was used to capture GFP fluorescence (excitation: 488 nm; emission: 505 to 530 nm), RFP fluorescence (excitation: 561 nm; emission: 570 to 620 nm) and plastid autofluorescence (excitation: 633, emission: 650-750 nm). Images were taken using a LD C-Apochromat 40x/1.1 W Korr objective using a sequential acquisition mode. For time series acquisition, images were taken at low resolution scanning and maximum speed mode. Images were

processed using ImageJ (http://rsb.info.nih.gov/ij), ZEN 2012 (Zeiss) and Adobe Photoshop software.

Quantification of fluorescence

For the analyses of GFP fluorescent intensity of AZI1 and variants in plastids, confocal images were captured using two channels: plastid autofluorescence (blue, 650-750 nm) and GFP fluorescence (green, 505 to 530 nm) as described above. Using the Fiji software (https://imagej.net/), individual plastids were identified in the blue channel and a spherical region of interest (ROI) was drawn around each plastid such that it incorporated the entire region of autofluorescence. The intensity of the GFP signal within the ROI was measured. Four or more images from independent experiments were analyzed for each construct and 4-5 plastids were quantified per image to calculate the mean plastid GFP fluorescence +/- standard error. To test the significance across values, one-way ANOVA followed by Tukey's HSD post hoc tests were performed. For the analyses of GFP signal that colocalized with RFP-TUB6, confocal image channels for GFP (green, 505 to 530 nm) and RFP fluorescence (red, 570 to 620 nm nm) were used. The ImageJ Colocalization plugin (http://rsb.info.nih.gov/ij/plugins/colocalization.html) was used to generate ROIs from GFP/RFP colocalized signal regions (using thresholds= 50 % and ratio= 50 %). The intensity of the total GFP signal and within the ROI was measured for each image. Six or more images from independent experiments were analyzed to calculate the percentage of GFP fluorescence +/- standard error that colocalize with RFP-TUB6 with respect to total. To test the significance, one-way ANOVA followed by Tukey's HSD post hoc tests was performed.

Fractionation

Microsomal fractions were obtained as described in (Zhang *et al.*, 2014). 1 g of *N. benthamiana* leaf tissue expressing the different constructs was used for the fractionation. Plastids were isolated from 1 g of *Arabidopsis* or *N. benthamiana* leaves following the protocol described in (Cecchini *et al.*, 2015b). Chlorophyll content was measured by spectrophotometric analysis as described in Lamppa (1995). For *N. benthamiana* transiently expressing AZI1 deletion variants V, VIII, IXc, and X, plastids were isolated from 1 g of leaves following the protocol described in Cecchini et al., 2015b with a slight modification. The total/impure plastids were separated at 4^{o}C on two percoll gradients (80%-40%), initially in 2mL microfuge tubes then again in 4mL polycarbonate tubes. To enrich for plastid envelopes, purified plastids were frozen in liquid nitrogen to lyse membranes then thawed on ice. Thawed samples were centrifuged at 13000g, the supernatant was collected, then the pellet was resuspended in ice-cold dH_2O (with protease inhibitor cocktail) and frozen at -80C o/n to further lyse membranes. The envelope fraction was again centrifuged at 13000g, the supernatant fraction was collected, then the pellet was resuspended in 1X PBS (1% SDS). Successful fractionation was confirmed by the absence of chlorophyll in the soluble supernatant fractions.

Western blot analysis and immunoprecipitations

Total proteins or different fractions were separated by SDS-PAGE. Concentrations of protein in the samples were calculated by Bradford assay (Bradford, 1976). The primary antibodies used for Western blots were: GFP antibody (Covance MMS-118P, 1:5000), HA antibody (Covance 16B12,

1:1750), HA antibody (Cell Signaling 14031S, 1:1200) , RFP antibody (Agrisera AS15 3028, 1:2000 or 1:3000), MPK3 antibody (Sigma-Aldrich M8318, 1:3000), MPK6 antibody (Sigma-Aldrich A7104, 1:3000), phospho-p44/42 MAPK (Erk1/2) (Thr202/Tyr204) antibody (Cell Signaling Technologies 9101S, 1:1000) (Bartels *et al.*, 2009; Beckers *et al.*, 2009), H^+ATPase antibody (Agrisera AS07260, 1:7500), cytosolic FBP antibody (Agrisera AS04 043, 1:3000), BiP2 antibody (Agrisera AS09 481, 1:4000), and rat monoclonal tubulin (yol1/34) antibody (gift from Michael Glotzer, 1:1000). For analysis of native AZI1/EARLI1 proteins an anti- AZI1/EARLI1 polyclonal antibody (Zhang and Schläppi, 2007) was used (1:750). The loading buffer for AZI1/EARLI1 western blot samples does not contain reducing agents as described (Zhang and Schläppi, 2007). Secondary horseradish peroxidase conjugated anti-rabbit or anti-mouse antibodies (Thermo Scientific) were used at 1:1000. SuperSignal Stable Peroxidase (Thermo Scientific) was used to detect the bands. To quantify by densitometry the Western blot bands and Coomassie Blue staining Gel-Pro analyzer™ software was used.

For immunoprecipitations, 5 g of leaves of *Arabidopsis* WT or transgenic plants expressing AZI1-HA was used. Input extracts used for the immunoprecipitation were isolated in extraction buffer (50 mM Tris-HCL pH8.0, 10 % glycerol, 0.5 % sodium deoxycholate, 1 % Igepal CA-630 (Sigma-Aldrich, USA) and complete protease inhibitor cocktail from Roche) as previously described (Cecchini *et al.*, 2015b). Proteins were immunoprecipitated using an anti-HA affinity matrix (rat monoclonal 3F10, Roche). Matrix was washed 4 times with extraction buffer and then resuspended in loading buffer for western blot analysis.

flg22 treatment and systemic resistance induction

To analyze AZI1/EARLI1 levels and localization after flg22 peptide treatment, *Arabidopsis* WT and *mpk3* and *mpk6* mutant leaves were infiltrated with 1 µM flg22 or mock (H_2O). Total or plastid fraction protein samples were obtained after different times post-infiltration as indicated in Figure legends. Plants were treated soon after lights were turned on in the morning.

To evaluate the local and systemic resistance induced by flg22 (mSAR; (Mishina and Zeier, 2007; Cecchini *et al.*, 2015b)), 3 lower leaves were infiltrated with 200 nM flg22 or H_2O (mock). After two days local or distal leaves were syringe-inoculated with virulent *Pseudomonas cannabina* pv *alisalensis* (formerly called *P. syringae* pv. *maculicola* ES4326 (Bull *et al.*, 2010)) carrying an empty vector (*Pma*DG3) (OD_{600}=0.0003) (Guttman and Greenberg, 2001). Bacteria growth was quantified 3 days post infection using 8 leaves from 8 different plants.

Exogenous application of actin and microtubules inhibitors

Solutions of Latrunculin B (20 µM, Sigma-Aldrich, USA) or oryzalin (40 µM, Sigma-Aldrich, USA) inhibitors were directly infiltrated into leaves with a needleless syringe. In *Arabidopsis*, treated leaves were analyzed by microscopy or total and plastid fraction proteins isolated after 3 hs. In *N. benthamiana*, discs were immediately cut after leaves' infiltration and floated in the inhibitor solutions for 16-18 hs before the microscopy analysis.

Statistical analysis

Analyses in this study were done with the software SigmaPlot v11.0 (Systat Software, Inc.). ANOVA (log-transformed data for bacterial growth curves) followed by the Tukey or Newman-Keuls (SNK) post hoc test and one-tailed Student's *t*-test were used as indicated in Figure legends.

ACKNOWLEDGMENTS

This research was supported by National Science Foundation grant IOS1456904 to JTG. NMC is a Career Investigator of CONICET, Argentina. DJ Speed was supported by National Institutes of Health training grant T32 GM007183, the Ford Foundation Predoctoral Fellowship, and the Howard Hughes Medical Institute Gilliam Fellowship for Advanced Study. We thank Zeeshan Z. Banday for helpful discussions. We thank Michael Glotzer for rat monoclonal tubulin (yol1/34) antibody.

AUTHOR CONTRIBUTIONS

NMC and JTG conceived and designed the experiments. NMC, DJS, and SR performed the experiments. JTG, NMC, DJS, and SR analyzed and interpreted data. NMC, DJS and JTG wrote the paper.

CONFLICT OF INTEREST

The authors declare that they have no conflict of interests.

SHORT SUPPORTING LEGENDS

Figure S1. Quantification of the AZI1:GFP that colocalize with RFP-TUB6 and anti-tubulin western blot of total and plastid fractions from *N. benthamiana* expressing AZI1$^{\Delta 2\text{-}25}$:GFP (X), AZI1$^{\Delta 2\text{-}30}$:GFP (XI), or mock-treated.

Figure S2. Flg22 treatment affects the levels of AZI1/EARLI1 and phosphorylation state of MPK3/MPK6 in *mpk3* and *mpk6* mutants.

Movie S1. Live imaging microscopy of AZI1:GFP and RFP-TUB6 expressing *N. benthamiana*.

Table S1**.** A summary of the *in vivo* microscopy and fractionation plastid association data for AZI1 variants.

Table S2. Vectors, constructs and primers list used in this study.

REFERENCES

- **Ambrose, C., Allard, J.F., Cytrynbaum, E.N. and Wasteneys, G.O.** (2011) A CLASP-modulated cell edge barrier mechanism drives cell-wide cortical microtubule organization in Arabidopsis. *Nat. Commun.*, **2**, 430.
- **Beckers, G.J.M., Jaskiewicz, M., Liu, Y., Underwood, W.R., He, S.Y., Zhang, S. and Conrath, U.** (2009) Mitogen-activated protein kinases 3 and 6 are required for full priming of stress responses in Arabidopsis thaliana. *Plant Cell*, **21**, 944–53.
- **Bigeard, J. and Hirt, H.** (2018) Nuclear signaling of plant MAPKs. *Front. Plant Sci.*, **9**, 1–18.
- **Blée, E.** (2002) Impact of phyto-oxylipins in plant defense. *Trends Plant Sci.*, **7**, 315–22.
- **Boller, T. and Felix, G.** (2009) A renaissance of elicitors: perception of microbe-associated molecular patterns and danger signals by pattern-recognition receptors. *Annu. Rev. Plant Biol.*, **60**, 379–406.
- **Bradford, M.M.** (1976) A rapid and sensitive method for the quantitation of microgram quantities of protein utilizing the principle of protein-dye binding. *Anal. Biochem.*, **72**, 248–54.
- **Breuers, F.K.H., Bräutigam, A. and Weber, A.P.M.** (2011) The plastid outer envelope - A highly dynamic interface between plastid and cytoplasm. *Front. Plant Sci.*, **2**, 97.
- **Bruce, B.D.** (2000) Chloroplast transit peptides: Structure, function and evolution. *Trends Cell Biol.*, **10**, 440–447.
- **Bull, C.T., Manceau, C., Lydon, J., Kong, H., Vinatzer, B.A. and Fischer-Le Saux, M.** (2010) Pseudomonas cannabina pv. cannabina pv. nov., and Pseudomonas cannabina pv. alisalensis (Cintas Koike and Bull, 2000) comb. nov., are members of the emended species Pseudomonas cannabina (ex Sutic & Dowson 1959) Gardan, Shafik, Belouin, Brosch, Grimont & . *Syst. Appl. Microbiol.*, **33**, 105–15.
- **Caplan, J.L., Kumar, A.S., Park, E., Padmanabhan, M.S., Hoban, K., Modla, S., Czymmek, K. and Dinesh-Kumar, S.P.** (2015) Chloroplast stromules function during

innate immunity. *Dev. Cell*, **34**, 45–57.

- **Caplan, J.L., Mamillapalli, P., Burch-Smith, T.M., Czymmek, K. and Dinesh-Kumar, S.P.** (2008) Chloroplastic protein NRIP1 mediates innate immune receptor recognition of a viral effector. *Cell*, **132**, 449–62.
- **Cecchini, N.M., Jung, H.W., Engle, N.L., Tschaplinski, T.J. and Greenberg, J.T.** (2015a) ALD1 regulates basal immune components and early inducible defense responses in Arabidopsis. *Mol. Plant. Microbe. Interact.*, **28**, 455–66.
- **Cecchini, N.M., Roychoudhry, S., Speed, D.J., et al.** (2019) Underground azelaic acid-conferred resistance to Pseudomonas syringae in Arabidopsis. *Mol. Plant. Microbe. Interact.*, **32**, 86–94.
- **Cecchini, Nicolás M, Steffes, K., Schläppi, M.R., Gifford, A.N. and Greenberg, J.T.** (2015b) Arabidopsis AZI1 family proteins mediate signal mobilization for systemic defence priming. *Nat. Commun.*, **6**, 7658.
- **Cesari, S.** (2018) Multiple strategies for pathogen perception by plant immune receptors. *New Phytol.*, **219**, 17–24.
- **Chanda, B., Xia, Y., Mandal, M.K., et al.** (2011) Glycerol-3-phosphate is a critical mobile inducer of systemic immunity in plants. *Nat. Genet.*, **43**, 421–7.
- **Chaturvedi, R., Venables, B., Petros, R. a, Nalam, V., Li, M., Wang, X., Takemoto, L.J. and Shah, J.** (2012) An abietane diterpenoid is a potent activator of systemic acquired resistance. *Plant J.*, **71**, 161–72.
- **Chinchilla, D., Bauer, Z., Regenass, M., Boller, T. and Felix, G.** (2006) The Arabidopsis receptor kinase FLS2 binds flg22 and determines the specificity of flagellin perception. *Plant Cell*, **18**, 465–76.
- **Conrath, U., Beckers, G.J.M.M., Langenbach, C.J.G.G. and Jaskiewicz, M.R.** (2015) Priming for enhanced defense. *Annu. Rev. Phytopathol.*, **53**, 97–119.
- **Daniotti, J.L., Pedro, M.P. and Valdez Taubas, J.** (2017) The role of S-acylation in protein trafficking. *Traffic*, **18**, 699–710.
- **Dvoráková, L., Cvrcková, F. and Fischer, L.** (2007) Analysis of the hybrid proline-rich protein families from seven plant species suggests rapid diversification of their sequences and expression patterns. *BMC Genomics*, **8**, 412.
- **Emanuelsson, O., Brunak, S., Heijne, G. von and Nielsen, H.** (2007) Locating proteins in the cell using TargetP, SignalP and related tools. *Nat. Protoc.*, **2**, 953–71.
- **Emanuelsson, O., Nielsen, H., Brunak, S. and Heijne, G. Von** (2000) Predicting subcellular localization of proteins based on their N-terminal amino acid sequence. *J. Mol. Biol.*, **300**, 1005–1016.
- **Erickson, J.L., Kantek, M. and Schattat, M.H.** (2017) Plastid-nucleus distance alters the behavior of stromules. *Front. Plant Sci.*, **8**, 1135.
- **Erickson, J.L. and Schattat, M.H.** (2018) Shaping plastid stromules — principles of in vitro membrane tubulation applied in planta. *Curr. Opin. Plant Biol.*, **46**, 48–54.

- **Gao, Q.M., Yu, K., Xia, Y., Shine, M.B., Wang, C., Navarre, D., Kachroo, A. and Kachroo, P.** (2014) Mono- and digalactosyldiacylglycerol lipids function nonredundantly to regulate systemic acquired resistance in plants. *Cell Rep.*, **9**, 1681–1692.
- **Gómez-Gómez, L. and Boller, T.** (2000) FLS2: An LRR receptor-like kinase involved in the perception of the bacterial elicitor flagellin in Arabidopsis. *Mol. Cell*, **5**, 1003–1011.
- **Grant, M.R. and Jones, J.D.G.** (2009) Hormone (dis)harmony moulds plant health and disease. *Science*, **324**, 750–2.
- **Gu, Y., Zavaliev, R. and Dong, X.** (2017) Membrane trafficking in plant immunity. *Mol. Plant*, **10**, 1026–1034.
- **Guttman, D.S. and Greenberg, J.T.** (2001) Functional analysis of the type III effectors AvrRpt2 and AvrRpm1 of Pseudomonas syringae with the use of a single-copy genomic integration system. *Mol. Plant. Microbe. Interact.*, **14**, 145–55.
- **Hames, B.D.** (1998) Gel Electrophoresis of Proteins: A Practical Approach. *Oxford Univ. Press. 3rd Edition.*
- **Hemsley, P.A.** (2015) The importance of lipid modified proteins in plants. *New Phytol.*, **205**, 476–489.
- **Jalmi, S.K. and Sinha, A.K.** (2015) ROS mediated MAPK signaling in abiotic and biotic stress- striking similarities and differences. *Front. Plant Sci.*, **6**, 769.
- **Jayasinghe, S., Hristova, K. and White, S.H.** (2001) Energetics, stability, and prediction of transmembrane helices. *J Mol Biol*, **312**, 927–934.
- **Jones, J.D.G. and Dangl, J.L.** (2006) The plant immune system. *Nature*, **444**, 323–329.
- **Jung, H.W., Tschaplinski, T.J., Wang, L., Glazebrook, J. and Greenberg, J.T.** (2009) Priming in systemic plant immunity. *Science*, **324**, 89–91.
- **Kang, Y., Jelenska, J., Cecchini, N.M., Li, Y., Lee, M.W., Kovar, D.R. and Greenberg, J.T.** (2014) HopW1 from Pseudomonas syringae disrupts the actin cytoskeleton to promote virulence in Arabidopsis. *PLoS Pathog.*, **10**, e1004232.
- **Khaled, S. Ben, Postma, J. and Robatzek, S.** (2015) A moving view: subcellular trafficking processes in pattern recognition receptor–triggered plant immunity. *Annu. Rev. Phytopathol.*, **53**, 379–402.
- **Kim, D.H. and Hwang, I.** (2013) Direct targeting of proteins from the cytosol to organelles: the ER versus endosymbiotic organelles. *Traffic*, 1–9.
- **Kumar, A.S., Park, E., Nedo, A., Alqarni, A., Ren, L., Hoban, K., Modla, S., McDonald, John H, et al.** (2018) Stromule extension along microtubules coordinated with actin-mediated anchoring guides perinuclear chloroplast movement during innate immunity. *Elife*, **7**, pii: e23625.
- **Lamberti, G., Gügel, I.L., Meurer, J., Soll, J. and Schwenkert, S.** (2011) The cytosolic kinases STY8, STY17, and STY46 are involved in chloroplast differentiation in Arabidopsis. *Plant Physiol.*, **157**, 70–85.

- **Lee, D.W., Lee, J. and Hwang, I.** (2017) Sorting of nuclear-encoded chloroplast membrane proteins. *Curr. Opin. Plant Biol.*, **40**, 1–7.
- **Lee, D.W., Yoo, Y.-J., Razzak, M.A. and Hwang, I.** (2018) Prolines in transit peptides are crucial for efficient preprotein translocation into chloroplasts. *Plant Physiol.*, **176**, 663–677.
- **Lee, J., Kim, D.H. and Hwang, I.** (2014) Specific targeting of proteins to outer envelope membranes of endosymbiotic organelles, chloroplasts, and mitochondria. *Front. Plant Sci.*, **5**, 1–11.
- **Lee, J., Lee, H., Kim, J., Lee, S., Kim, D.H., Kim, S. and Hwang, I.** (2011) Both the hydrophobicity and a positively charged region flanking the C-terminal region of the transmembrane domain of signal-anchored proteins play critical roles in determining their targeting specificity to the endoplasmic reticulum or endosymbiotic org. *Plant Cell*, **23**, 1588–607.
- **Lim, G.-H., Shine, M.B., de Lorenzo, L., et al.** (2016) Plasmodesmata localizing proteins regulate transport and signaling during systemic acquired immunity in plants. *Cell Host Microbe*, **19**, 541–549.
- **Littlejohn, G.R., Gouveia, J.D., Edner, C., Smirnoff, N. and Love, J.** (2010) Perfluorodecalin enhances in vivo confocal microscopy resolution of Arabidopsis thaliana mesophyll. *New Phytol.*, **186**, 1018–25.
- **Liu, Y. and Zhang, S.** (2004) Phosphorylation of 1-aminocyclopropane-1-carboxylic acid synthase by MPK6, a stress-responsive mitogen-activated protein kinase, induces ethylene biosynthesis in Arabidopsis. *Plant Cell*, **16**, 3386–99.
- **Lu, H., Rate, D.N., Song, J.T. and Greenberg, J.T.** (2003) ACD6, a novel ankyrin protein, is a regulator and an effector of salicylic acid signaling in the Arabidopsis defense response. *Plant Cell*, **15**, 2408–20.
- **Macho, A.P. and Zipfel, C.** (2014) Plant PRRs and the Activation of Innate Immune Signaling. *Mol. Cell*, **54**, 263–272.
- **Mackenzie, S.A.** (2005) Plant organellar protein targeting: A traffic plan still under construction. *Trends Cell Biol.*, **15**, 548–554.
- **Martin, T., Sharma, R., Sippel, C., Waegemann, K., Soll, J. and Vothknecht, U.C.** (2006) A protein kinase family in Arabidopsis phosphorylates chloroplast precursor proteins. *J. Biol. Chem.*, **281**, 40216–23.
- **Martinez-Medina, A., Flors, V., Heil, M., Mauch-Mani, B., Pieterse, C.M.J., Pozo, M.J., Ton, J., Dam, N.M. van and Conrath, U.** (2016) Recognizing plant defense priming. *Trends Plant Sci.*, **21**, 818–822.
- **Medina-Puche, L., Tan, H., Dogra, V., et al.** (2020) A defense pathway linking plasma membrane and chloroplasts and co-opted by pathogens. *Cell*, 1–16.
- **Mishina, T.E. and Zeier, J.** (2007) Pathogen-associated molecular pattern recognition rather than development of tissue necrosis contributes to bacterial induction of systemic acquired resistance in Arabidopsis. *Plant J.*, **50**, 500–13.

- **Návarová, H., Bernsdorff, F., Döring, A.-C. and Zeier, J.** (2012) Pipecolic acid, an endogenous mediator of defense amplification and priming, is a critical regulator of inducible plant immunity. *Plant Cell*, **24**, 5123–41.
- **Nelson, B.K., Cai, X., Nebenführ, A. and Nebenfu, A.** (2007) A multicolored set of in vivo organelle markers for co-localization studies in Arabidopsis and other plants. *Plant J.*, **51**, 1126–36.
- **Nomura, H., Komori, T., Uemura, S., et al.** (2012) Chloroplast-mediated activation of plant immune signalling in Arabidopsis. *Nat. Commun.*, **3**, 926.
- **Park, S.-W., Kaimoyo, E., Kumar, D., Mosher, S. and Klessig, D.F.** (2007) Methyl Salicylate Is a Critical Mobile Signal for Plant Systemic Acquired Resistance. *Science*, **318**, 113–116.
- **Parker, J.E.** (2009) The quest for long-distance signals in plant systemic immunity. *Sci. Signal.*, **2**, pe31.
- **Pieterse, C.M.J., Zamioudis, C., Berendsen, R.L., Weller, D.M., Wees, S.C.M. van and Bakker, P. a H.M.** (2014) Induced systemic resistance by beneficial microbes. *Annu. Rev. Phytopathol.*, **52**, 347–75.
- **Pitzschke, A., Datta, S. and Persak, H.** (2014) Salt stress in Arabidopsis: lipid transfer protein AZI1 and its control by mitogen-activated protein kinase MPK3. *Mol. Plant*, **7**, 722–38.
- **Pitzschke, A., Xue, H., Persak, H., Datta, S. and Seifert, G.** (2016) Post-translational modification and secretion of azelaic acid induced 1 (AZI1), a hybrid proline-rich protein from Arabidopsis. *Int. J. Mol. Sci.*, **17**, 85.
- **Prost, I., Dhondt, S., Rothe, G., et al.** (2005) Evaluation of the antimicrobial activities of plant oxylipins supports their involvement in defense against pathogens. *Plant Physiol.*, **139**, 1902–13.
- **Rayapuram, N., Bigeard, J., Alhoraibi, H., Bonhomme, L., Hesse, A.M., Vinh, J., Hirt, H. and Pflieger, D.** (2018) Quantitative phosphoproteomic analysis reveals shared and specific targets of Arabidopsis mitogen-activated protein kinases (MAPKs) MPK3, MPK4, and MPK6. *Mol. Cell. Proteomics*, **17**, 61–80.
- **Ren, J., Wen, L., Gao, X., Jin, C., Xue, Y. and Yao, X.** (2008) CSS-Palm 2.0: An updated software for palmitoylation sites prediction. *Protein Eng. Des. Sel.*, **21**, 639–644.
- **Riedlmeier, M., Ghirardo, A., Wenig, M., et al.** (2017) Monoterpenes Support Systemic Acquired Resistance within and between Plants. *Plant Cell*, **29**, 1440–1459.
- **Rodriguez, M.C.S., Petersen, M. and Mundy, J.** (2010) Mitogen-activated protein kinase signaling in plants. *Annu. Rev. Plant Biol.*, **61**, 621–49.
- **Schwessinger, B., Roux, M., Kadota, Y., Ntoukakis, V., Sklenar, J., Jones, A. and Zipfel, C.** (2011) Phosphorylation-dependent differential regulation of plant growth, cell death, and innate immunity by the regulatory receptor-like kinase BAK1. *PLoS Genet.*, **7**, e1002046.
- **Smertenko, A.P., Deeks, M.J. and Hussey, P.J.** (2010) Strategies of actin reorganisation in

plant cells. *J. Cell Sci.*, **123**, 3019–28.

- **Spoel, S.H. and Dong, X.** (2012) How do plants achieve immunity? Defence without specialized immune cells. *Nat. Rev. Immunol.*, **12**, 89–100.
- **Su, J., Zhang, M., Zhang, L., Sun, T., Liu, Y., Lukowitz, W., Xu, J. and Zhang, S.** (2017) Regulation of stomatal immunity by interdependent functions of a pathogen-responsive MPK3/MPK6 cascade and abscisic acid. *Plant Cell*, **29**, 526–542.
- **Tateda, C., Zhang, Z., Shrestha, J., Jelenska, J., Chinchilla, D. and Greenberg, J.T.** (2014) Salicylic acid regulates Arabidopsis microbial pattern receptor kinase levels and signaling. *Plant Cell*, **26**, 4171–87.
- **Torres Zabala, M. de, Littlejohn, G., Jayaraman, S., et al.** (2015) Chloroplasts play a central role in plant defence and are targeted by pathogen effectors. *Nat. plants*, **1**, 15074.
- **Truman, W., Bennett, M.H., Kubigsteltig, I., Turnbull, C. and Grant, M.** (2007) Arabidopsis systemic immunity uses conserved defense signaling pathways and is mediated by jasmonates. *Proc. Natl. Acad. Sci. U. S. A.*, **104**, 1075–80.
- **Ueda, K., Matsuyama, T. and Hashimoto, T.** (1999) Visualization of microtubules in living cells of transgenic Arabidopsis thaliana Rapid communication. *Protoplasma*, **206**, 201–206.
- **Vanacker, H., Lu, H., Rate, D.N. and Greenberg, J.T.** (2001) A role for salicylic acid and NPR1 in regulating cell growth in Arabidopsis. *Plant J.*, **28**, 209–216.
- **Vinatzer, B.A., Teitzel, G.M., Lee, M.-W., Jelenska, J., Hotton, S., Fairfax, K., Jenrette, J. and Greenberg, J.T.** (2006) The type III effector repertoire of Pseudomonas syringae pv. syringae B728a and its role in survival and disease on host and non-host plants. *Mol. Microbiol.*, **62**, 26–44.
- **Waizenegger, T., Stan, T., Neupert, W. and Rapaport, D.** (2003) Signal-anchor domains of proteins of the outer membrane of mitochondria: Structural and functional characteristics. *J. Biol. Chem.*, **278**, 42064–42071.
- **Wang, C., El-Shetehy, M., Shine, M.B., Yu, K., Navarre, D., Wendehenne, D., Kachroo, A. and Kachroo, P.** (2014) Free radicals mediate systemic acquired resistance. *Cell Rep.*, **7**, 348–355.
- **Wang, H., Ngwenyama, N., Liu, Y., Walker, J.C. and Zhang, S.** (2007) Stomatal development and patterning are regulated by environmentally responsive mitogen-activated protein kinases in Arabidopsis. *Plant Cell*, **19**, 63–73.
- **Wang, W.-M., Liu, P.-Q., Xu, Y.-J. and Xiao, S.** (2016) Protein trafficking during plant innate immunity. *J. Integr. Plant Biol.*, **58**, 284–298.
- **Wittek, F., Hoffmann, T., Kanawati, B., et al.** (2014) Arabidopsis ENHANCED DISEASE SUSCEPTIBILITY1 promotes systemic acquired resistance via azelaic acid and its precursor 9-oxo nonanoic acid. *J. Exp. Bot.*, **65**, 5919–31.
- **Yu, K., Soares, J.M., Mandal, M.K., et al.** (2013) A feedback regulatory loop between G3P and lipid transfer proteins DIR1 and AZI1 mediates azelaic-acid-induced systemic immunity.

Cell Rep., **3**, 1266–78.

- **Zeier, J.** (2013) New insights into the regulation of plant immunity by amino acid metabolic pathways. *Plant, Cell Environ.*, **36**, 2085–2103.
- **Zhang, Y. and Schläppi, M.** (2007) Cold responsive EARLI1 type HyPRPs improve freezing survival of yeast cells and form higher order complexes in plants. *Planta*, **227**, 233–43.
- **Zhang, Z., Shrestha, J., Tateda, C. and Greenberg, J.T.** (2014) Salicylic acid signaling controls the maturation and localization of the Arabidopsis defense protein ACCELERATED CELL DEATH6. *Mol. Plant*, **7**, 1365–83.
- **Zoeller, M., Stingl, N., Krischke, M., Fekete, A., Waller, F., Berger, S. and Mueller, M.J.** (2012) Lipid profiling of the Arabidopsis hypersensitive response reveals specific lipid peroxidation and fragmentation processes: biogenesis of pimelic and azelaic acid. *Plant Physiol.*, **160**, 365–78.
- **Zuegge, J., Ralph, S., Schmuker, M., McFadden, G.I. and Schneider, G.** (2001) Deciphering apicoplast targeting signals – feature extraction from nuclear-encoded precursors of Plasmodium falciparum apicoplast proteins. *Gene*, **280**, 19–26.

SUPPLEMENTAL DATA

Supplemental Figure 3.1.

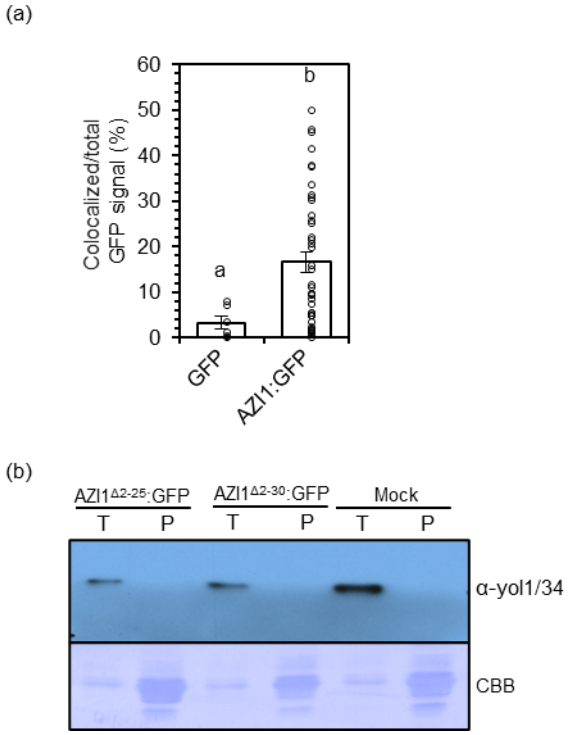

Figure S3.1. Quantification of the AZI1:GFP that colocalize with RFP:TUB6 and anti-tubulin Western blot of total and plastid fractions from N. benthamiana expressing AZI1$^{\Delta 2\text{-}25}$:GFP (X), AZI1$^{\Delta 2\text{-}30}$:GFP (XI), or mock-treated

(a) Quantification of the control GFP and AZI1:GFP that colocalize with RFP-TUB6. The averages +/- standard error of colocalized vs total GFP signal from one (control GFP) and five (AZI1:GFP) independent experiments are shown. Different letters indicate statistically significant differences ($P<0.05$, analysis of variance (ANOVA), Tukey test). Individual data points are shown on the bar chart as scatter-dots. (b) Western blot of total extracts from agrotransformed N. benthamiana tissues expressing AZI1Δ2-25:GFP (X), AZI1Δ2-30:GFP (XI), or mock (infiltration solution only). Bands were revealed using anti-yol34 (anti-tubulin) antibody. The blots stained with Coomassie blue (CBB) are presented to show loading.

Supplemental Figure 3.2.

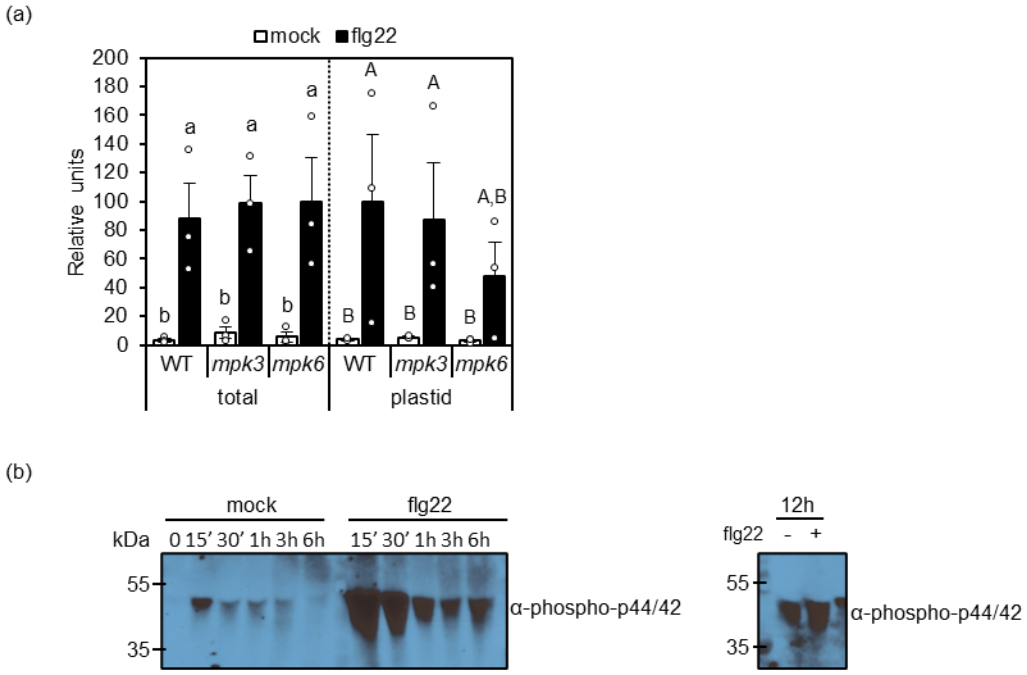

Figure S3.2. Flg22 treatment affects the levels of AZI1/EARLI1 and phosphorylation state of MPK3/MPK6 in *mpk3* and *mpk6* mutants.

(a) Quantitation of AZI1–EARLI1 protein levels total and plastid fraction from Arabidopsis leaves of WT Col-0 and *mpk3* and *mpk6* plants 6h post treatment with 1 µM flg22 or mock relative to the total protein content in each Coomassie blue membrane lane. The highest value in total or plastid fractions was set to 100 in the relative units. Averages with standard error from three independent experiments are shown. Different lower or uppercase letters indicate statistically significant differences ($P<0.01$, analysis of variance (ANOVA), Tukey test). The dotted line in the graph indicates that the total and plastid fractions were analyzed independently. Individual data points are shown on the bar chart as scatter-dots. **(b)** Western blot of total extracts from WT Col-0 Arabidopsis samples used in Figure 3a and 3b to test MPK3/6 activation at different times post infiltration with 1 µM flg22 (+) or mock (-). Bands were detected using phospho-p44/42 MAPK (Erk1/2) antibody that detect MPK3/MPK4/MPK6 phosphorylated kinase isoforms.

Table S3.1. Summary of the in vivo microscopy and fractionation plastid association data for AZI1 variants.

Variants	Mutated Regions	Plastid localization	
		in vivo (microscopy)	fractionation
AZI1	full length	++	+
AZI1$^{\Delta 77\text{-}161}$	LTP	++	+
AZI1$^{\Delta 40\text{-}76}$	PRR	-	-
AZI1$^{\Delta 32\text{-}76}$		-	-
AZI1$^{\Delta 28\text{-}76}$		-	-
AZI1$^{\Delta 31\text{-}37}$	CPR	+	+
AZI1^{C28A}	HD-cysteines	++	+
AZI1^{C30A}		++	+
AZI1$^{C28/30A}$		++	+
AZI1$^{\Delta 2\text{-}25}$	HD	- (+ contact points)	+
AZI1$^{\Delta 2\text{-}30}$		- (+ contact points)	+

(++), (+), (+/-), (-): indicate level of plastids association for each construct.

Table S3.2. Vectors, constructs and primers list used in this study

Plasmid	Parent vector	Description	Antibiotic[a)]	Reference
pBAV150	TA7001	Gateway binary plant expression vector (*Dex* promoter, C-terminal HA-tag)	Km^R/ Cm^R /$BASTA^R$	(Vinatzer *et al.*, 2006)
pBAV154	TA7001	Gateway binary plant expression vector (*Dex* promoter, C-terminal HA-tag)	Km^R/ Cm^R /$BASTA^R$	(Vinatzer *et al.*, 2006)
Lifeact-GFP	pMDC43	CaMV 35S:Lifeact-GFP	Km^R/Hyg^R	(Smertenko *et al.*, 2010)
RFP-TUB6	pCAMBIA1300	UBQ1::RFP:TUB6	Km^R/Hyg^R	(Ambrose *et al.*, 2011)
pSITE-4NA-MPK3	pSITE-4NA	35S::MPK3:mRFP1 (CD-1642)	Sp^R	This study
pSITE-4NA-MPK6	pSITE-4NA	35S-MPK6:mRFP1 (CD-1642)	Sp^R	This study
pBAV154-AZI1	pBAV154	Dex:AZI1:HA in a binary vector	Km^R /$BASTA^R$	(Cecchini *et al.*, 2015b)
pBAV150-I. AZI1:GFP	pBAV150	Dex:AZI1:GFP in a binary vector	Km^R /$BASTA^R$	(Cecchini *et al.*, 2015b)
pBAV150-II. $AZI1^{\Delta 77-161}$:GFP	pBAV150	Dex::AZI1-variant:GFP in a binary vector	Km^R /$BASTA^R$	(Cecchini *et al.*, 2015b)
pBAV150-III. $AZI1^{\Delta 38-161}$:GFP	pBAV150	Dex::AZI1-variant:GFP in a binary vector	Km^R /$BASTA^R$	This study
pBAV150-IV. $AZI1^{\Delta 38-161\_C28A/C30A}$:GFP	pBAV150	Dex::AZI1-variant:GFP in a binary vector	Km^R /$BASTA^R$	This study
pBAV150-V. $AZI1^{\Delta 40-76}$:GFP	pBAV150	Dex::AZI1-variant:GFP in a binary vector	Km^R /$BASTA^R$	This study

pBAV150-VI. AZI1$^{\Delta 32-76}$:GFP	pBAV150	Dex::AZI1-variant:GFP in a binary vector	Km^{R} /BASTA^{R}	(Cecchini *et al.*, 2015b)
pBAV154-VI. AZI1$^{\Delta 32-76}$:HA	pBAV154	Dex::AZI1-variant:HA in a binary vector	Km^{R} /BASTA^{R}	This study
pBAV150-VII. AZI1$^{\Delta 28-76}$:GFP	pBAV150	Dex::AZI1-variant:GFP in a binary vector	Km^{R} /BASTA^{R}	This study
pBAV150-VIII. AZI1$^{\Delta 31-37}$:GFP	pBAV150	Dex::AZI1-variant:GFP in a binary vector	Km^{R} /BASTA^{R}	This study
pBAV150-IX. AZI1^{C28A}:GFP	pBAV150	Dex::AZI1-variant:GFP in a binary vector	Km^{R} /BASTA^{R}	This study
pBAV150-IX. AZI1^{C28A}:GFP	pBAV150	Dex::AZI1-variant:GFP in a binary vector	Km^{R} /BASTA^{R}	This study
pBAV150-IX. AZI1$^{C28A/C30A}$:GFP	pBAV150	Dex::AZI1-variant:GFP in a binary vector	Km^{R} /BASTA^{R}	This study
pBAV150-X. AZI1$^{\Delta 2-25}$:GFP	pBAV150	Dex::AZI1-variant:GFP in a binary vector	Km^{R} /BASTA^{R}	This study
pBAV150-XI. AZI1$^{\Delta 2-30}$:GFP	pBAV150	Dex::AZI1-variant:GFP in a binary vector	Km^{R} /BASTA^{R}	This study
pBAV150-XII. AZI1$^{\Delta 2-30/\Delta 77-161}$:GFP	pBAV150	Dex::AZI1-variant:GFP in a binary vector	Km^{R} /BASTA^{R}	This study
pBAV150-XIII. AZI1$^{\Delta 2-77}$:GFP	pBAV150	Dex::AZI1-variant:GFP in a binary vector	Km^{R} /BASTA^{R}	This study
pBAV150-XIV. AZI1$^{\Delta 2-30/\Delta 103-161}$:GFP	pBAV150	Dex::AZI1-variant:GFP in a binary vector	Km^{R} /BASTA^{R}	This study
pBAV150-XV. AZI1$^{\Delta 2-52/\Delta 103-161}$:GFP	pBAV150	Dex::AZI1-variant:GFP in a binary vector	Km^{R} /BASTA^{R}	This study
pBAV150-XVI. AZI1$^{\Delta 2-52}$:GFP	pBAV150	Dex::AZI1-variant:GFP in a binary vector	Km^{R} /BASTA^{R}	This study

Primers		
Name	Sequence (5’-3’)	Purpose
Actin qPCR F	GAGCGGGAAATTGTCAGGGA	Purpose
Actin qPCR R	GAGCGGGAAATTGTCAGGGA	Purpose
AZI1-cacc-FW	GAGCGGGAAATTGTCAGGGA	Purpose
AZI1-nostop-RV	GAGCGGGAAATTGTCAGGGA	Purpose
AZI1_SP+CPR_RV	GAGCGGGAAATTGTCAGGGA	Purpose
AZI1 signalP-C-LTP RV	GAGCGGGAAATTGTCAGGGA	Purpose
AZI1 C-LTP FW	GAGCGGGAAATTGTCAGGGA	Purpose
SP+CPR---Cterm RV	GAGCGGGAAATTGTCAGGGA	Purpose
SP+CPR---AZI1 C-LTP FW	GAGCGGGAAATTGTCAGGGA	Purpose
SP-CxC-CPR---Cterm RV	GAGCGGGAAATTGTCAGGGA	Purpose
SP-CxC-CPR---AZI1 C-LTP FW	GAGCGGGAAATTGTCAGGGA	Purpose
AZI1w-oCPR_RV	GAGCGGGAAATTGTCAGGGA	Purpose
AZI1w-oCPR_FW	GAGCGGGAAATTGTCAGGGA	Purpose
AZI1_C28A_RV	GAGCGGGAAATTGTCAGGGA	Purpose
AZI1_C28A_FW	GAGCGGGAAATTGTCAGGGA	Purpose
AZI1_C30A_RV	GAGCGGGAAATTGTCAGGGA	Purpose
AZI1_C30A_FW	GAGCGGGAAATTGTCAGGGA	Purpose
AZI1_C28A-C30A_RV	GAGCGGGAAATTGTCAGGGA	Purpose
AZI1_C28A-C30A_FW	GAGCGGGAAATTGTCAGGGA	Purpose
AZI1-LTP_FW	GAGCGGGAAATTGTCAGGGA	Purpose
AZI1-SP_atg_FW	GAGCGGGAAATTGTCAGGGA	Purpose

caccATG_AZI1 woSP woCxC_FW	GAGCGGGAAATTGTCAGGGA	Purpose
AZI1 N-term -RV	GAGCGGGAAATTGTCAGGGA	Purpose
AZI1_307-Q102_RV	GAGCGGGAAATTGTCAGGGA	Purpose
AZI1_157-P53_FW	GAGCGGGAAATTGTCAGGGA	Purpose
MPK3 FW	GAGCGGGAAATTGTCAGGGA	Purpose
MPK3RV	GAGCGGGAAATTGTCAGGGA	Purpose
MPK6 FW	GAGCGGGAAATTGTCAGGGA	Purpose
MPK6RV	GAGCGGGAAATTGTCAGGGA	Purpose

a) BASTA^R, BASTA (glufosinate ammonium) resistance; Cm^R, chloroamphenicol resistance; Km^R, kanamycin resistance; Sp^R, spectinomycin resistance; Rif^R, rifampicin resistance; Tet^R, tetracycline resistance.

CHAPTER 4

THE ROLE OF THE AZI1 PROTEIN FAMILY IN SYSTEMIC DEFENSE AND AZELAIC ACID SIGNALING

Preface

This chapter includes a new, unpublished from collaborative work performed with Dr. Claire Parent that was completed under the supervision of Professor Jean Greenberg. I authored this chapter alone with helpful comments from Professor Greenberg. My contributions to the project are as follows:

I developed the CRISPR/Cas9 mutagenesis project and selected the targets with Dr. Parent. Dr. Parent designed the gRNA adaptors (Table 4.2), locus-specific and sequencing primers (Table 4.1), and cloned the constructs into the destination vector.

Dr. Parent and I transformed the CRISPR/Cas9 destination vectors into the plants and selected mutants with Dr. Parent performing the majority of the BASTA treatments and transformations. Dr. Parent selected and collected seed from T2 plants with the help of Dr. Zeeshan Banday. I sequenced T3 plants to characterize their mutations in AZI3, AZI4, AZI5, or AZI6 and collected seed from plants with biallelic mutations.

I performed each of the experiments described herein. Jessica Morgan assisted with one replicate of the systemic disease resistance assays (Fig 4.2A).

4.1 Introduction

Azelaic acid (AZA) is present and active in both aerial and underground plant organs, primes the induction of SAR-like systemic immune responses when exogenously applied to either leaves or roots, and restricts primary root elongation while enhancing lateral root density when applied to roots (Bouain et al., 2018; Cecchini et al., 2015; Chapter 2, Cecchini et al., 2019; Jung et al., 2009; Yu et al., 2013). Sensitivity to and systemic transport of AZA require the SAR- and ISR-essential LTPs AZI1 and EARLI1, which are induced by AZA, pathogen effectors, and infections (Bouain et al., 2018; Cecchini et al., 2015, Chapter 2, Cecchini et al., 2019; Cecchini et al., 2021; Jung et al., 2009). *azi1-1* and *earli1-1* plants mutants fail to mount systemic defenses after the application of AZA to roots and show reduced changes in root morphology (Chapter 2, Cecchini et al., 2019). Whereas wild-type plants show more severely inhibited primary root elongation and greatly enhanced lateral root density, loss of either *AZI1* or *EARLI1* causes a more moderate reduction in primary root elongation and a weak increase in lateral root density (Bouain et al., 2018; Chapter 2, Cecchini et al., 2019).

In addition to *AZI1* and *EARLI1*, the AZI1 gene family encodes five additional proteins that are tandemly arrayed on chromosome 4 and show a high degree of sequence similarity to *AZI1* and *EARLI1* (Fig. 1.3). These seven genes encode highly similar proteins that can be divided into three main domains based on amino acid sequence: 1) an N-terminal HD; 2) an internal PRR of varying length; 3) and a C-terminal LTP domain, which contains a highly conserved 8-cysteine motif (Cecchini et al., 2015; Dvořáková et al., 2007, 2012).

AZI1's N-terminal HD and PRR form a novel bipartite plastid targeting signal which localizes the protein to plastid envelope membranes (Fig 1.2 and 1.3; Cecchini et al., 2015; Cecchini, Speed et al., 2021). AZI1's HD shows a degree of hydrophobicity similar to signal

anchor proteins and is sufficient to drive membrane association (Kim et al., 2011; Lee et al., 2014; Cecchini et al., 2015; Cecchini, Speed et al., 2021). Although deletion of the HD disrupts AZI1's ring-like association with plastids, only deletion of the PRR completely abolishes AZI1's plastid association, which posits the PRR as a plastid targeting signal (Cecchini, Speed et al., 2021). Furthermore, AZI3, which has a PRR similar to AZI1 and EARLI also targets to plastids when transiently expressed in tobacco leaves (Cecchini et al., 2015). In contrast, AZI5, AZI6, and AZI7, which have a very short or no PRRs, do not target to plastids like AZI1, EARLI1, or AZI3.

The AZI1 family genes and the proteins they encode are highly similar, have coding regions comprising <700 bases each, and lack introns. Thus, it is likely that they function as natural variants of each other similar to an allelic series (Fig. 1.3). Furthermore, *AZI5* and *AZI6* have identical coding sequences and the immune-priming defects in *azi1* mutants can be rescued by overexpression of *EARLI1* (Cecchini et al., 2015). This also suggests a degree of interchangeability and similar functionality among the (plastid-targeted) AZI1 family proteins (Cecchini et al., 2015). As such, I hypothesized that the AZI1 family proteins with PRRs similar to AZI1 are essential for systemic defense priming and signal mobilization. Although null mutants for *azi1* and *earli1* exist and permit the analysis of their roles in various signaling and defense priming pathways, no such mutants exist for *AZI3*, *AZI4*, *AZI5*, *AZI6*, or *AZI7*.

Thus, in collaboration with Dr. Claire Parent, I employed a CRISPR/Cas9 mutagenesis strategy to induce targeted mutations in individual AZI1 family genes. CRISPR/Cas9 systems employ a bacterial endonuclease to permit the induction of targeted double strand breaks in the DNA backbone. We employed such a system to introduce mutations into the *AZI3*, *AZI4*, *AZI5*, and *AZI6* gene loci. Herein, I characterize three novel mutants of *azi3*, one novel mutant of *azi4*,

and two novel mutants of *azi5azi6* (Fig 4.1). Because the coding regions of AZI5 and AZI6 are identical, the genes could not be targeted individually.

I assessed these mutants' ability to prime SAR and respond to root-applied AZA similar to *azi1* and *earli1*. Because root-applied AZA can prime defenses in aerial tissues and induces changes in root morphology, I assessed the impacts of root-applied AZA on the development of leaf tissues (Bouain et al., 2018; Chapter 2, Cecchini et al., 2019). I also assessed if loss (*azi1-1*) or mutation (*azi1* family CRISPR mutants) of the AZI1 family proteins affected root development when exposed to high concentrations of salt.

4.2 Material and Methods

Plants, bacteria, and plasmids

All plants used for infections were 25- to 28-day-old *Arabidopsis thaliana* in the Columbia-0 (Col-0; wild-type/WT) background. *azi1-1* and *earli1-1* t-DNA mutants were previously described. Plants were grown in soil under 12-h day (08:00 to 20:00) and 12-h night conditions at 20°C, 200–230µmol $s^{-1}m^{-2}$ light at rosette level and 50–70% relative humidity.

Transgenic *Arabidopsis* were generated by the floral dip method (cite). Transformants were selected by spraying 10-day-old seedlings grown in soil with BASTA (120mg/L + 0.5% Silwet-77). BASTA treatment was re-applied every 3-4 days for a total of four treatments. To determine the genotype of the T3 plants, DNA was extracted from 3 leaf discs collected from an individual T3 plant using a Cetyltrimetyl ammonium bromide (CTAB)-based method (Clarke, 2009). The target region was PCR-amplified using the appropriate locus-specific primers (Table 4.1), confirmed via agarose gel electrophoresis, cleaned using a QIAquick PCR

Figure 4.1 Sequence Alignment and Cartoons Diagramming the *azi1* family CRISPR mutants

A)

>**AZI3**

MASKNSASLA LFFALNILFF TLTAGTNCRC NPSPKPRPLP NPKVPSPKVP TPSVPSPYVP
TPSVPSPSVP TPSVPSPSVP SPNPTPVIPP RTPGSSGNCP IDALRLGVCA NVLSGLLNVQ
LGQPSPQPCC SLIQGLVDLD AAVCLCTALR ANVLGINLNV PISLSVLLNV CNRRLPSNFQ
CA

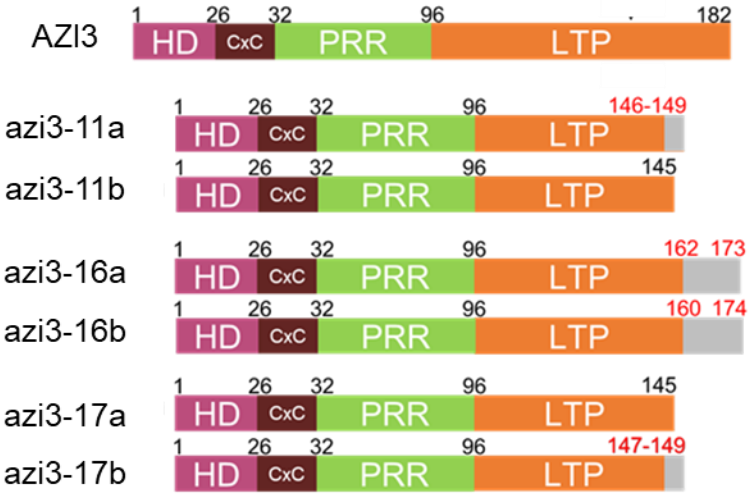

>**azi3.11a**

MASKNSASLA LFFALNILFF TLTAGTNCRC NPSPKPRPLP NPKVPSPKVP TPSVPSPYVP
TPSVPSPSVP TPSVPSPSVP SPNPTPVIPP RTPGSSGNCP IDALRLGVCA NVLSGLLNVQ
LGQPSPQPCC SLIQGLVDLD AAVCLWHCS

>**azi3.11b**

MASKNSASLA LFFALNILFF TLTAGTNCRC NPSPKPRPLP NPKVPSPKVP TPSVPSPYVP
TPSVPSPSVP TPSVPSPSVP SPNPTPVIPP RTPGSSGNCP IDALRLGVCA NVLSGLLNVQ
LGQPSPQPCC SLIQGLVDLD AAVCL

>**azi3.16a**

MASKNSASLA LFFALNILFF TLTAGTNCRC NPSPKPRPLP NPKVPSPKVP TPSVPSPYVP
TPSVPSPSVP TPSVPSPSVP SPNPTPVIPP RTPGSSGNCP IDALRLGVCA NVLSGLLNVQ
LGQPSPQPCC SLIQGLVDLD AAVCLCTALR ANVLGINLNV PDAHSLLFKI ITV

>**azi3.16b**

MASKNSASLA LFFALNILFF TLTAGTNCRC NPSPKPRPLP NPKVPSPKVP TPSVPSPYVP
TPSVPSPSVP TPSVPSPSVP SPNPTPVIPP RTPGSSGNCP IDALRLGVCA NVLSGLLNVQ
LGQPSPQPCC SLIQGLVDLD AAVCLCTALR ANVLGINLNA QYDAHSLLFK IITV

>**azi3.17a**

MASKNSASLA LFFALNILFF TLTAGTNCRC NPSPKPRPLP NPKVPSPKVP TPSVPSPYVP
TPSVPSPSVP TPSVPSPSVP SPNPTPVIPP RTPGSSGNCP IDALRLGVCA NVLSGLLNVQ
LGQPSPQPCC SLIQGLVDLD AAVCL

>**azi3.17b**

MASKNSASLA LFFALNILFF TLTAGTNCRC NPSPKPRPLP NPKVPSPKVP TPSVPSPYVP
TPSVPSPSVP TPSVPSPSVP SPNPTPVIPP RTPGSSGNCP IDALRLGVCA NVLSGLLNVQ
LGQPSPQPCC SLIQGLVDLD AAVCLCHCS

Figure 4.1 Sequence Alignment and Cartoons Diagramming the *azi1* family CRISPR mutants

B)

>AZI4

MASKNSTSLA LFFALNILFF TLTTATDCRC NLSPKPRTVP SPKVPSPKYP SPSIPSPSVP
TPSVPTPSVP TPSVPSPNPT PVTPPRTPGS SGNCPIDALR LGVCANVLSG LLNVQLGQPS
AQPCCSLIQG LVDLDAAICL CTALRANVLG INLNVPISLS VLLNVCNRRL PSDFQCA

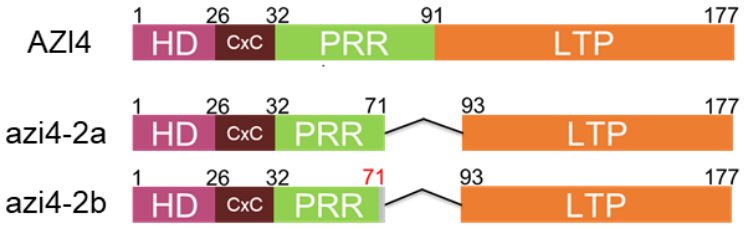

>azi4-2a

MASKNSTSLA LFFALNILFF TLTTATDCRC NLSPKPRTVP SPKVPSPKYP SPSIPSPSVP
TPSVPTPSVP TNCPIDALRL GVCANVLSGL LNVQLGQPSA QPCCSLIQGL VDLDAAICLC
TALRANVLGI NLNVPISLSV LLNVCNRRLP SDFQCA

>azi4-2b

MASKNSTSLA LFFALNILFF TLTTATDCRC NLSPKPRTVP SPKVPSPKYP SPSIPSPSVP
TPSVPTPSVP KNCPIDALRL GVCANVLSGL LNVQLGQPSA QPCCSLIQGL VDLDAAICLC
TALRANVLGI NLNVPISLSV LLNVCNRRLP SDFQCA

C)

>AZI5/6

MASKISASLV IFLTFNILFF TLTTACGGGC SSTPKPKPKP KSTGSCPKDT LKLGVCANVL
KDLLKIQLGT PPVKPCCSLL NGLVDLEAAA CLCTALKAKV LGINLNVPVS LSLLLNVCGK
KVPSGFVCA

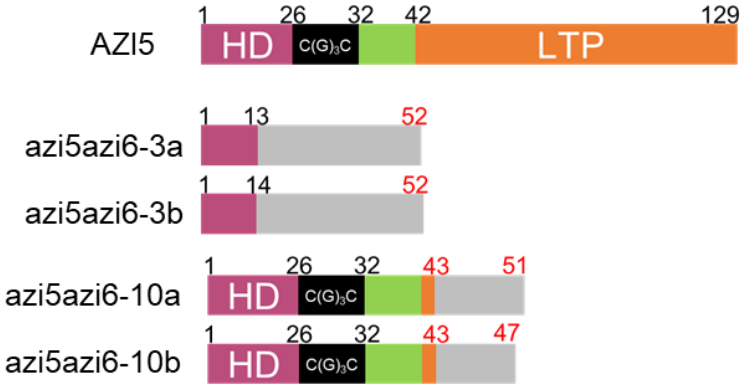

>azi5azi6-3a

MASKISASLV IFPLNPNLSP SPPEAALKTL SSSAFAPMFS RIFSKFSWEH HQ

>azi5azi6-3b

MASKISASLV IFLLNPNLSP SPPEAALKTL SSSAFAPMFS RIFSKFSWEH HQ

>azi5azi6-10a

MASKISASLV IFLTFNILFF TLTTACGGGC SSTPKPKPKP KSSLVVRSSM V

>azi5azi6-10b

MASKISASLV IFLTFNILFF TLTTACGGGC SSTPKPKPKP KSHRKLP

Figure 4.1 Sequence Alignment and Cartoons Diagramming the azi1 family CRISPR mutants
A) WT (Top) and mutant (bottom) amino acid sequences of B) AZI3, C) AZI4, and D) AZI5/6 (AZI5 and AZI6 are identical). The PRR starting at amino acid 32 is underlined in each WT sequence. The HD comprises amino acids 1-25 in AZI3, AZI4, and AZI5/6. Amino acids 26-32 contain a putative acylation site in AZI3 and AZI4 (CxC, brown). The PRR is underlined in each WT sequence. Sequences in grey are not present in the WT protein. Note that the CRISPR allele of AZI4 deletes two highly conserved regions in the PRR that are indicated by the red boxes in Figure 1.3B.

Purification/Clean-up kit (QIAgen, # 28104) and Sanger-sequenced using the specific sequencing primers (Table 4.1). To determine allelic heterogeneity, sequencing results were analyzed using the Degenerate Sequence Decode program (DsDecode; Liu et al., 2015; Ma et al., 2016). The individual alleles revealed by DsDecode were then re-aligned to the reference sequences using SnapGene (Insightful Science, snapgene.com) and expasy.org/translate to determine the amino acid sequence of each allele. Three biallelic mutants of *AZI3*, one biallelic mutant of *AZI4*, and two biallelic double mutants of *AZI5AZI6* were identified in this screen and selected for further study. T4 seeds from one individual plant per sequenced T3 line that was sequenced was used for experiments.

Table 4.1 – Locus-Specific and Sanger Sequencing Primers Employed in the Characterization of *azi1* Family CRISPR Mutants

Name	Sequence (5'-3')	length
AZI3 locus primer 1F	TGCGCGGAAAAAGATAACGC	20
AZI3 locus primer 1R	TAGGCCGCTCCCAAATCCTA	20
AZI3 sequencing primer 1F	AGAGTAAACTGTGTGCGTCGT	21
AZI3 sequencing primer 1R	AGTCCTAACCCTACGCCAGT	20
AZI4 locus primer 1F	CAACTGCACGTTAAGTAGACCAC	23
AZI4 locus primer 1R	ACACTAAAGAAAATACCAATGGCTT	25

AZI4 sequencing primer 1F	GAGCATCGATAGGACAGTTTCCG	23
AZI4 sequencing primer 1R	AACCACTGCTACTGATTGTCGAT	23
AZI5/6 locus primer 1F	GAAGGCTGAGAGAGACGGGA	20
AZI5/6 locus primer 1R	ACCACTCTCTTTTGGCAATACT	22
AZI5/6 sequencing primer 1F	AACTTTAGCCTTTAGGGCGGTG	22
AZI5/6 sequencing primer 1R	AGCCTCTCTTGTCATTTTCCTCA	23
AZI7 locus primer 1F	TGTTCCCTTAACAGTATTTCCCT	23
AZI7 locus primer 1R	TGCCCAAGAGACGTTCTCAA	20
AZI7 sequencing primer 1F	TGGATGTTAGACAAAACCAATTCA	24
AZI7 sequencing primer 1R	ACCAGCTATGAGGCCTTGTT	20

Nicotiana benthamiana were grown at 24℃ and with 16-h day light. Plants were grown for 4 weeks before *Agrobacterium tumefaciens*-mediated transient transformation.

Generation of AZI1 Family CRISPR Alleles

CRISPR/Cas9 gene editing technology was used to introduce mutations into *AZI3*, *AZI4*, *AZI5*, and *AZI6* as according to the method described by Ma and Liu, 2016. Two guide RNA (gRNA) adaptors were designed for each gene of interest to increase targeting and editing efficiency (Table 4.2). Target adaptors were ligated into a Bsa-I digested plasmids (Addgene #66198 and 66201) to construct the sgRNA intermediate plasmid which contained: 1) the Arabidopsis U6 small nuclear RNA promoter; 2) the binding scaffold for Cas9 nuclease; 3) and the two target adaptors. The final CRISPR/Cas9 expression vectors were assembled by

recombining the sgRNA cassettes into Addgene vector 66188, which also contains a BASTA herbicide resistance gene and a Cas9 gene expression cassette driven by the maize ubiquitin promoter. All constructs were transformed into and purified from *Escherichia coli* DH5α cells and expression vectors were subsequently transformed into *Agrobacterium tumefaciens* GV3101.

Table 4.2 – sgRNA Adaptors Used to Target AZI3, AZI4, and AZI5/AZI6

Name	Sequence (5'-3')
AZI3 -1U3dF	gtcaTTTGGTTGACCTTGACGCTG
AZI3 -1U3dR	aaacATGCACTGCTCTTAGGGCTA
AZI4 -1U3dF	aaacAGGACGGTCCCAAGTCCAAA
AZI4 -1U3dR	aaacAAGTCCAAAGGTCCCGAGTC
AZI5-1U3dF	gtcaAACCTAAGCCCAAGTCCAC
AZI5-1U3R	aaacGTGAAGCCTTGTTGTTCGC

Surface Sterilization of Seeds using Chlorine Gas

Seeds were surface sterilized using chlorine gas (Lindsey et al., 2017). ~5µL seed were added to a pre-labeled 1.5mL Eppendorf tube. 100mL of 7.5% NaOCl (Clorox) were added to a 250mL beaker placed inside a desiccator inside an active fume hood. The 1.5mL tube(s) containing the seeds was re-labeled over the previous label to reduce bleaching of the label due to the chlorine gas. The tubes were transferred to the desiccator which contained the 7.5% NaOCl, then carefully opened. 3mL of 37% HCl (Sigma) were slowly added to the top of the 7.5% NaOCl using a transfer pipette which was used to very gently stir the solution. The lid was then placed on the desiccator then sealed with parafilm. After 2.5-3hrs, the tubes were closed using aseptic technique then removed from the desiccator and transferred to a sterile fume hood. Within the sterile hood, the tubes were relabeled then opened and allowed to vent for 15-30mins.

After venting, the seeds were plated on ½MS (1% sucrose; Sigma Aldrich) agar plates in 100x100mm polystyrene petri dishes (Fisherbrand). After three days of vernalization at 4°C, plates were transferred to the growth chamber with 16-h light (120 μmol s^{-1} m^{-2}) and 8-h dark cycles at 21°C.

Oxylipin Treatment of Seedlings on Plates

For oxylipin treatment assays, 12-15 seedlings germinated from gas-sterilized seeds were transferred to new ½MS plates (1% sucrose; Sigma Aldrich) supplemented with either 40μM azelaic acid (AZA) in 5mM MES or 40μM suberic acid (C8) in 5mM MES or 5mM MES alone (mock) in 120x120mm polystyrene petri dishes (Grenier Bio) two days post-germination. 10mM stock solutions of AZA and C8 were prepared in 5mM MES buffer at pH 5.7. To limit contact between the aerial tissues and the media, sterile 18x18mm or sterile 24x30mm glass coverslips placed on top of the media. The seedlings were gently transferred onto the coverslips such that only the nascent root was in contact with the media. Images were collected using an Epson scanner at 10- and 17-days post-transfer for root and leaf growth assessments, respectively. For fresh weight measurements, individual seedlings were collected and the mass of the aerial tissue cleaved from the roots was measured using a standard bench scale. Mean data from two (*azi3-17*, *azi5azi6-10*) or three (*wild-type*, *azi1-1*, *azi3-16*, *azi4-2*, and *azi5azi6-3*) independent experiments is plotted. 1 genotype per plate; n = 11-15 seedlings per plate. Error bars are SEM and color-coded letters above bars indicate statistical differences by anova, SNK test. $p<0.05$.

All root lengths and lateral root numbers were measured using ImageJ.

Salt Treatment of Seedlings on Plates

For basal growth and salt response assays, 7-8 seedlings germinated from gas-sterilized seeds were transferred to new ½MS plates (1% sucrose) supplemented with either 150mM NaCl or dH_2O in 100x100mm polystyrene petri dishes (Grenier Bio) 7-days post-germination. Images were collected at 7-days post-transfer using an Epson scanner. Mean data from two independent experiments is plotted; n = 7-8 seedlings per genotype per experiment. Error bars are SEM and color-coded letters above bars indicate statistical differences by anova, SNK test. $p<0.05$.

All root lengths and lateral root numbers were measured using ImageJ.

Disease Resistance Assays

The evaluation of bacterial growth was carried out as described (Jung et al., 2009). To evaluate basal disease resistance, three lower leaves were infiltrated with *Pseudomonas cannabina pv. alisalensis* an avirulent isogenic strain expressing avrRpt2 (PmaDG6) at a concentration wherein optical density at wavelength of 600nm (OD_{600}) = 0.0001 (Guttman and Greenberg, 2001). Bacterial growth was quantified from 8 discs collected from inoculated leaves from separate plants 3-days post-inoculation.

To evaluate systemic resistance, two lower leaves were syringe-inoculated with avirulent PmaDG6 at OD_{600} = 0.01. Two days later, the inoculated leaves were excised then two systemic (and uninoculated) upper leaves were inoculated with the virulent pathogen *P. cannabina* without avrRpt2 (PmaDG3) at OD_{600}=0.0001 (Guttman and Greenberg, 2001). Growth was quantified from discs collected from eight leaves from eight separate plants for each genotype assessed 3-days post-inoculation.

Plotting and Statistical Analysis

All root and leaf growth-related graphs were plotted and statistics were performed using GraphPad Prism Version 9.3.1. Pathogen infection graphs and statistics were performed using RStudio (Figure S4.1 and S4.2).

4.3 Results

4.3.1 Characterization of *azi1* family CRISPR mutants

Given the roles and localizations of AZI1 and EARLI1 in systemic immunity priming, I investigated whether AZI1 family proteins with (predicted) similar localization patterns would show similar pro-immunity functions. To test for possible differential roles of the AZI1 family proteins in AZA signaling and systemic defense priming, we induced targeted mutations in *AZI3*, *AZI4*, and *AZI5/AZI6*. We used two guide RNAs (gRNAs) per gene to increase editing efficiency. To identify allelic variances, I employed a combination of Sanger sequencing followed by analysis using DsDecode (Liu et al., 2015; Ma et al., 2016). Using this method, I identified three lines with mutations in *AZI3*, one line with mutations in *AZI4*, and two lines with mutations in *AZI5* and *AZI6* (Fig. 4.1).

Each of the *azi3* mutations partially deletes the 8-cysteine motif conserved among the AZI1 family proteins and the greater HyPRP family (Fig. 1.3B and C; Fig. 4.1A). Alleles *azi3-11b* and *azi3-17a* have identical mutations wherein amino acids 146-182 have been deleted. *azi3-11a* and *azi3-17b* consist of similar but distinct frameshift mutations. *azi3-11a* has a mutation resulting in the deletion of wild-type amino acids 146-182 and the addition of new amino acids 146-149. *azi3-17b* has a mutation resulting in the deletion of wild-type amino acids 147-182 and the addition of new amino acids 147-149. Both *azi3-16* alleles have frameshift mutations

resulting in the deletion of wild-type amino acids 162-182 (*azi3-16a*) and 160-182 (*azi3-16b*) and the addition of 11 and 14 new amino acids, respectively.

The *azi4-2* mutant has similar biallelic mutations resulting in the loss of wild-type amino acids 72-92; *azi4-2b* contains an additional T71K mutation (Fig 4.1B). In both cases, this region encompasses 20 amino acids that are highly conserved within the plastid targeting regions of AZI1, EARLI1, and AZI3 (Fig. 1.3B; Cecchini et al., 2015; Chapter 3, Cecchini, Speed et al., 2021).

The *azi5azi6* double mutants contain the most severe mutations from the wild-type sequences. Both mutants display total deletions of the 8-cysteine motif within the LTP domain (Fig. 4.1C). *azi5azi6-3* is comprised of biallelic frameshift mutations resulting in the loss of wild-type amino acids 14-129 (*azi5azi6-3a*) and 15-129 (*azi5azi6-3b*) and the addition of 39 and 38 new mutant amino acids, respectively. *azi5azi6-10* has biallelic frameshift mutations resulting in the loss of wild-type amino acids 44-129 and the addition of 8 (*azi5azi6-10a*) and 4 (*azi5azi6-10b*) new amino acids. These mutations remove most of the targeting signal (HD) from *azi5azi6-3*, whereas *azi5azi6-10* has an intact targeting signal (Cecchini et al., 2015; Chapter 4, Cecchini, Speed et al., 2021).

4.3.2 Plastid-Targeted AZI1 Family Proteins Contribute to Priming of Systemic Defenses

To determine if AZI3, AZI4, and AZI5/AZI6 contribute to SAR, I primed systemic defenses as previously described (Jung et al., 2009). Three lower leaves were inoculated with the avirulent pathogen *P. cannabina* PmaDG6 or 10mM $MgSO_4$ infiltration solution alone (mock). Later, the inoculated lower leaves were removed and two upper leaves were challenged by secondary inoculation with the virulent pathogen PmaDG3 (*P. cannabina* lacking AvrRpt2).

Figure 4.2. The Plastid-Targeted AZI1 Family Proteins Contribute to SAR

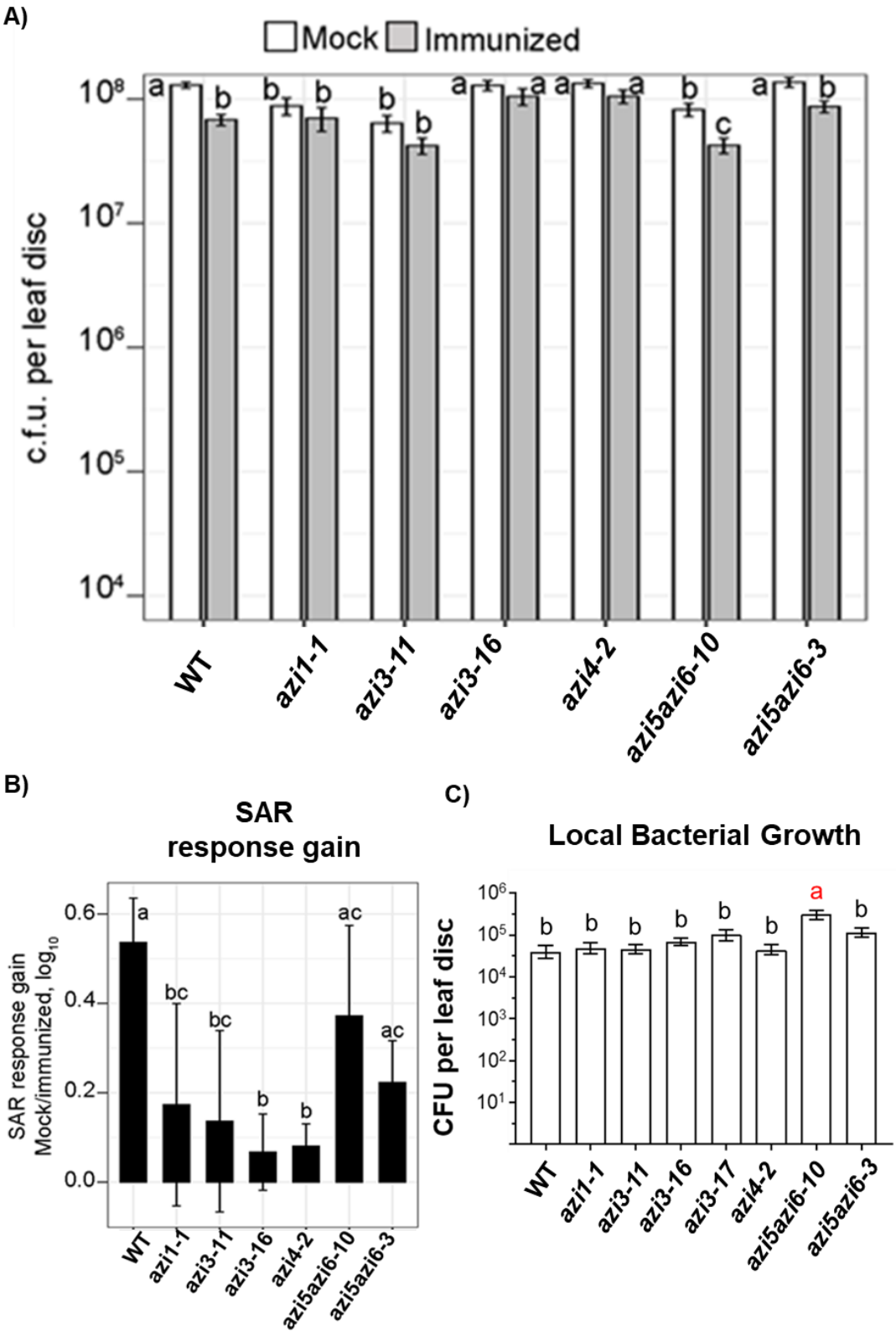

Figure 4.2. The Plastid-Targeted AZI1 Family Proteins Contribute to SAR
A) SAR assay showing the growth of virulent bacteria *Pma*DG3 in systemic leaves of WT, *azi1* (negative control), *azi3*, *azi4*, and *azi5/azi6* mutants and B) response gain of SAR due to *Pma*DG6 immunization in (A). The plants were immunized in three lower leaves with avirulent pathogen PmaDG6 (OD_{600} = 0.01) or mock. Two days later, the immunized leaves were removed and two upper, systemic leaves were infected with the virulent pathogen *Pma*DG3 (OD_{600} = 0.0001). Bacterial growth was sampled from the systemic leaves. C) Local bacterial growth assay showing the growth of avirulent bacteria *Pma*DG6 in local leaves of WT, *azi1*, *azi3*, *azi4*, and *azi5/azi6* mutants. Three lower leaves were infected with avirulent pathogen *Pma*DG6 (OD_{600} = 0.0001) and bacteria were sampled from the same leaves three days later. In (A), the mean CFU of two-six experiments with eight leaves per WT or mutant line is plotted; error bars show SEM. In (B), error bars represent variation among replicates. In C) the mean CFU is plotted from two experiments with seven-eight leaves per WT or mutant line per experiment; error bars show SEM. Color-coded letters above bars indicate statistical differences by anova, SNK test. $p<0.05$.

Consistent with previous findings, *azi1-1* failed to mount SAR after the initial priming infection (Fig. 4.2A). In comparison, systemic wild-type leaves showed significantly enhanced bacterial resistance after the priming infection.

Similar to *azi1-1*, mutation of *AZI3* (which targets plastids similarly to AZI1) or *AZI4* (which has a PRR similar to AZI1) resulted in an attenuated SAR response wherein bacteria-primed plants showed a similar degree of bacterial colonization as mock-treated plants (Fig 4.2A). In contrast, neither of the *azi5azi6* mutants showed a noticeable SAR defect. To quantify the magnitude of each immune response due to the initial immunization, I calculated the response gain to SAR using a mathematical model derived by Jiang et al., 2021. Compared to wild-type, only *azi1*, *azi3* and *azi4* mutants showed significantly reduced response gains in SAR (Fig. 4.2B). The lack of SAR in *azi3* and *azi4* may be due to an inability to recognize the SAR-inducing pathogen PmaDG6 as opposed to a general defect in defense priming. Therefore, I also assessed each mutant's basal/unprimed bacterial resistance and found that *azi3* and *azi4* displayed wild-type levels of basal disease resistance (Fig. 4.2C). Interestingly, the *azi5azi6-10* double mutant appeared to show a weaker basal disease resistance than wild-type.

These results suggests that the AZI1 protein family may weakly contribute to local defense signaling and that the non-plastid-targeted AZI1 family proteins are dispensable to systemic defense signaling.

4.3.3 The AZI1 Gene Family Regulates Root Growth During AZA Signaling

The full root and shoot responses to AZA require AZI1 and EARLI1, which poises the AZI1 protein family as critical components of such a root-to-shoot developmental signaling mechanism (Bouain et al., 2018; Jung et al., 2009; Cecchini et al., 2015, Chapter 2, Cecchini et al., 2019, Cecchini, Speed et al., 2021). However, our findings that the non-plastid targeted AZI5/AZI6 are dispensable for SAR presents the possibility that the AZI1 family proteins may have differential functions in AZA signaling as well (Fig. 4.2)

To test if the plastid-targeted and non-plastid-targeted AZI1 family proteins contribute to root-based AZA signaling, I measured the impacts of prolonged root exposure to AZA in the *azi1* family mutants (Fig. 4.3-4.9). As a measure for oxylipin specificity in the root morphology response, I separately exposed roots to the 8-carbon oxylipin suberic acid (C8), which is structurally similar to AZA but does not prime systemic defenses (Jung et al., 2009). As performed previously, 2-day-old seedlings grown on ½MS media were gently transferred to fresh ½MS plates supplemented with either 40uM AZA, 40uM C8, or 5mM MES (Fig 4.3; Chapter 2, Cecchini et al., 2019). To limit contact between the aerial tissues and the media, the seedlings were placed on glass coverslips such that only the root was in contact with the media (Fig 4.3A).

Figures 4.3-4.8 demonstrate that exposure of roots to either AZA or C8 severely limits primary and lateral root growth however, AZA causes a much greater inhibition of primary root elongation than C8 in wild-type seedlings (Fig 4.4A and B). In contrast, AZA and C8 had more similar impacts on lateral root elongation (Fig. 4.4C and D). The *azi1*, *azi3*, *azi4*, and *azi5azi6*

mutants showed similar primary root length after either lipid treatment, which could be suggestive of both an attenuated sensitivity to AZA and/or a heightened response to C8. Due to the similar impacts of AZA and C8 on primary root growth, I directly compared the primary root length on either compound to measure the relative sensitivity to either oxylipin (Fig. 4.4B and D). Measured in arbitrary units, RS = 1 when the root growth on AZA is equivalent to the root growth on C8 and suggests equal levels of sensitivity to AZA and C8. An RS < 1 occurs when there is greater growth on AZA than C8 and suggests greater sensitivity to AZA than to C8; when RS > 1, plants appear more sensitive to C8 than AZA.

As suggested from the primary root lengths, wild-type seedlings showed a much greater sensitivity to AZA than C8 (RS < 1; 4.4B). In contrast, each of the *azi1* family mutants showed a greater sensitivity for C8 than AZA (RS > 1). Though the impact on lateral root elongation is more subtle, loss or mutation of the AZI1 family genes generally decreased the relative sensitivity for AZA similar to the effect seen on primary root development (Fig 4.4B and D). These data show that AZA inhibits primary and lateral root elongation and suggests that the *AZI1* gene family may regulate developmental specificity for oxylipins. The greater degree of primary root growth inhibition and the greater relative sensitivity to AZA than C8 seen in wild-type plants also suggests that similar but distinct oxylipins may induce the formation of distinct root structures in a manner dependent on the AZI1 gene family.

To further assess the role of the AZI1 family proteins in AZA-induced root development, I assessed the impact of AZA and C8 treatment on the initiation of new lateral roots (Fig 4.5). wild-type seedlings showed a significant increase in lateral root density in response to either treatment (Fig 4.5A). However, similar to the response seen in the primary root, AZA causes a much greater increase in lateral root density than C8 treatment. This heightened response to AZA

Figure 4.3. Root-applied Oxylipins Severely Inhibit Root Growth

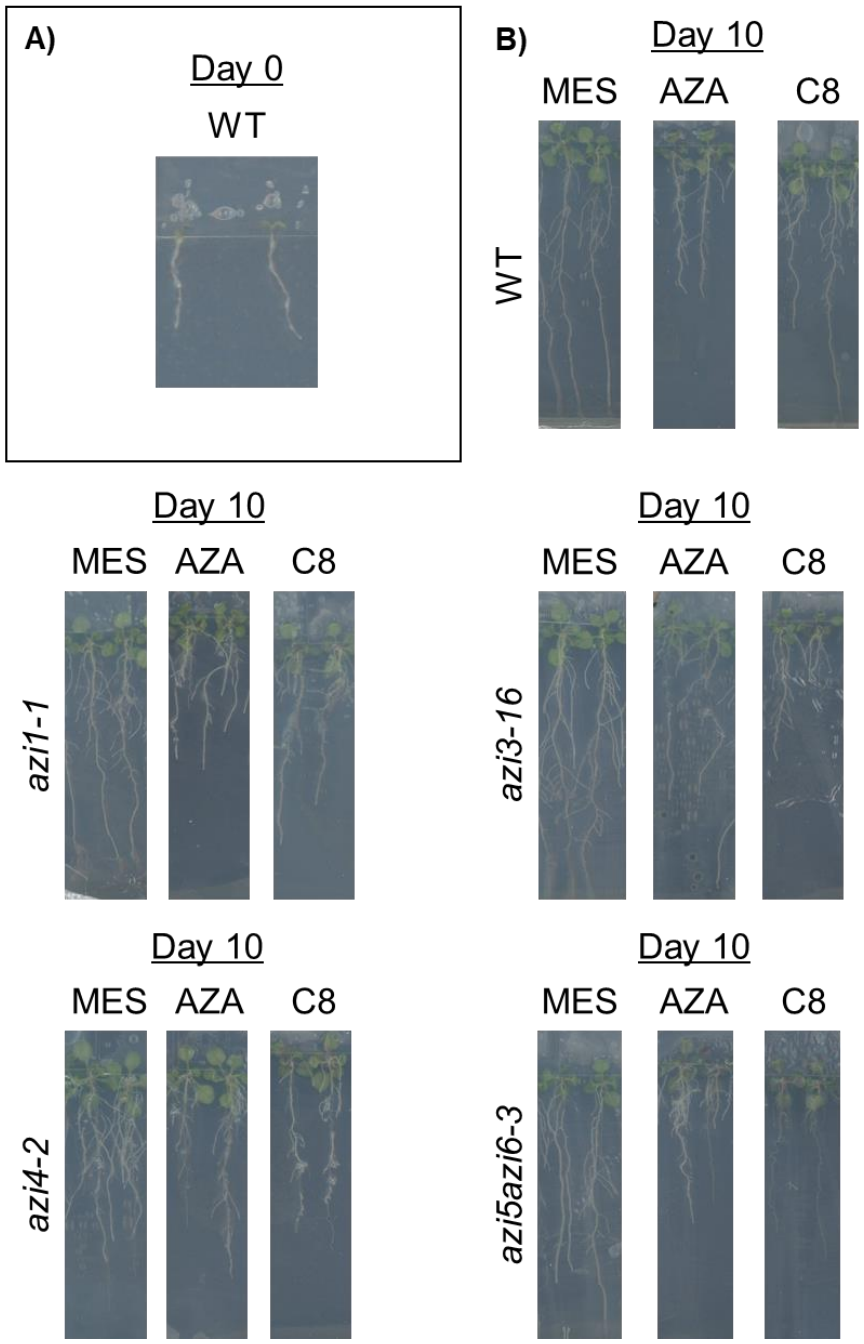

Figure 4.3. Root-applied Oxylipins Severely Inhibit Root and Shoot Growth
A) 2-days after germination on ½MS agar, WT, *azi1*, *azi3*, *azi4*, and *azi5azi6* seedlings were gently transferred to onto sterile coverslips placed on new ½MS agar supplemented with either 40 µM azelaic acid (AZA) or 40 µM suberic acid (C8) in 5mM MES or 5mM MES alone (mock) so as to limit contact between the aerial tissues and media. B**)** Select WT *azi1*, *azi3*, *azi4*, and *azi5azi6* mutants 10 days after transfer onto sterile coverslips on ½MS agar supplemented with either 40 µM azelaic acid or 40µM suberic acid in 5mM MES or 5mM MES alone (mock). 11-15 seedlings per plate; example seedlings from 1 of 3 replicates shown. Images collected with an Epson brand scanner. Select images shown; similar results were observed among different mutations for the same gene.

Figure 4.4. The AZI1 Gene Family Affects the Root Elongation Response to Oxylipin Treatment

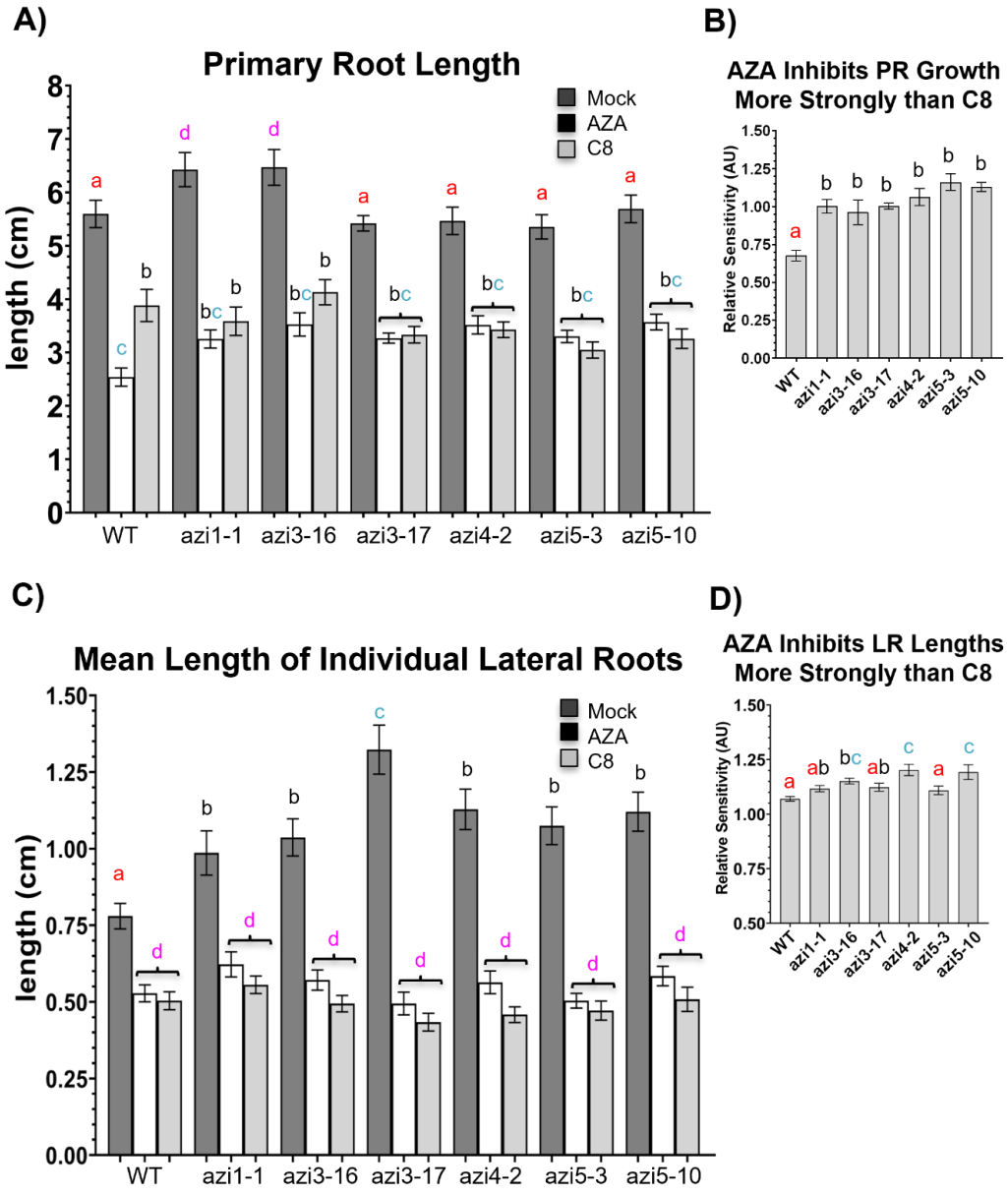

Figure 4.4. The AZI1 Gene Family Affects Root Elongation in Response to Oxylipin Treatment
The mean length of each primary root A) or lateral root C) of WT and *azi1* family mutant seedlings was measured days after transfer to sterile coverslips on ½MS agar supplemented with either 40 µM azelaic acid (AzA) or 40 µM suberic acid (C8) in 5mM MES or 5mM MES alone (mock) as in Figure 9. B) Primary root length or D) individual lateral root lengths on the AzA plates were divided by the primary or lateral root lengths on C8 to calculate the relative sensitivity to either compound. Relative Sensitivity = $Length^{AzA}/Length^{C8}$. Mean data from two (*azi3-11*, *azi3-17*, *azi5/azi6-10*) or three (*WT*, *azi1-1*, *azi3-16*, *azi4-2*, and *azi5/azi6-10*) independent experiments is plotted; n = 11-15 seedlings per genotype per experiment. Error bars are SEM and color-coded letters above bars indicate statistical differences by anova, SNK test. $p<0.05$.

Figure 4.5 Root-Applied Oxylipins Increase Lateral Root Density

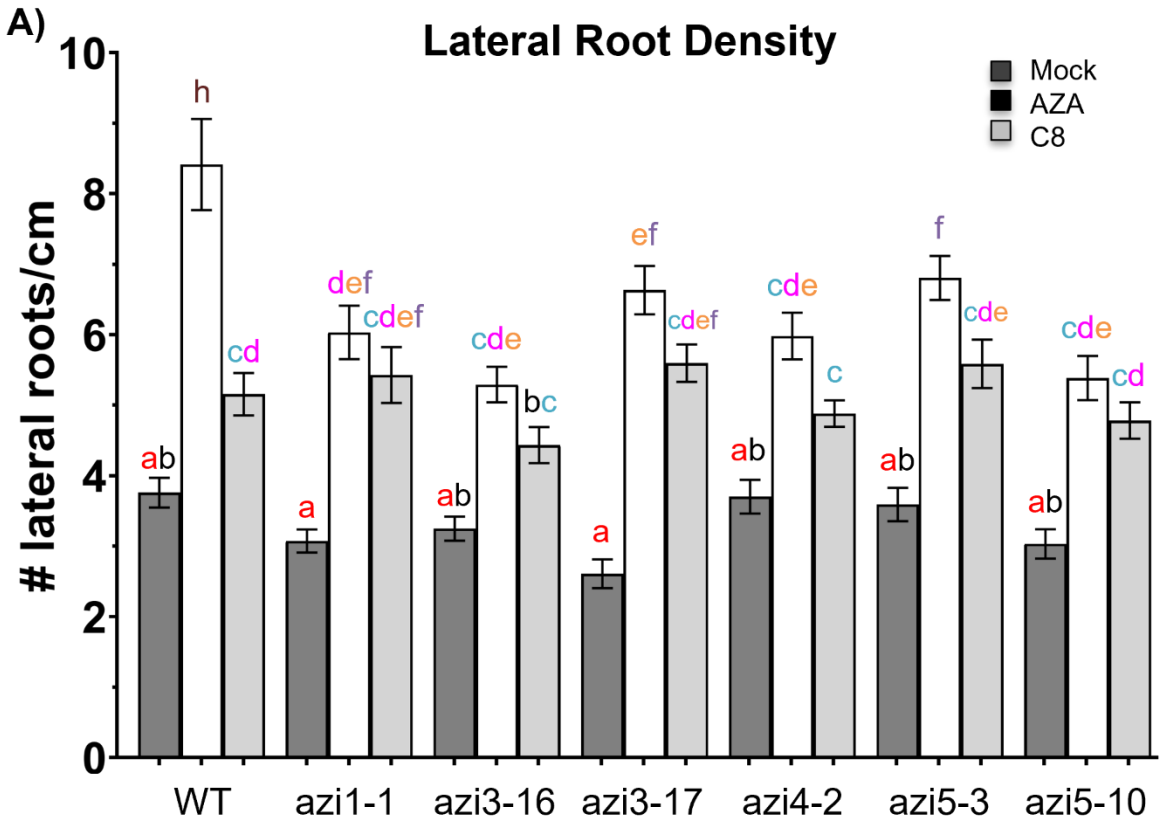

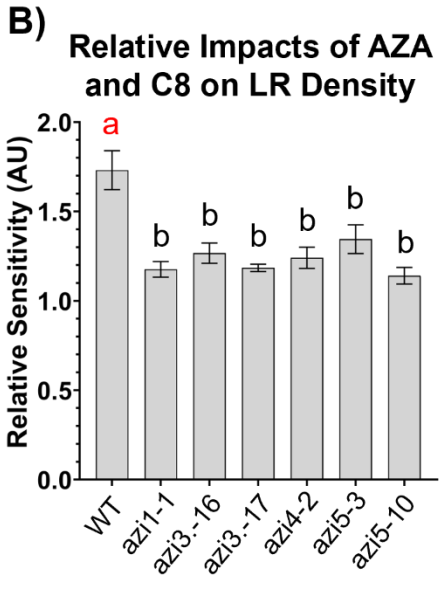

Figure 4.5 Root-Applied Oxylipins Increase Lateral Root Density

A) Mean lateral root density of WT and *azi1*-family mutant seedlings was measured 10 days after transfer to sterile coverslips on ½MS agar supplemented with either 40 µM azelaic acid (AzA) or 40 µM suberic acid (C8) in 5mM MES or 5mM MES alone (mock) as in Figure 4.3. B) Mean lateral root density on the AzA plates was divided by mean lateral root density on C8 to calculate the relative sensitivity to either compound. F) Mean lateral root length on AzA was divided by mean lateral root length on C8 to calculate the relative sensitivity to either compound. Relative Sensitivity = $Length^{AzA}/Length^{C8}$. Mean data from two (*azi3-11*, *azi3-17*, *azi5/azi6-10*) or three (*WT*, *azi1-1*, *azi3-16*, *azi4-2*, and *azi5/azi6-10*) independent experiments is plotted; n = 11-15 seedlings per genotype per experiment. Error bars are SEM and color-coded letters above bars indicate statistical differences by anova, SNK test. $p<0.05$.

relative to C8 involves the *AZI1* gene family (Fig 4.5B; Bouain et al., 2018; Chapter 2, Cecchini et al., 2019). In contrast to wild-type seedlings, the *azi1* family mutants showed much weaker inhibition of lateral roots in response to AZA. In fact, the *azi3*, *azi4*, and *azi5azi6* mutants showed an increased inhibition of overall lateral root growth when grown on C8 compared to AZA (Fig. 4.6A). Wild-type seedlings showed a similar response to either compound when viewing the overall impact on lateral root growth (Fig 4.6A and B). To assess the individual impacts of AZA and C8 on root growth, I normalized the total root growth after either lipid treatment against the total root growth after the mock treatment to measure the fold change in root growth and thus the level of growth inhibition caused by either compound (Fig 4.6C). Deeper analysis of the fold repression in lateral root growth induced by either compound reveals that *azi3*, *azi4*, and *azi5azi6* show a much greater level of responsiveness to C8 than wild-type, while showing similar overall responses to AZA. Though *azi1-1* still weakly responds to AZA, its greater apparent relative sensitivity to AZA than C8 is due to a lessened response to C8 rather than a heightened response to AZA. (Fig 4.6B and C).

Although their specific impacts on primary and lateral root development vary slightly, AZA and C8 have overall similar effects on root growth (Fig 4.7). Both compounds restrict primary root growth and increase lateral root density however, AZA causes a much greater effect than C8 in either case. Collectively, this suggests that AZA-treated plants may show a slight increase in the development of lateral roots relative to primary root development in comparison to plants treated with C8. Consistent with this expectation, AZA and C8 cause differential shifts in the balance between primary and lateral root growth (Fig 4.8). Furthermore, loss (*azi1-1*) or disruption (*azi1* family CRISPR mutants) resulted in a decreased sensitivity to AZA and increased responsiveness to C8 (Fig 4.7B and C).

A root's total growth results from the balance of two developmental factors: 1) the initiation of new lateral roots; and 2) elongation of existing primary and lateral roots. Measuring the percentage of total root growth that is due to lateral root growth (% LR) reveals that AZA, but not C8, significantly increases the % LR in wild-type plants (Fig. 4.8A). In fact, C8 slightly reduces % LR (Fig. 4.8C). Comparing the relative sensitivity of the mutants and wild-type for AZA and C8 reveal that the mutants generally show a lessened relative sensitivity for AZA when it comes to lateral root induction (Fig. 4.8B). In contrast, each of the *azi1* family mutants shows a significantly reduced induction of lateral rooting in response to AZA. The *azi1* family CRISPR mutants also showed a strong reduction in lateral rooting after C8 treatment in contrast to the weak response displayed by wild-type plants.

Since root-applied AZA affects root development and primes aerial defenses, prolonged activation of AZA-induced (defense) signaling might impact shoot growth (Fig 4.3-4.8; Jung et al., 2009; Cecchini et al., 2015; Chapter 2, Cecchini et al., 2019). Thus, I assessed the impact of root-applied AZA and C8 on shoot growth (Fig 4.9A-D). Changes in shoot growth caused by the oxylipin treatments were subtle and difficult to detect by eye, however the leaves of wild-type roots exposed to AZA and C8 appeared slightly smaller than the leaves of mock-treated roots (Fig. 4.9A). Quantification of fresh leaf mass confirmed that prolonged root exposure to either treatment significantly inhibited leaf growth, though wild-type leaves showed a greater relative sensitivity for AZA than C8 (Fig. 4.9B and C). In contrast, each of the *azi1* family mutants also showed reduced leaf mass after either treatment and a greater relative sensitivity for C8 than for AZA (Fig 4.9C). Additionally, each of the CRISPR-generated mutants showed a heightened level of growth repression due to C8 when compared to either wild-type or the *azi1* null mutant (Fig. 4.9D).

Collectively, these SAR and AZA signaling results indicate that the AZI1 family mediates both developmental responses to defense-priming signals and the transmission of root-autonomous developmental cues to aerial tissues.

4.3.4 The AZI1 Gene Family Regulates Root Growth During Salt Stress

My data show that mutation of either *AZI3* or *AZI4*, which target and are predicted to target to plastids, respectively, attenuates SAR similar to *azi1* (Fig 4.2). In contrast, the *azi5azi6* double mutants show no noticeable defect in their ability to mount SAR after an immunizing infection. I also found that root-application of AZA negatively impacts shoot growth (Fig. 4.9). However, all *azi1* family mutants assessed show an attenuated response to root-applied AZA (Fig 4.4-4.8). Additionally, several *azi1* family mutants demonstrate increased lateral root growth in the presence of salt when compared to wild-type seedlings, which suggests a role for the AZI1 family in the control of lateral root growth during stress (Fig 4.10-4.16).

Excessive soil salinity induces osmotic stress and blocks the absorption of water and nutrients, and thus reduces photosynthesis, energy, lipid, and protein metabolism, which restricts plant growth and crop yields (Zhao et al., 2021). Exposure to high salt concentrations both induces bleaching in leaves and inhibits root growth in Arabidopsis seedlings (Pitzschke et al., 2014; Yan et al., 2021). AZI1 and EARLI1 are reported to promote seedling survival during salt stress (Pitzschke et al., 2014). The kinase MPK3, which is required for SAR, ISR, and root and shoot responses to AZA, also promotes seedling survival during salt stress (Yan et al., 2021). Given the impact of the AZI1 family proteins, and their regulatory kinases, in plant salt tolerance and defense-associated root development, I assessed if the *AZI1* family genes also impacted root growth in response to the abiotic salt stress (Fig. 4.10).

Figure 4.6 Root-Applied Oxylipins Inhibit Overall Lateral Root Growth

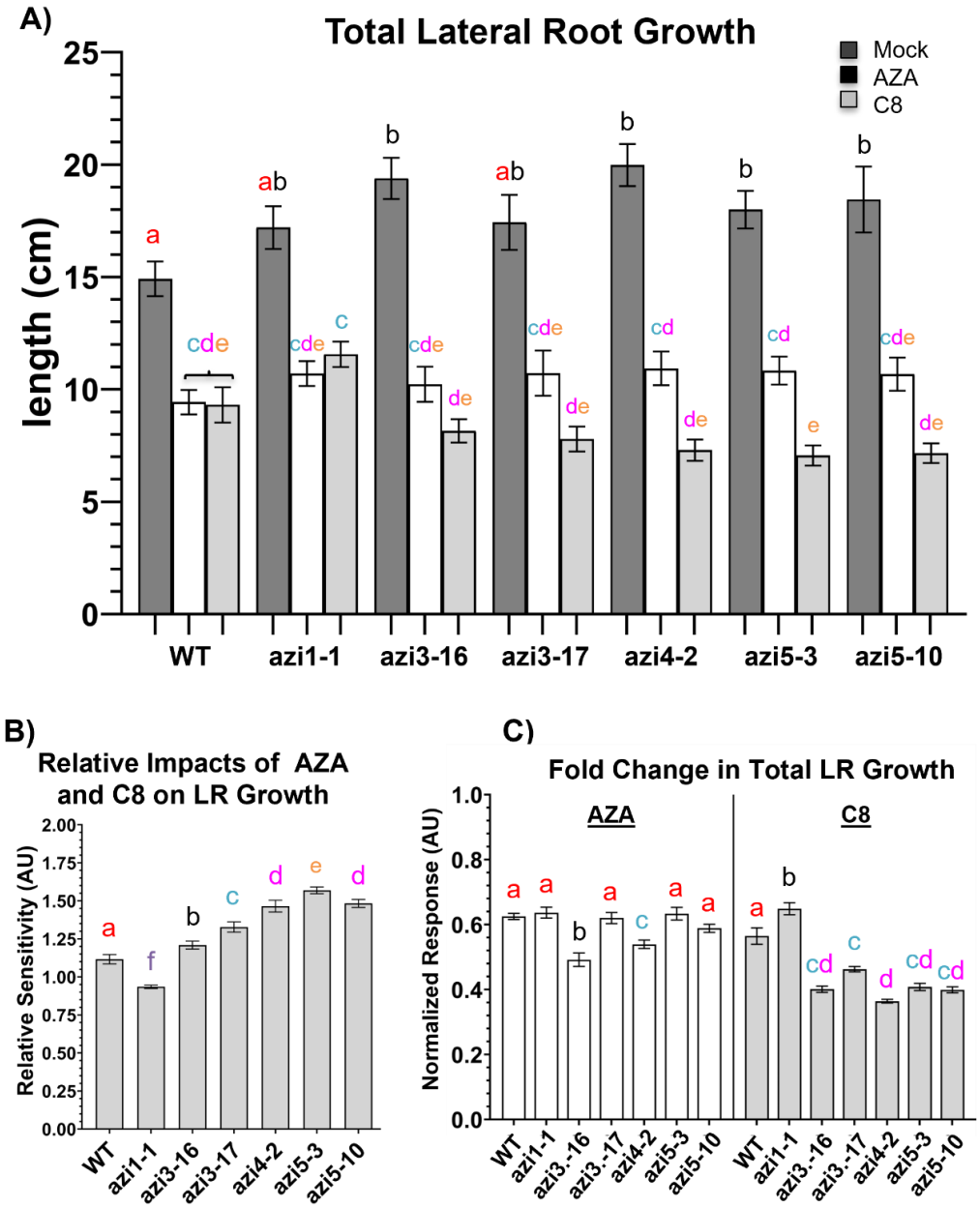

Figure 4.6 Root-Applied Oxylipins Inhibit Overall Lateral Root Growth

A) The total amount of lateral root growth in WT and *azi1*-family mutant seedlings was measured 10 days after transfer to sterile coverslips on ½MS agar supplemented with either 40 µM azelaic acid (AzA) or 40 µM suberic acid (C8) in 5mM MES or 5mM MES alone (mock) as in Figure 4.3. B) Total lateral root length on azelaic acid was divided by total lateral root length on suberic acid to calculate the relative sensitivity to either compound. C) Total lateral root length on each lipid treatment condition was divided by primary root growth on MES to calculate the normalized response to either compound. Relative Sensitivity = $Length^{AzA}/Length^{C8}$. Mean data from two (*azi3-11*, *azi3-17*, *azi5/azi6-10*) or three (*WT*, *azi1-1*, *azi3-16*, *azi4-2*, and *azi5/azi6-10*) independent experiments is plotted; n = 11-15 seedlings per genotype per experiment. Error bars are SEM and color-coded letters above bars indicate statistical differences by anova, SNK test, $p<0.05$.

Fig 4.7 Disruption of the AZI1 Gene Family Increases the Root Response to Suberic Acid

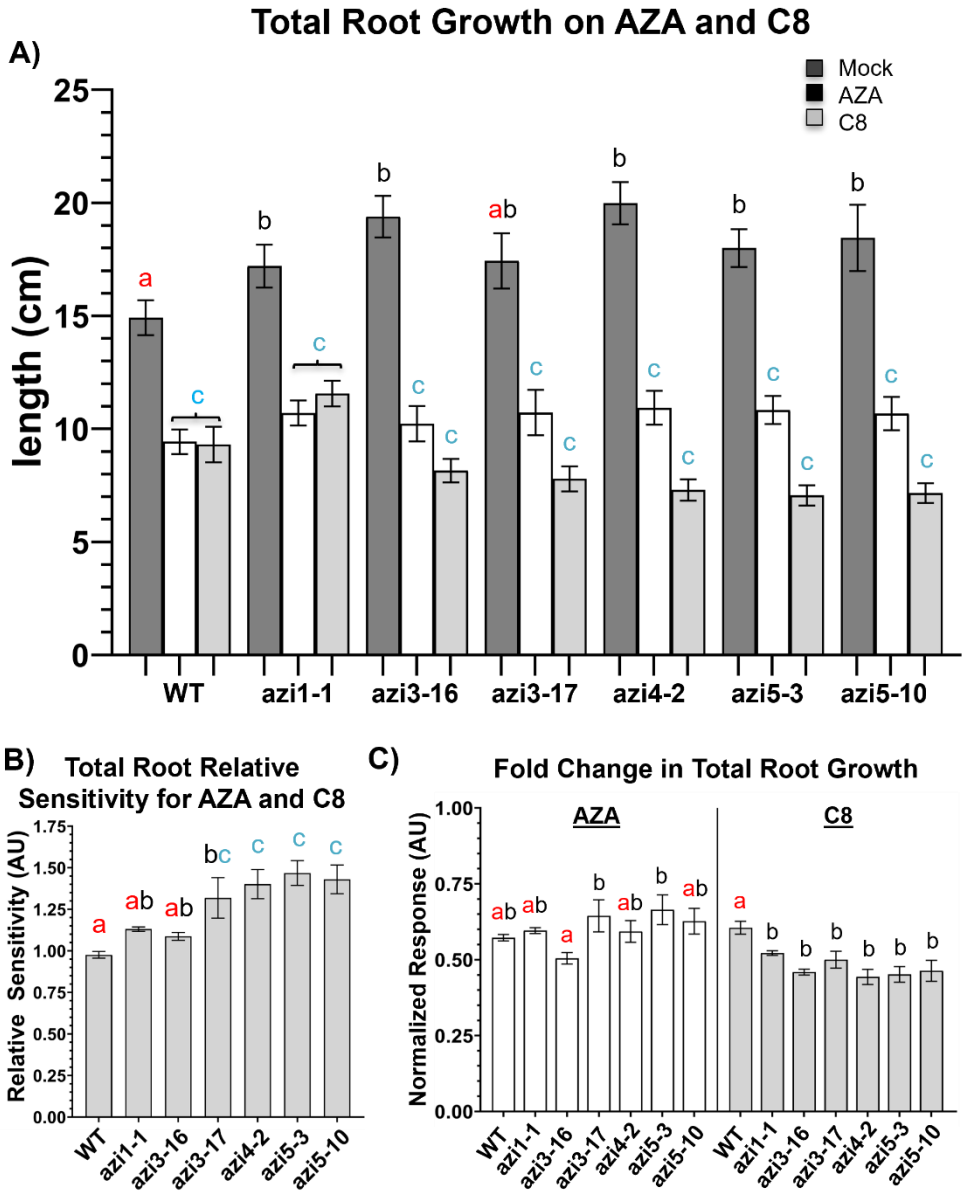

Figure 4.7. Disruption of the AZI1 Gene Family Increases the Total Root Response to Suberic Acid

A) Total root growth of WT and *azi1*-family mutant seedlings was measured 10 days after transfer to sterile coverslips on ½MS agar supplemented with either 40 µM azelaic acid (AzA) or 40 µM suberic acid (C8) in 5mM MES or 5mM MES alone (mock) as in Figure 4.4. B) Total root growth on azelaic acid was divided by total root growth on suberic acid to calculate the relative sensitivity to either compound. Mean data from two (*azi3-11*, *azi3-17*, *azi5/azi6-10*) or three (*WT*, *azi1-1*, *azi3-16*, *azi4-2*, and *azi5/azi6-10*) independent experiments is plotted; n = 11-15 seedlings per genotype per experiment. Error bars are SEM and color-coded letters above bars indicate statistical differences by anova, SNK test. $p<0.05$.

Figure 4.8 AzA Treatment Promotes a Bias for Lateral Root Growth

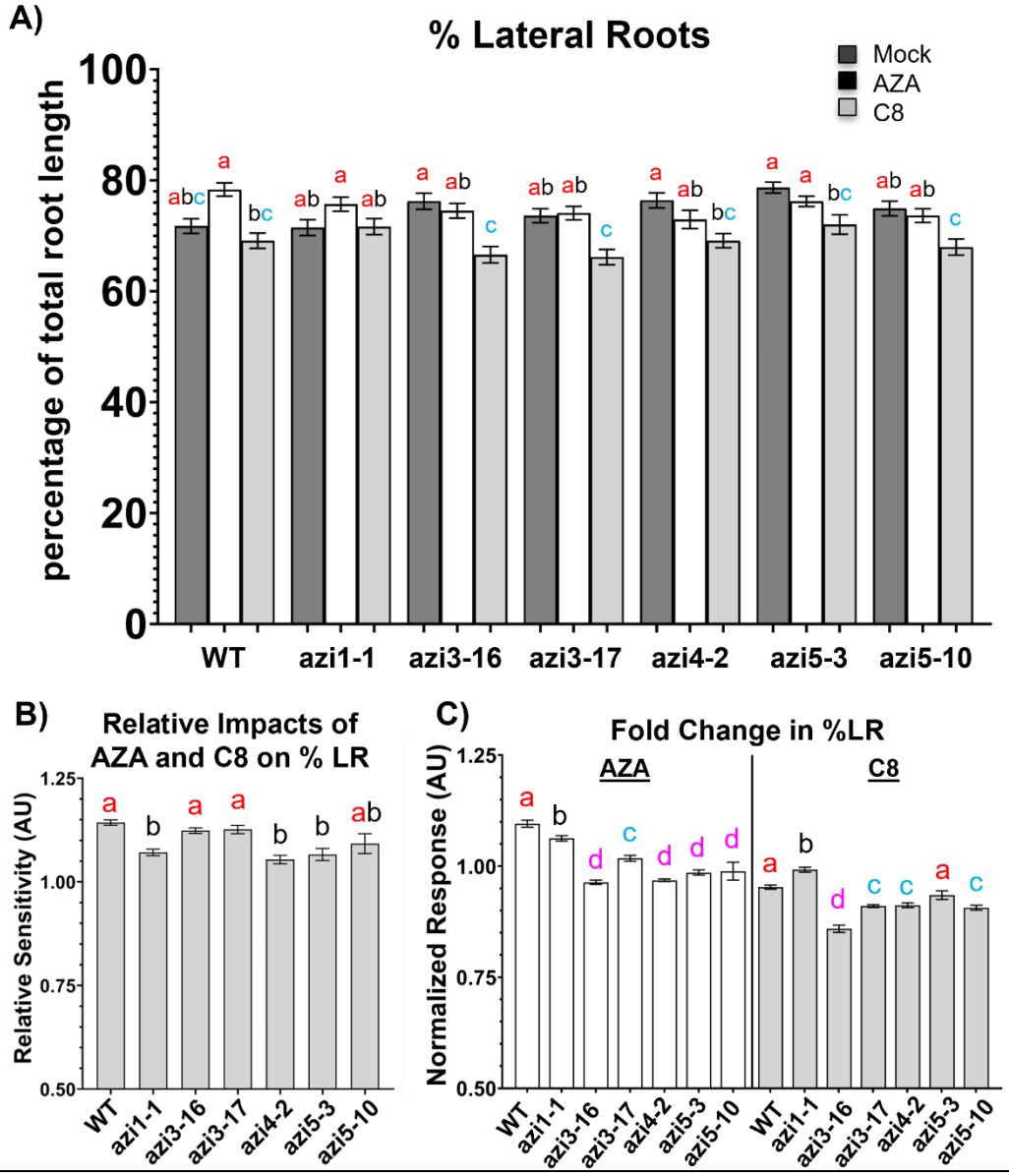

Figure 4.8 AzA Treatment Promotes a Bias for Lateral Root Growth

A) The seedling bias toward lateral root development (% LR) was measured as the total amount of lateral root lengths (Fig 4.6) divided by the total root length (Fig 4.8). Root lengths in WT and mutant seedlings were measured 10 days after transfer to sterile coverslips on ½MS agar supplemented with either 40 µM azelaic acid (AzA) or 40 µM suberic acid (C8) in 5mM MES or 5mM MES alone (mock) as in Figure 4.3. B) % LR after growth on azelaic acid was divided by % LR after growth on suberic acid to calculate the relative sensitivity to either compound. Relative Sensitivity = $Length^{AzA}/Length^{C8}$. C) LR % after growth on either lipid treatment condition was divided by primary root growth on the mock treatment to calculate the normalized response to either compound. Normalized Responsiveness = $Length^{Lipid}/Length^{MES}$. Mean data from two (*azi3-11*, *azi3-17*, *azi5/azi6-10*) or three (*WT*, *azi1-1*, *azi3-16*, *azi4-2*, and *azi5/azi6-10*) independent experiments is plotted; n = 11-15 seedlings per genotype per experiment. Error bars are SEM and color-coded letters above bars indicate statistical differences by anova, SNK test. $p<0.05$.

Fig 4.9 Root-Applied Oxylipins Inhibit Shoot Growth

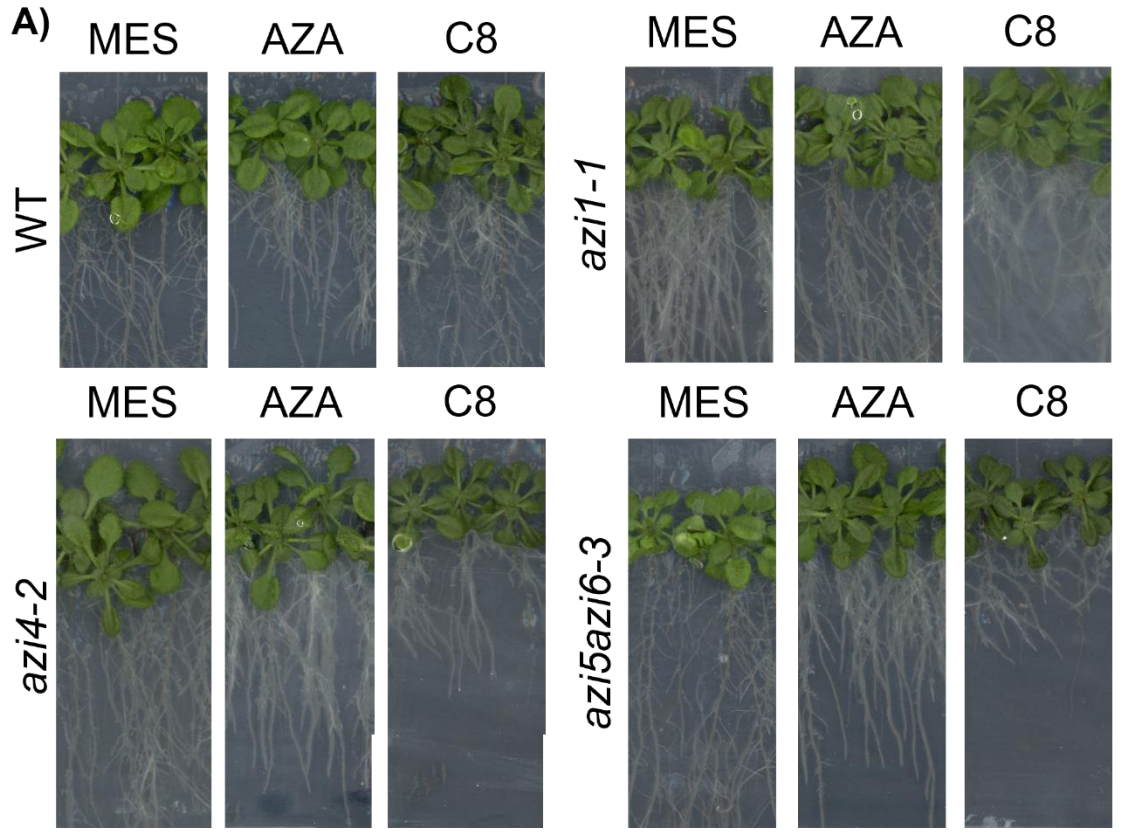

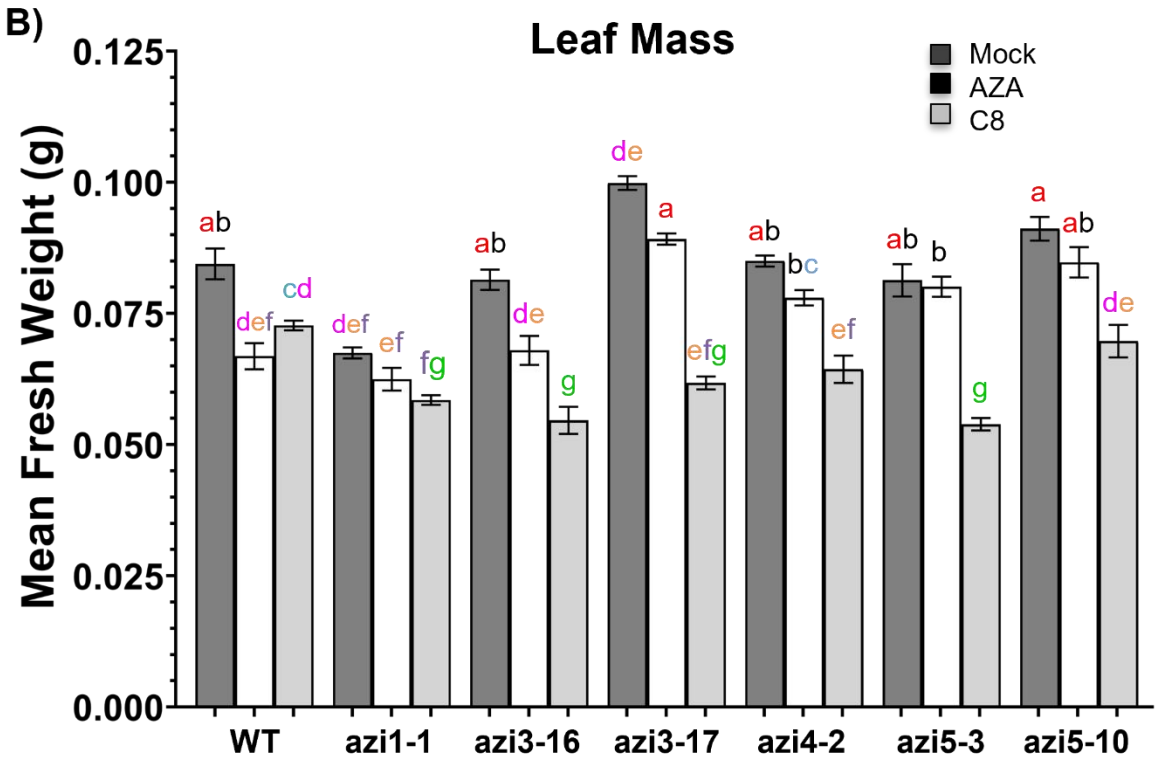

Figure 4.9 Root-Applied Oxylipins Inhibit Shoot Growth

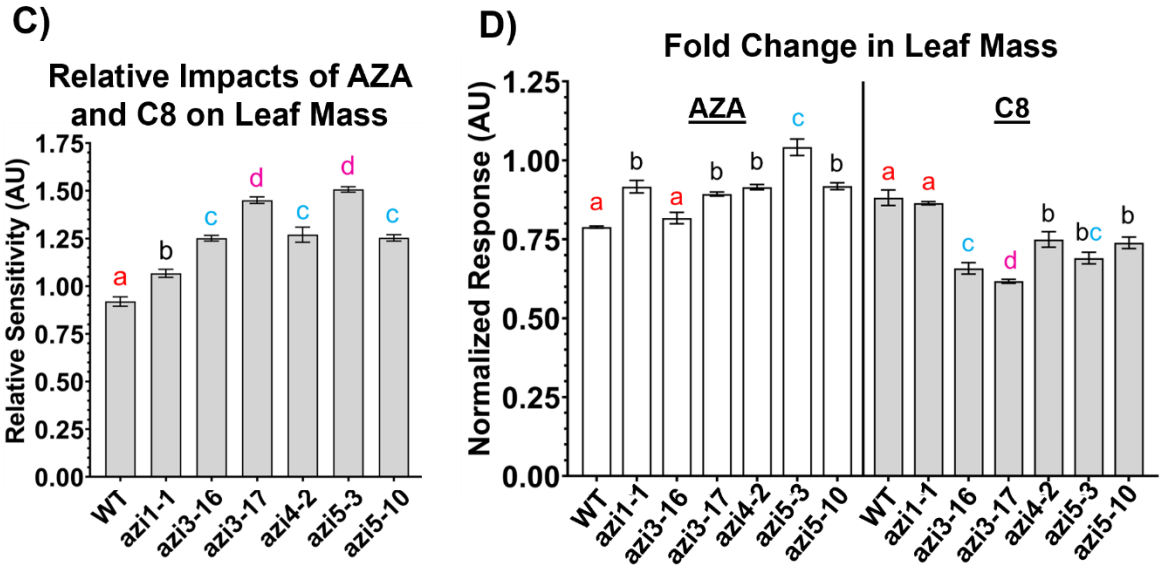

Figure 4.9 Root-Applied Oxylipins Inhibit Shoot Growth

A) Representative images of WT, azi1, azi3, azi4, and azi5azi6 mutant seedlings after 17-days of root exposure to oxylipins. B) Mean leaf fresh weight of WT and *azi1*-family mutant seedlings was measured 17 days after transfer to sterile coverslips on ½MS agar supplemented with either 40 µM azelaic acid (AzA) or 40 µM suberic acid (C8) in 5mM MES or 5mM MES alone (mock) as in Figure 4.3. C) Leaf fresh weight on AzA was divided by leaf fresh weight on C8 to calculate the relative sensitivity to either compound. Relative Sensitivity = $Length^{AzA}/Length^{C8}$. D) Leaf fresh weight after exposure to azelaic acid (left) or suberic acid (right) was divided by leaf fresh weight on MES to calculate the normalized response to either compound. Normalized Responsiveness = $Length^{Lipid}/Length^{MES}$. Mean data from two (*azi3-11*, *azi3-17*, *azi5/azi6-10*) or three (*WT*, *azi1-1*, *azi3-16*, *azi4-2*, and *azi5/azi6-10*) independent experiments is plotted; n = 11-15 seedlings per genotype per experiment. Error bars are SEM and color-coded letters above bars indicate statistical differences by anova, SNK test. $p<0.05$.

Fig 4.11A and B demonstrate the near-complete abrogation of root growth caused by salt stress and suggests that mutation of some *AZI1* family genes, especially *AZI3* and *AZI4*, may partially enhance total root growth during salt stress. Salt stress appears to less severely impact primary root growth (Fig 4.12) than lateral root growth (Fig 4.13). Wild-type seedlings display a ~40% reduction in primary root growth when salt stressed (Fig 4.12B); in contrast, the total lateral root length is reduced to <10% of the unchallenged growth (Fig 4.13B). Similar to the

response to AZA, loss (*azi1-1*) or mutation (*azi1* family CRISPR mutants) of the AZI1 proteins attenuates the lateral root response to salt which results in greater root growth during salt stress. Further analysis of lateral root development revealed that the (slightly) greater root growth demonstrated by some mutants during salt stress was primarily due to an increased lateral root synthesis during salt stress relative to wild-type (Fig 4.14B); primary root length and later root density were only weakly impacted by salt stress or mutation to the *AZI1* gene family (Fig. 4.12B and 4.15). Interestingly, the *azi1* family CRISPR mutants, especially *azi4-2*, showed a slight decrease in the elongation of unchallenged lateral roots.

Collectively, the enhanced lateral root elongation and stunted primary root growth seen in salt-stressed *azi1* family mutants results in an increased bias towards lateral root formation compared to wild-type plants during salt stress (Fig. 4.16A and B). These data suggest the *AZI1* gene family may restrict lateral root development during salt stress. When viewed with the roles of the AZI1 genes in prioritizing lateral root development over primary root growth during AZA signaling, these data suggest the AZI1 family mediate root morphological responses to biotic and abiotic stress signaling by affecting the development of lateral root systems.

Figure. 4.10 High Salt Concentrations Severely Impact Root Growth

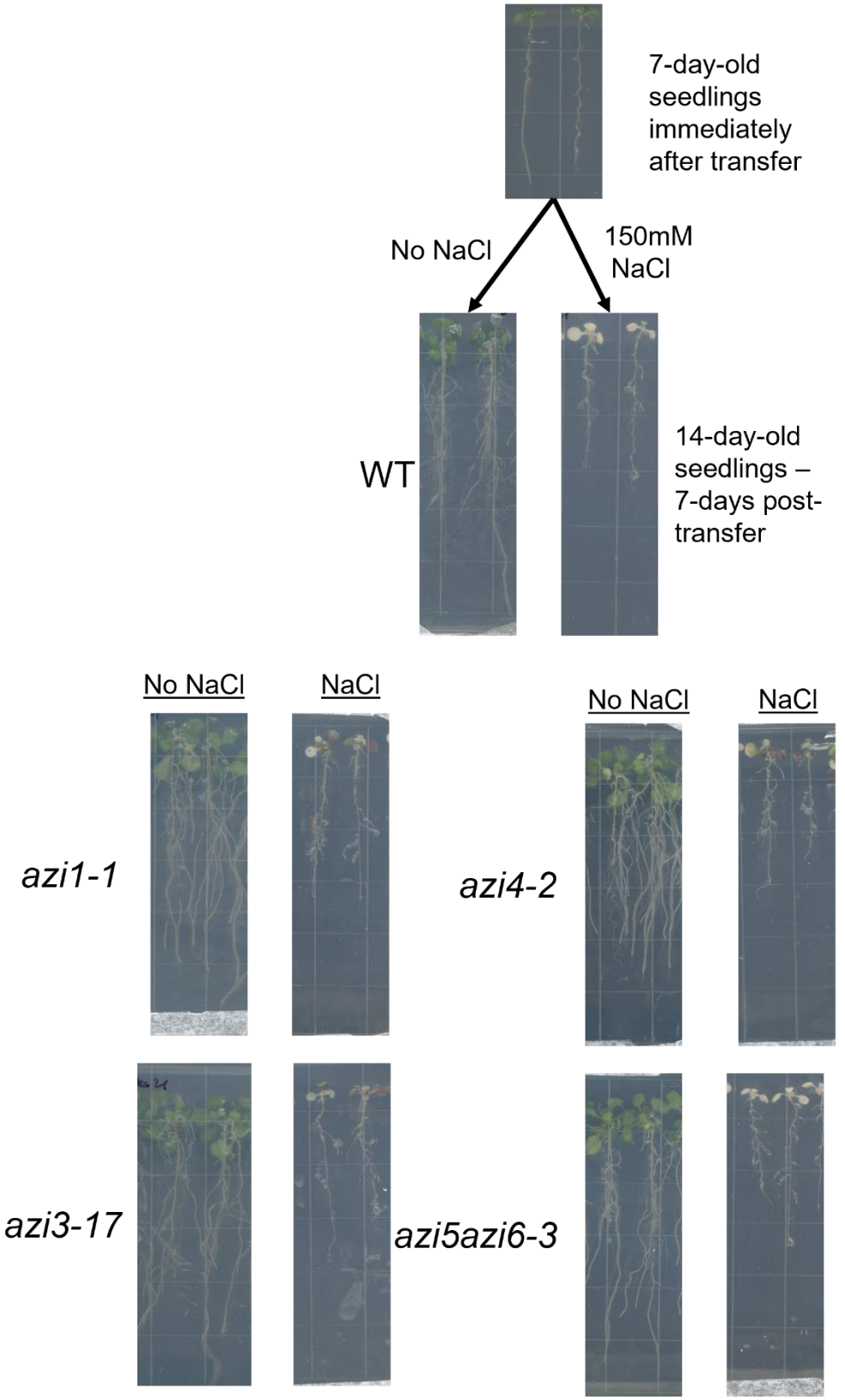

Figure. 4.10 High [Salt] Negatively Impacts Plant Growth
Surface-sterilized seedlings were germinated in unchallenging conditions on ½MS agar. 7-days-post-germination, 7-8 seedlings were transferred from the germination plates to new ½MS agar plates either supplemented with 150mM NaCl (NaCl) or dH_2O (No NaCl). Images were collected at 7-days-post transfer using an Epson scanner and root lengths were assessed using ImageJ. Two technical replicates per experiment. Select images shown; similar phenotypes observed among different mutations for the same gene.

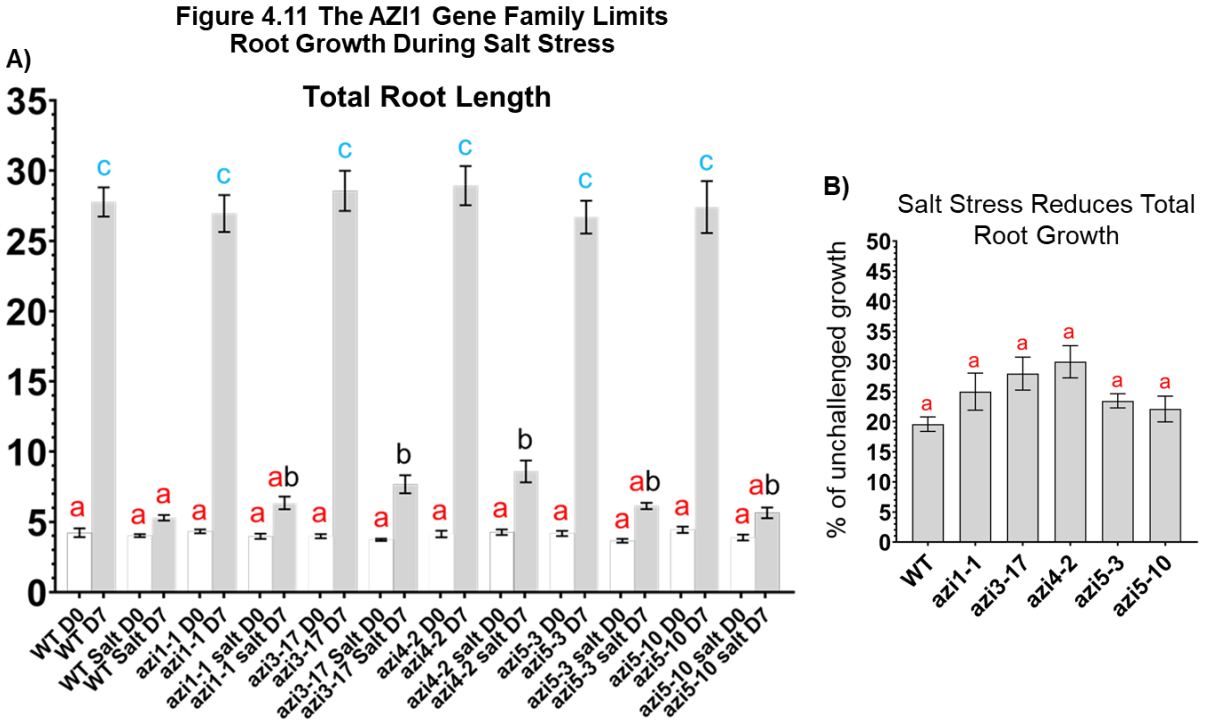

Figure 4.11 The AZI1 Gene Family Affects Root Growth During Salt Stress
A) Total root growth of WT and *azi1*-family mutant seedlings measured 10 days after transfer to ½MS agar supplemented with 150 mM NaCl as in Figure 4.10. B) The change in total root length from Day 0 to Day 7 in the unchallenged and salt-challenged seedlings is plotted. C) To measure the level of root growth inhibit induced by osmotic stress, total root length in the osmotically-challenged plants is plotted as a percentage of the total root length in the unchallenged plants. Mean data from two independent experiments is plotted; n = 7-8 seedlings per genotype per experiment. Error bars are SEM and color-coded letters above bars indicate statistical differences by anova, SNK test. $p<0.05$.

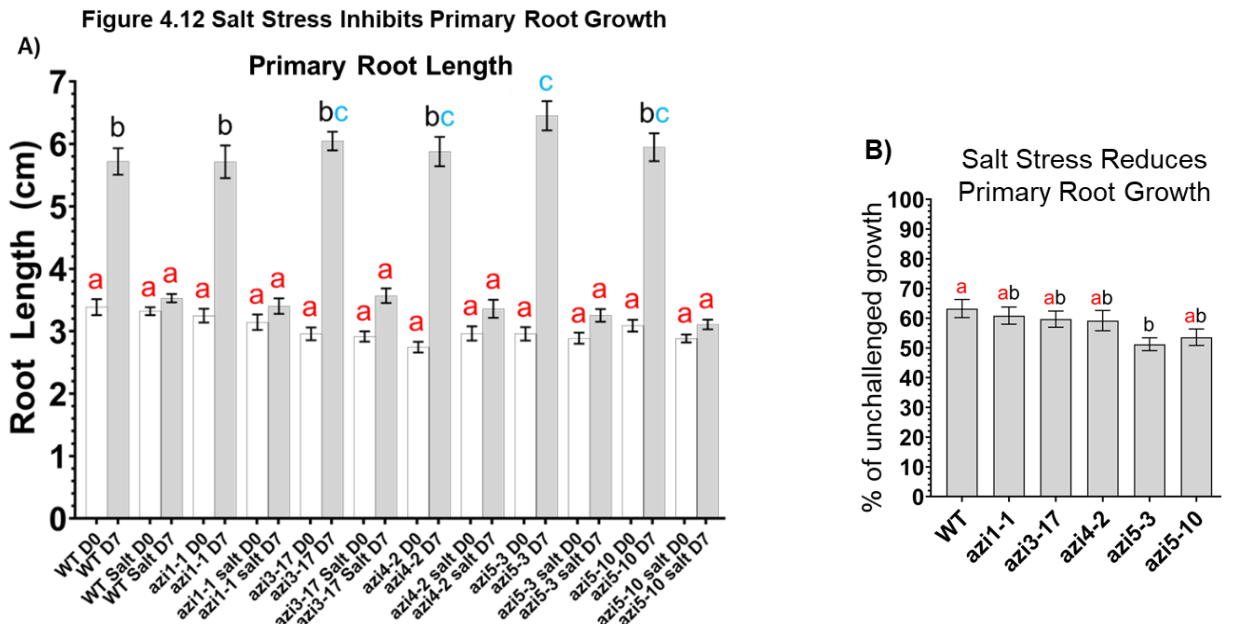

Figure 4.12 Salt Stress Inhibits Primary Root Growth
A) Primary root length of WT and *azi1*-family mutant seedlings was measured 10 days after transfer to ½MS agar supplemented with 150 mM NaCl as in Figure 4.10. B) To measure the level of root growth inhibition caused by osmotic stress, primary root length in the osmotically-challenged plants is plotted as a percentage of the primary root length in the unchallenged plants. Mean data from two independent experiments is plotted; n = 7-8 seedlings per genotype per experiment. Error bars are SEM and color-coded letters above bars indicate statistical differences by anova, SNK test. $p<0.05$.

Discussion

Immune and stress responses generally negatively impact plant growth. For example, the gain of function mutant, *acd6-1* has constitutively active immune signaling and displays a severely dwarfed growth phenotype (Rate et al., 1999; Zhang et al., 2014, 2017). Furthermore, *acd6-1* also has constitutively active MPK3 signaling and accumulates AZI1/EARLI1 in plastids similar during actual infections (Zhang et al. 2014, 2017; Chapter 3; Cecchini et al., 2021).

In recent years, the importance of AZI1 and EARLI1 to plant biotic and abiotic stress responses has been clearly documented. However, analysis of the other AZI1 family genes, and their association or non-association with plastids, has been limited due to the lack of stable

Arabidopsis mutants for AZI3, AZI4, AZI5/AZI6, or AZI7. Herein, we used CRISPR/Cas9-based mutagenesis to demonstrate that similar to AZI1 and EARLI1, the other AZI1 family genes also contribute to AZA signaling, systemic defenses, and root development.

We have recently published evidence for a role of the plastid targeting of AZI1 and EARLI1 during systemic defense priming (Chapter 2, Cecchini et al., 2019, Cecchini, Speed et al., 2021). Here, I report additional findings that the non-plastid-targeted AZI1 family proteins (AZI5/AZI6) are dispensable to SAR, whereas the plastid-associated AZI3 and AZI4 contribute to systemic defenses in leaves. Even small deletions encompassing only one of the cysteines within the 8-cysteine motif of the *azi3* mutants is sufficient to impair SAR, which supports some critical function of the 8-cysteine motif (Fig. 4.1B, Fig. 4.2). In contrast to the *azi3* mutations, the *azi4-2* mutations delete a region within the distal end of the PRR that is completely conserved within AZI1, EARLI1, AZI3, and AZI4. That deleting this region from AZI4 disrupts SAR suggests some critical role of this region in the function of the AZI1 family proteins. It is unlikely that deletion of this small region abolishes plastid targeting, however this region may be modified during defense signaling and could contribute to protein-protein interactions and/or the enhancement of AZI1/EARLI1's plastid targeting during defense signaling (Cecchini et al., 2015; Chapter 3, Cecchini, Speed et al., 2021; Lim et al., 2016; Pitzschke et al., 2014; Jack Riley, Greenberg lab – informal communications).

Figure 4.13 The AZI1 Gene Family Limits Lateral Root Growth during Salt Stress

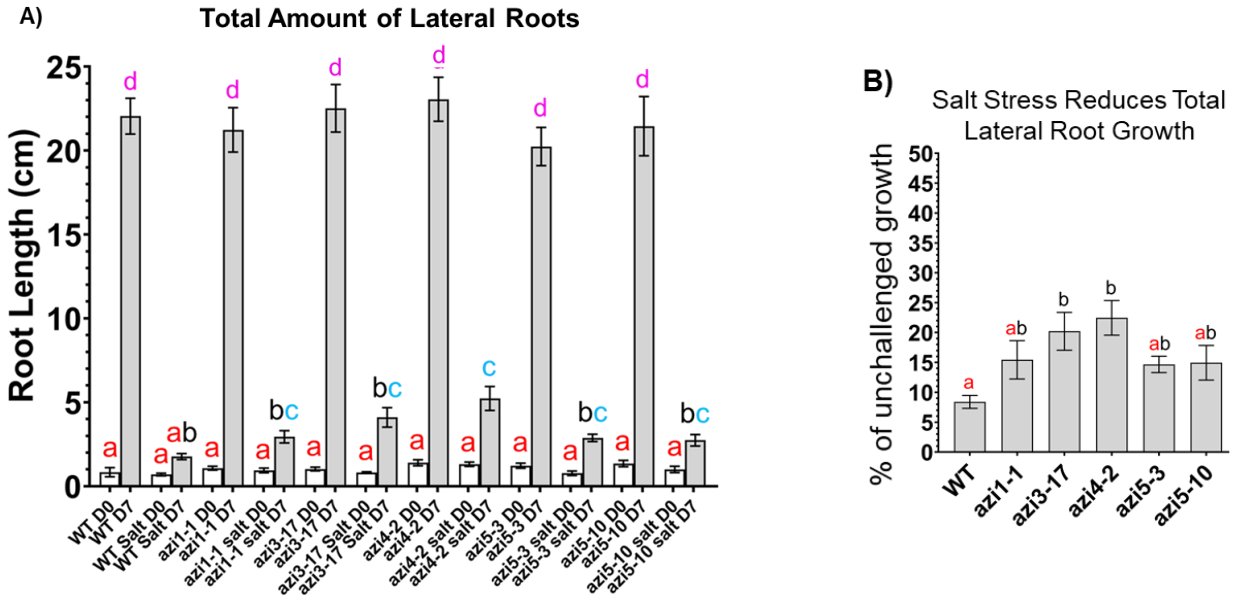

Figure 4.13 The AZI1 Gene Family Inhibits Lateral Root Growth during Salt Stress
A) Total lateral root length of WT and *azi1*-family mutant seedlings was measured 10 days after transfer to ½MS agar supplemented with 150 mM NaCl as in Figure 4.10. B) To measure the level of root growth inhibition caused by osmotic stress, total lateral root length in the osmotically-challenged plants is plotted as a percentage of the total lateral root length in the unchallenged plants. Mean data from two independent experiments is plotted; n = 7-8 seedlings per genotype per experiment. Error bars are SEM and color-coded letters above bars indicate statistical differences by anova, SNK test. $p<0.05$.

Figure 4.14 The AZI1 Gene Family Limits Lateral Root Elongation during Salt Stress

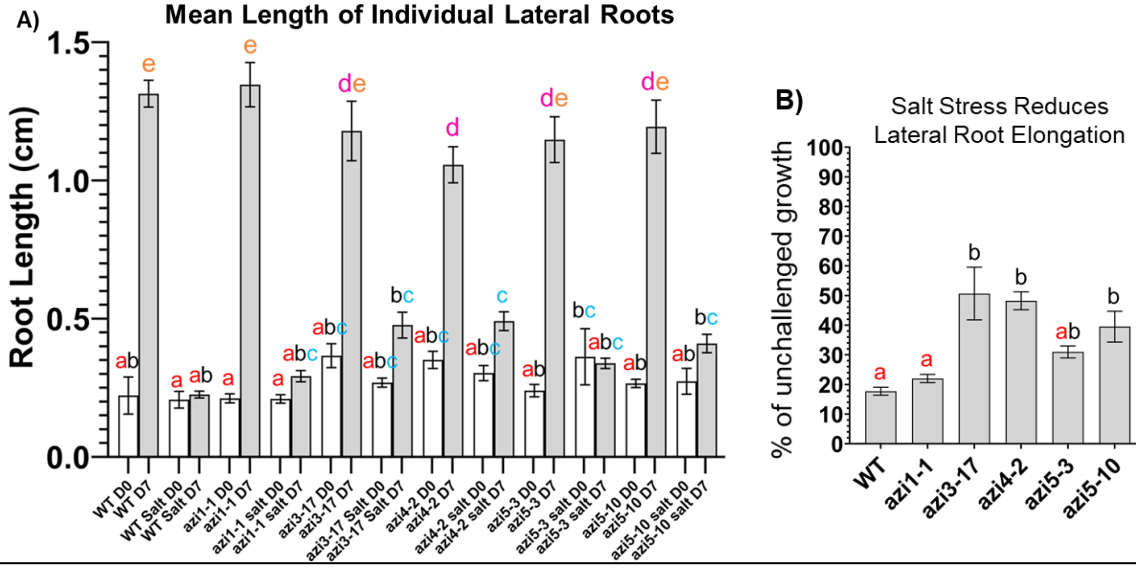

Figure 4.14 The AZI1 Gene Family Inhibits Lateral Root Elongation during Salt Stress
A) The length of individual lateral roots in WT and *azi1*-family mutant seedlings was measured 10 days after transfer to ½MS agar supplemented with 150 mM NaCl as in Figure 4.10. B) To measure the level

Figure 4.14 The AZI1 Gene Family Inhibits Lateral Root Elongation during Salt Stress (cont)
of root growth inhibition caused by osmotic stress, individual lateral root lengths in the osmotically-challenged plants is plotted as a percentage of the total individual lateral root length in the unchallenged plants. Mean data from two independent experiments is plotted; n = 7-8 seedlings per genotype per experiment. Error bars are SEM and color-coded letters above bars indicate statistical differences by anova, SNK test. $p<0.05$.

regulate them during defense signaling (Chapter 2, Cecchini et al., 2019). Here I showed that the root developmental responses to AZA also involve both the plastid-associated (AZI3 and AZI4) and non-plastid-associated (AZI5/AZI6) AZI1 family proteins. I further demonstrated that root-applied AZA limits growth in aerial tissues similar to its effects on root development and leaf defenses and that this aerial growth inhibition also requires the AZI1 gene family.

That local and systemic developmental responses to root-autonomous AZA requires the non-plastid associated AZI1 family proteins, which are not essential for SAR, suggests several possibilities for the roles of the AZI1 family proteins (and their plastid targeting) in coordinating AZA's regulation of plant defense and development: 1) the plastid targeting of the AZI1 family proteins is essential for SAR and defense signaling but not developmental responses to AZA; 2) the plastid targeting of the AZI1 family proteins is non-essential for SAR, defense signaling, and developmental responses to AZA; or 3) the AZI1 family proteins have overlapping but distinct functions. In the third case, the plastid-targeting of only a threshold amount of certain AZI1 family members may be required for systemic defense signaling and/or developmental responses to AZA.

In each of these cases, however, the impact of the root-applied AZA on aerial growth without shootward movement suggests the generation or existence of some second signal that transmits the effects of AZA signaling from roots to shoots. Whether this signaling involves the canonical AZA-G3P signaling pathway or some novel signaling components remains to be discovered. Our previous findings that root-applied AZA primes aerial defenses in a SAR- and

ISR-independent mechanism also suggests that locally applied AZA may stimulate the generation of a second systemic signal in roots, possibly due to some antimicrobial product generated during AZA signaling. However, our present findings that the developmental impacts of AZA are transmitted from root to shoot in an AZI1 family-dependent manner suggests that this signal is most likely lipidic in nature.

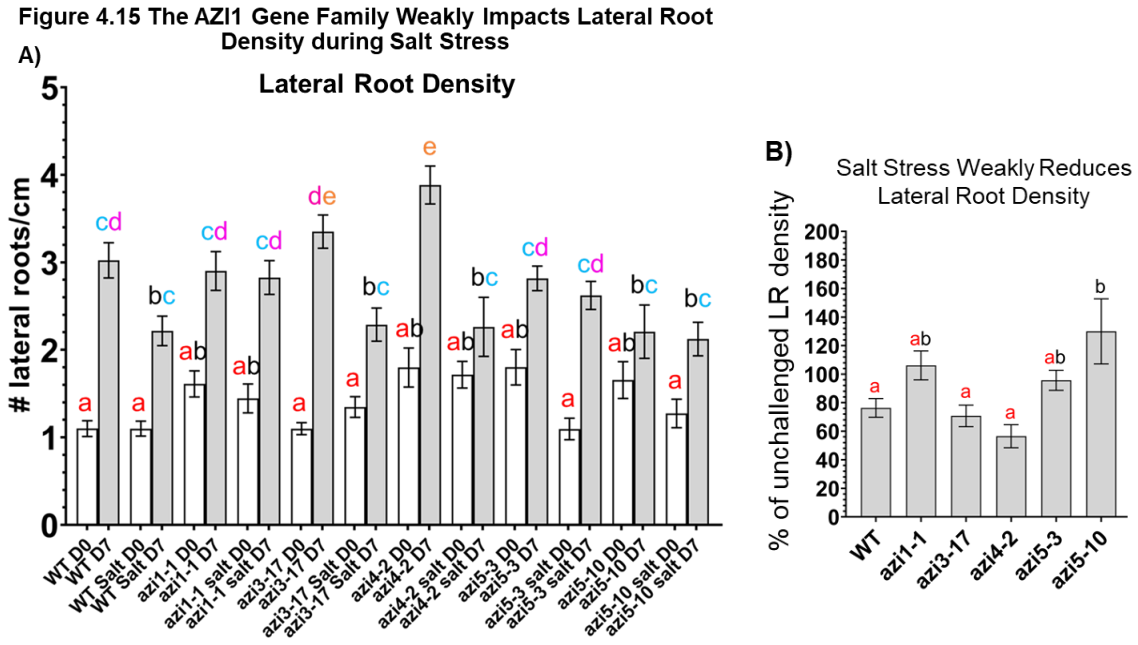

Figure 4.15 The AZI1 Gene Family Weakly Impacts Lateral Root Density during Salt Stress
A) To measure the initiation of new lateral roots, the number of lateral roots per centimeter (LR density) of primary root in WT and *azi1*-family mutant seedlings was measured 10 days after transfer to ½MS agar supplemented with 150 mM NaCl as in Figure 4.10. B) To measure the level of root cell initiation inhibition caused by osmotic stress, LR density in the osmotically-challenged plants is plotted as a percentage of the LR density in the unchallenged plants. Mean data from two independent experiments is plotted; n = 7-8 seedlings per genotype per experiment. Error bars are SEM and color-coded letters above bars indicate statistical differences by anova, SNK test. $p<0.05$.

Interestingly, I found that C8 also impacts root development and has similar but slightly different effects than AZA. I also found that the *azi1* family mutants often showed both a reduced response to AZA and a greater response to C8 when compared to wild-type. AZI1 and EARLI1 interact with DIR1 and defense-associated plasmodesmata proteins to promote defense signaling and the systemic movement of defense signals (Cecchini et al., 2015; Lim et al., 2016;

Yu et al., 2013). It is likely that these and other yet to be discovered proteins contribute to an LTP-based signaling complex that confers responsiveness to several lipid signals. The AZI1 family proteins may confer specificity for AZA to such a complex; loss of these proteins may thus reduce sensitivity to AZA and increase the response to similar lipid compounds.

I also showed that the AZI1 genes negatively impact lateral root development during salt stress. Salt stress largely inhibits plant growth through the generation of negative osmotic pressure that inhibits water uptake from the salt. Though some information is known about the development of roots under osmotic stress induced by drought, it is unknown if similar root phenotypes would develop from salt-induced osmotic stress as high salt concentrations generally completely arrest plant growth and development. Here, I assessed the impact of salt on root development by transferring 7-day-old seedlings to the salt condition instead of germinating the seedlings on salt. Surprisingly, I found that the *azi1* family mutants typically showed greater root growth on the salt condition than wild-type seedlings and that this effect was largely due to increased lateral root elongation in the *azi1* mutants. I also found that several *azi1* family mutants, *azi4-2* in particular, showed a decrease in the basal length of individual lateral roots when compared to wild-type.

Our data indicate that the AZI1 family proteins regulate the root responses to stress, likely by impacting lateral root development. Though AZA and high salt concentrations both limit root growth, AZA more strongly inhibits primary root growth relative to the development of lateral roots. In contrast, salt stress more strongly inhibits lateral root growth than primary root growth. That both these effects on lateral root development involve the AZI1 family proteins suggests a role for this gene family in regulating the balance between primary and lateral root growth during stress.

Figure 4.16 The AZI1 Gene Family Reduces the Bias for Lateral Root Development During Salt Stress

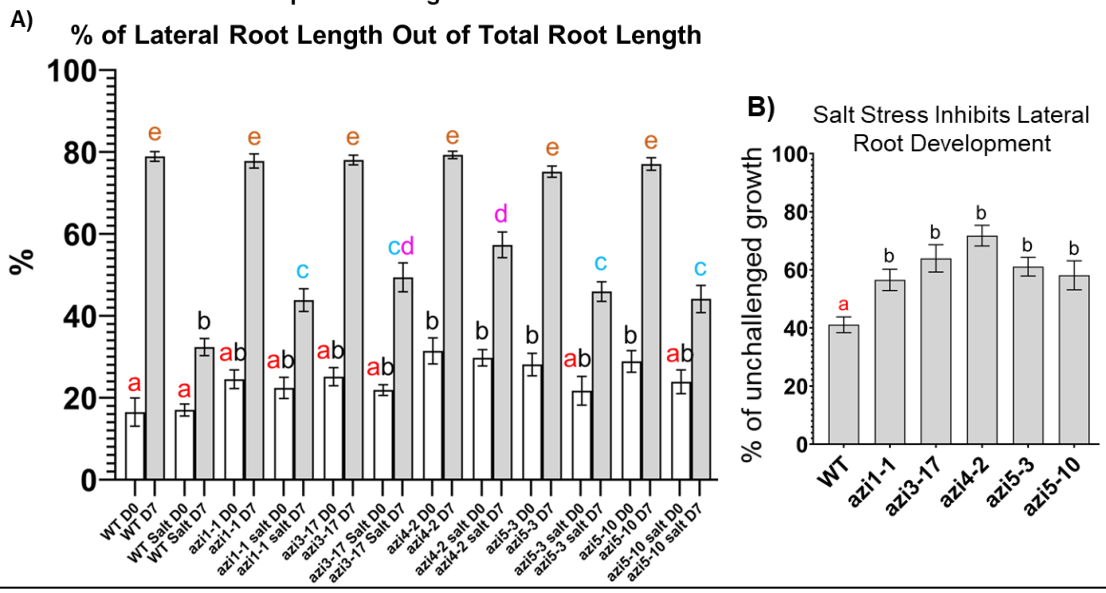

Figure 4.16 The AZI1 Gene Family Lowers the Commitment to Lateral Root Development During Salt Stress

A) To measure the impact of osmotic stress on commitment to lateral root development, the total lateral root growth is plotted as a percentage of the total root growth (% LR) of WT and *azi1*-family mutant seedlings measured 10 days after transfer to ½MS agar supplemented with 150 mM NaCl as in Figure 4.10. B) The change in % LR from Day 0 to Day 7 in the unchallenged and osmotically-challenged seedlings is plotted. C) To measure the level of inhibition of lateral root development induced by osmotic stress, % LR in the osmotically-challenged plants is plotted as a percentage of the %LR in the unchallenged plants. Mean data from two independent experiments is plotted; n = 7-8 seedlings per genotype per experiment. Error bars are SEM and color-coded letters above bars indicate statistical differences by anova, SNK test. $p<0.05$.

The kinases MPK3 and MPK6 regulate root growth during basal and stress conditions as well as plant survival during osmotic stress (Lu et al., 2020; Shao et al., 2020; Yan et al., 2021; Zhu et al., 2019). That MPK3 and MPK6 affect the plastid targeting of AZI1 and EARLI1, are essential for the same immune and developmental responses as the AZI1 gene family, and regulate root growth during stress signaling suggests that the AZI1 family proteins contribute to the MPK3/MPK6-mediated coordination of root growth and defense signaling (Cecchini et al., 2015; Chapter 2, Cecchini et al., 2019; Chapter 3, Cecchini et al., 2021).

I also found an increased local pathogen susceptibility in *azi5azi6-10*, but not the *azi5azi6-3* mutation. *azi5azi6-10* retains the entirety of its HD and (small) PRR in contrast to

azi5azi6-3 which retains less than half of its HD. In light of our recent findings that AZI1's HD is sufficient to confer membrane association, it is possible the *azi5azi6-10* gene product has a dominant negative effect on local defenses by interfering with proteins that normally interact with the AZI1 family proteins (Chapter 3, Cecchini, Speed et al., 2021). Consistent with this possibility, the *azi3*, *azi4*, and *azi5azi6* partial deletion mutants often showed a greater response to C8 than the *azi1-1* null mutant. Genetic analysis of *azi3*, *azi4*, and *azi5azi6* CRISPR alleles via crossing or transformation into wild-type plants could clarify the mechanisms of their effects on SAR and AZA signaling.

It remains to be determined if AZA-induced root development contributes to defense signaling. It has been recently proposed that AZA contributes to the control of the tomato rhizosphere through a root-based systemic signaling mechanism termed SIREM (systemically induced root exudation of metabolites; Korenblum et al., 2020).

ACKNOWLEGDEMENTS

This research was supported by National Science Foundation grant IOS1456904 to JTG. DJ Speed was supported by National Institutes of Health training grant T32 GM007183, the Ford Foundation Predoctoral Fellowship, and the Howard Hughes Medical Institute Gilliam Fellowship for Advanced Study. I thank Claire Parent for selecting the CRISPR target sites and cloning the CRISPR constructs. I thank Zeeshan Z. Banday for helpful discussions and for plotting the bacterial resistance data. I thank Jessica Morgan for assistant with one of the SAR experiments.

Supplemental Figure 4.1: R Script for SAR

```
> library(ggplot2)
library(dplyr)
setwd("~/Desktop")
filename <- "SAR-rdata/DJdataSAR_allcombined.txt"
my_data <- read.delim (filename, header=TRUE)
my_data$Samples<-factor(my_data$Samples, levels = c("sample1 mock","sample1 DG6","sample2 mock", "sample2 DG6"))
my_data$genotype<-factor(my_data$genotype, levels = c("WT","mutant1","mutant2"))
clean_data <- my_data %>%
  group_by (Samples, genotype) %>%
  summarize(mean_cfu = mean(cfu), sd_cfu = sd(cfu), count = n(), se_cfu = (sd_cfu/(sqrt(count))))
ggplot(clean_data, aes(x=genotype, y=mean_cfu, fill = Samples, group= Samples)) +
  geom_bar(stat="identity", color="black", position = position_dodge(width = 0.7), width = 0.6)+
  theme_bw()+
  scale_y_log10(breaks = scales::trans_breaks("log10", function(x) 10^x),
                labels = scales::trans_format("log10", scales::math_format(10^.x))) +
  scale_x_discrete(labels=c("WT mock \n\n WT DG6","mutant1 mock \n\n mutant1 DG6","mutant2 mock \n\n mutant2 DG6")) +
  scale_fill_manual(values=c("white", "grey", "white", "grey", "white", "grey"))+
  geom_errorbar(aes(ymin = mean_cfu-se_cfu, ymax = mean_cfu+se_cfu),
                position = position_dodge(width = 0.7), width = 0.2)+
  theme(axis.text.x = element_text(angle = 90, size = 10, hjust =1, vjust = 0.5), axis.text.y = element_text(size=10),
        axis.ticks.length.y = unit(.20, "cm"),
        axis.ticks.length.x = unit(.15, "cm"), axis.title.x = element_blank())+ ylab(expression(log[10]~CFU/leaf~disc))
 ### anova snk.test
library(agricolae)
model<-aov(cfu~Samples, data=my_data)
out <- SNK.test(model,"samples", console=TRUE)
print(SNK.test(model,"samples", group=FALSE))
```

Supplemental Figure 4.2: R Script for SAR Response Gain

```
> library(ggplot2)
library(dplyr)
setwd("~/Desktop")
filename <- "SAR-rdata/DJdata_SAR_response gain.txt"
my_data <- read.delim (filename, header=TRUE)
my_data$samples<-factor(my_data$samples, levels = c("sample1","sample2"))
my_data$genotype<-factor(my_data$genotype, levels = c("WT","mutant1","mutant2"))
clean_data <- my_data %>%
  group_by(samples) %>%
  group_by(genotype) %>%
  group_by(error) %>%
  summarize(mean_gain = mean(gain), sd_gain = sd(gain), count = n(), se_gain = (sd_gain/(sqrt(count))))
View(clean_data)
ggplot(clean_data, aes(x=genotype, y=mean_gain, fill = genotype)) +
  geom_bar(stat="identity", color="black", position = position_dodge(width = 0.7), width = 0.6)+
  theme_bw()+
  scale_x_discrete(labels=c("WT","mutant1","mutant2"))+
  scale_fill_manual(values=c("black","black","black"))+
  geom_errorbar(aes(ymin = mean_gain-error, ymax = mean_gain+error), width = 0.2)
```

CHAPTER 5

CONCLUSION

In the preceding chapters, I showed that the AZI1 gene family is required for root responses to AZA, AZA-induced defense priming, SAR, and ISR (Cecchini et al., 2019; Cecchini, Speed et al., 2021). Together with collaborators, I demonstrated that AZI1's HD and PRR form a bipartite targeting signal that localizes AZI1 to plastid envelopes. We also revealed that the kinases MPK3 and MPK6 are essential for the priming of root-triggered (ISR) and leaf-triggered (SAR), AZA-induced defense priming, increases in lateral root density due to AZA treatment (Chapter 2, Cecchini et al., 2019; Chapter 4). Our findings that MPK3 and MPK6 also promote the accumulation of AZI1 and EARLI1 at plastids, the site of defense signal production, during infections presents the possibility that the AZI1 protein family serves as a downstream target of MAPK signaling that coordinates the defense and development activities of MPK3 and MPK6 (Fig. 5.1; Chapter 3, Cecchini et al., 2021).

MAPK cascades contribute to a wide array of developmental and stress responses (Chai et al., 2014; Sopeña-Torres et al., 2018; Yan et al., 2021; Zhu et al., 2019). These highly conserved cascades amplify signals from plasma membrane receptors to stimulate various downstream response pathways (Sun et al., 2022; Xu et al., 2015). In general, the perception of stimuli by cell surface or cytosolic receptors causes activation of MAPKKKs (MAPK kinase kinases) which phosphorylate and activate MAPKKs. The subsequent activation and phosphorylation of MAPKs like MPK3 and MPK6 induces the downstream modification of many substrates and the regulation of the requisite signaling pathways like pathogen (PTI)- and effector (ETI)-triggered immune signaling (Jones and Dangl, 2000; Rodriguez et al., 2010).

PTI and ETI activate the kinases MPK3 and MPK6 and induce expression of the *AZI1* gene family, which are also required for normal responses to pathogen infection (Beckers et al., 2009; Jung et al., 2009; Cecchini et al., 2015; Chapter 2, Cecchini et al., 2019; Chapter 3; Cecchini et al., 2021). That MPK3 and MPK6 are required for the normal localization of AZI1/EARLI1 during infections, suggests that the plastid targeting of AZI1 proteins may be important for their defense signaling ability. Consistent with this expectation, the non-plastid-targeted AZI5 and AZI6 appear dispensable for SAR. In contrast, even partial deletion of AZI3 or AZI4, which target to plastids (AZI3) and have PRRs similar to AZI1/EARLI1 (AZI3 and AZI4) is sufficient to disrupt SAR. Additionally, AZI1, EARLI1, AZI3, and AZI4 are upregulated upon infection with SAR-inducing bacteria, colonization with ISR-promoting bacteria, or treatment with the MAMP flg22, whereas AZI5 and AZI6 are downregulated in response to *P. simiae* or flg22 treatment (Gupta et al., 2017; Jung et al., 2009; Stringlis et al., 2018; Chapter 3, Cecchini, Speed et al., 2021; Howard et al., 2013; Mohr and Cahill, 2007; Qutob et al., 2006; Thilmony et al., 2006; Zamioudis et al., 2014).

Interestingly, although the AZI4-2 variant proteins occur within the PRR, I expect the *azi4-2* mutants to localize to plastids (Banday et al., *in rev*; Jack Riley, Greenberg lab - informal communications). Each of the *azi4-2* alleles has a deletion encompassing 2 short amino acid motifs conserved within the PRRs of AZI1, EARLI1, and AZI3 (Fig. 1.3; Fig. 4.1B). Though the function of these motifs remains to be determined, it is possible they contribute to the MPK3-dependent accumulation of AZI1/EARLI1 at plastids during infections (Chapter 3, Cecchini et al., 2021). Modification of this region by MPK3 may alter AZI1's interactions with defense-associated proteins or chaperones that might affect its subcellular targeting (Cecchini et al., 2015; Kim et al., 2011; Lee et al., 2014; Lim et al., 2016; Pitzschke et al., 2014). In support of

this possibility, AZI1$^{\Delta 2\text{-}25}$:GFP, which still contains the PRR, stably associates with microtubule filaments (Chapter 3; Cecchini, Speed et al., 2021). Salt stress activates a Protein Tyrosine Phosphatase 1 (PTP1)-MPK3/MPK6 signaling cascade that promotes microtubule depolymerization in cortical cells, which are critical to cell elongation (Bartels et al., 2009). Given AZI1's potential interactions with microtubules and our findings that the AZI1 gene family negatively regulates lateral root growth during salt stress, AZI1 may function as a downstream component of PTP1-MPK3/MPK6-dependent microtubule depolymerization. Additional regulatory components of MPK3- and AZI1-dependent lateral root growth may be found within the YDA-MKK4/MKK5-MPK3/MPK6 signaling cascades (Shao et al., 2020; Yan et al., 2021; Zhu et al., 2019).

The YDA-MPK3/MPK6 signaling cascade is activated during PTI and ETI and regulates floral organ abscission and broad-spectrum resistance to fungi (Sopena-Torres et al., 2018). *yda*, *mkk4mkk5*, and *mpk3mpk6* mutants show a short root phenotype associated with reduced expression of auxin-responsive genes, PLT1 and PLT2, which control root cell differentiation (Santuari et al., 2016; Shao et al., 2020).

Recently, it was shown that this cascade also directly regulates lateral root development, which suggests this signaling cascade may coordinate defense signaling with development (Zhu et al., 2019). Analysis of *mpk3mpk6* and *mkk4mkk5* mutants revealed a significant reduction in lateral root growth due to defects in MPK3/MPK6-dependent pectin degradation at the site of lateral root emergence (Zhu et al., 2019). Identical lateral root emergence and floral abscission defects are observed due to loss of function mutations in *HAE/HSL2* or *IDA*, a receptor-like kinase and the gene encoding its ligand, respectively. Overexpression of MKK4 in an *ida* or *hae/hsl2* background activates MPK3/MPK6 in roots and rescues the lateral root defects seen in

these mutants and exogenous application of IDA to roots stimulates activation of MPK3/MPK6 in *ida* but not *hae/hsl2* mutants. Collectively, this data suggests that MKK4/MKK5 and MPK3/MPK6 function downstream of IDA and HAE/HSL2 in YDA-mediated lateral root development (Fig 5.1).

Hybrid Proline-Rich Proteins and other non-specific LTPs are widely distributed among plants and promote bacterial resistance and tolerance to abiotic stress similar to the AZI1 family (Liu et al., 2016). In tomato, the 8-cysteine motif-containing HyPRP1 and DEA1 have been recently identified as regulators of disease, salt, drought, and extreme temperature responses (Debbarma et al., 2021; Saikia et al., 2020; Saradadevi et al., 2021; Weyman et al., 2021). Determining how the AZI1 protein family interacts with other downstream targets of YDA-MKK4/MKK5-MPK3/MPK6 that regulate plant growth during like the salt-responsive ARR1/10/12 (Arabidopsis Response Regulators) could greatly elucidate how the AZI1 protein family coordinates plant development with defense (Yan et al., 2021).

Fig. 5.1 The AZI1 Gene Family May in MPK3/MPK6-dependent Control of Root Development during Stress

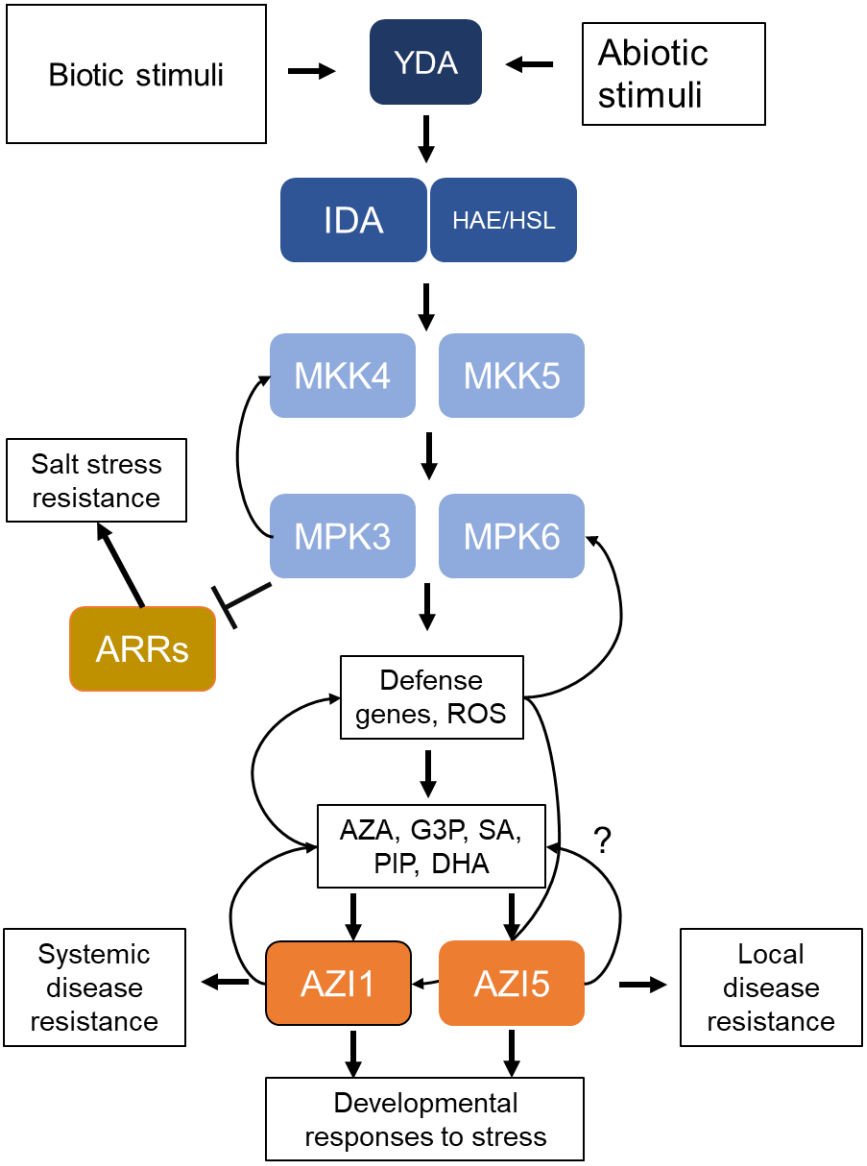

Figure. 5.1 The AZI1 Gene Family May in MPK3/MPK6-dependent Control of Root Development during Stress

AZI1 and *EARLI1* are essential components of several defense and developmental pathways that involve activity from the YDA-MKK4/MKK5-MPK3/MPK6 signaling cascades. YDA-MKK4/MKK5-MPK3/MPK6 signaling activates defense genes and generates reactive oxygen species that prime the production of defense and development signals like AZA. AZA triggers the expression of AZI1 and EARLI1 which promote systemic AZA signaling and primes responses to biotic and abiotic stresses. The precise placement of AZI1 within YDA-MKK4/MKK5-MPK3/MPK6 signaling cascades and how it interacts with known YDA-MKK4/MKK5-MPK3/MPK6 signals like the ARRs proteins remains to be determined.

Note: AZI1 = AZI1, EARLI1, AZI3, and AZI4; AZI5 = AZI5, AZI6, and AZI7.

REFERENCES

1. Acosta, I. F., & Farmer, E. E. (2010). Jasmonates. The Arabidopsis Book, 8, e0129-e0129. https://doi.org/10.1199/tab.0129
2. Báez, R. R., & Nemhauser, J. L. (2021). Expansion and innovation in auxin signaling: Where do we grow from here? In Development (Cambridge) (Vol. 148): Company of Biologists Ltd.
3. Banday, Z. Z., Cecchini, N. M., Scott, A. T., Hu, C. T., Filzen, R. C., Agbo, E., & Greenberg, J. T. Friend or Foe: Hybrid proline-rich proteins determine how plants interact with and 1 respond to beneficial and pathogenic microbes 2. https://academic.oup.com/plcell/pages/General-Instructions
4. Bartels, S., Anderson, J. C., González Besteiro, M. A., Carreri, A., Hirt, H., Buchala, A., Métraux, J. P., Peck, S. C., & Ulm, R. (2009). Map kinase phosphatase1 and protein tyrosine phosphatase1 are repressors of salicylic acid synthesis and SNC1 -mediated responses in Arabidopsis. Plant Cell, 21(9), 2884-2897. https://doi.org/10.1105/tpc.109.067678
5. Berendsen, R. L., Pieterse, C. M. J., & Bakker, P. A. H. M. (2012). The rhizosphere microbiome and plant health. Trends in Plant Science, 17(8), 478-486. https://doi.org/10.1016/j.tplants.2012.04.001
6. Blatt, M. R., Chaumont, F., & Farquhar, G. (2014). Focus on water. In Plant Physiology (Vol. 164, pp. 1553-1555): American Society of Plant Biologists.
7. Carella, P. (2020). Xylem-Mobile Oxylipins Are Critical Regulators of Induced Systemic Resistance in Maize. The Plant cell, 32(1), 13-14. https://doi.org/10.1105/tpc.19.00924
8. Cecchini, N. M., Roychoudhry, S., Speed, D. Q. J., Steffes, K., Tambe, A., Zodrow, K., Konstantinoff, K., Jung, H. W., Engle, N. L., Tschaplinski, T. J., & Greenberg, J. T. (2019). Underground azelaic acid–conferred resistance to pseudomonas syringae in arabidopsis. Molecular Plant-Microbe Interactions, 32(1), 86-94. https://doi.org/10.1094/MPMI-07-18-0185-R
9. Cecchini, N. M., Speed, D. Q. J., Roychoudhry, S., & Greenberg, J. T. (2021). Kinases and protein motifs required for AZI1 plastid localization and trafficking during plant defense induction. Plant Journal, 105(6), 1615-1629. https://doi.org/10.1111/tpj.15137
10. Cecchini, N. M., Steffes, K., Schlappi, M. R., Gifford, A. N., & Greenberg, J. T. (2015). Arabidopsis AZI1 family proteins mediate signal mobilization for systemic defence priming. Nature Communications, 6(May). https://doi.org/10.1038/ncomms8658
11. Chai, J., Liu, J., Zhou, J., & Xing, D. (2014). Mitogen-activated protein kinase 6 regulates NPR1 gene expression and activation during leaf senescence induced by salicylic acid. Journal of Experimental Botany, 65(22), 6513-6528. https://doi.org/10.1093/jxb/eru369
12. Chini, A., Boter, M., & Solano, R. (2009). Plant oxylipins: COI1/JAZs/MYC2 as the core jasmonic acid-signalling module. In FEBS Journal (Vol. 276, pp. 4682-4692): Blackwell Publishing Ltd.

13. Comas, L. H., Becker, S. R., Cruz, V. M. V., Byrne, P. F., & Dierig, D. A. (2013). Root traits contributing to plant productivity under drought. In Frontiers in Plant Science (Vol. 4): Frontiers Research Foundation.

14. Crombez, H., Motte, H., & Beeckman, T. (2019). Tackling Plant Phosphate Starvation by the Roots. In Developmental Cell (Vol. 48, pp. 599-615): Cell Press.

15. de León, I. P., Hamberg, M., & Castresana, C. (2015). Oxylipins in moss development and defense. Frontiers in Plant Science, 6(JULY), 1-12. https://doi.org/10.3389/fpls.2015.00483

16. Durrant, W. E., & Dong, X. (2004). Systemic acquired resistance. In Annual Review of Phytopathology (Vol. 42, pp. 185-209).

17. Dvořáková, L., Cvrčková, F., & Fischer, L. (2007). Analysis of the hybrid proline-rich protein families from seven plant species suggests rapid diversification of their sequences and expression patterns. BMC Genomics, 8, 1-16. https://doi.org/10.1186/1471-2164-8-412

18. Dvořaková, L., Srba, M., Opatrny, Z., & Fischer, L. (2012). Hybrid proline-rich proteins: Novel players in plant cell elongation? Annals of Botany, 109(2), 453-462. https://doi.org/10.1093/aob/mcr278

19. Efthimiadou, A., Katsenios, N., Chanioti, S., Giannoglou, M., Djordjevic, N., & Katsaros, G. (2020). Effect of foliar and soil application of plant growth promoting bacteria on growth, physiology, yield and seed quality of maize under Mediterranean conditions. Scientific Reports, 10(1). https://doi.org/10.1038/s41598-020-78034-6

20. Fitoussi, N., Borrego, E., Kolomiets, M. V., Qing, X., Bucki, P., Sela, N., Belausov, E., & Braun Miyara, S. (2021). Oxylipins are implicated as communication signals in tomato–root-knot nematode (Meloidogyne javanica) interaction. Scientific Reports, 11(1). https://doi.org/10.1038/s41598-020-79432-6

21. Gao, Q. M., Zhu, S., Kachroo, P., & Kachroo, A. (2015). Signal regulators of systemic acquired resistance. Frontiers in Plant Science, 6(APR). https://doi.org/10.3389/fpls.2015.00228

22. Grebner, W., Stingl, N. E., Oenel, A., Mueller, M. J., & Berger, S. (2013). Lipoxygenase6-dependent oxylipin synthesis in roots is required for abiotic and biotic stress resistance of Arabidopsis. Plant Physiology, 161(4), 2159-2170. https://doi.org/10.1104/pp.113.214544

23. Gudesblat, G. E., Iusem, N. D., & Morris, P. C. (2007). Guard cell-specific inhibition of Arabidopsis MPK3 expression causes abnormal stomatal responses to abscisic acid and hydrogen peroxide. New Phytologist, 173(4), 713-721. https://doi.org/10.1111/j.1469-8137.2006.01953.x

24. Gupta, A., & Senthil-Kumar, M. (2017). Transcriptome changes in Arabidopsis thaliana infected with Pseudomonas syringae during drought recovery. Scientific Reports, 7(1). https://doi.org/10.1038/s41598-017-09135-y

25. Guttman, D. S., & Greenberg, J. T. (2001). Functional Analysis of the Type III Effectors AvrRpt2 and AvrRpm1 of Pseudomonas syringae with the Use of a Single-Copy Genomic Integration System (/ 145 MPMI, Issue.

26. Haeggström, J. Z., & Funk, C. D. (2011). Lipoxygenase and leukotriene pathways: Biochemistry, biology, and roles in disease. In Chemical Reviews (Vol. 111, pp. 5866-5896).

27. Haney, C. H., Samuel, B. S., Bush, J., & Ausubel, F. M. (2015). Associations with rhizosphere bacteria can confer an adaptive advantage to plants. Nature Plants, 1(6). https://doi.org/10.1038/nplants.2015.51

28. Howard, B. E., Hu, Q., Babaoglu, A. C., Chandra, M., Borghi, M., Tan, X., He, L., Winter-Sederoff, H., Gassmann, W., Veronese, P., & Heber, S. (2013). High-Throughput RNA Sequencing of Pseudomonas-Infected Arabidopsis Reveals Hidden Transcriptome Complexity and Novel Splice Variants. PLoS ONE, 8(10). https://doi.org/10.1371/journal.pone.0074183

29. Jiang, M., Zhang, Y., Li, P., Jian, J., Zhao, C., & Wen, G. (2022). Mitogen-Activated Protein Kinase and Substrate Identification in Plant Growth and Development. International Journal of Molecular Sciences, 23(5), 2744-2744. https://doi.org/10.3390/ijms23052744

30. José-Estanyol, M., Gomis-Rüth, F. X., & Puigdomènech, P. (2004). The eight-cysteine motif, a versatile structure in plant proteins. In Plant Physiology and Biochemistry (Vol. 42, pp. 355-365).

31. Jung, H. W., Tschaplinski, T. J., Wang, L., Glazebrook, J., & Greenberg, J. T. (2009). Priming in systemic plant immunity. Science, 324(5923), 89-91. https://doi.org/10.1126/science.1170025

32. Kim, D. H., Xu, Z. Y., Na, Y. J., Yoo, Y. J., Lee, J., Sohn, E. J., & Hwang, I. (2011). Small heat shock protein Hsp17.8 functions as an AKR2A cofactor in the targeting of chloroplast outer membrane proteins in arabidopsis. Plant Physiology, 157(1), 132-146. https://doi.org/10.1104/pp.111.178681

33. Korenblum, E., Dong, Y., Szymanski, J., Panda, S., Jozwiak, A., Massalha, H., Meir, S., Rogachev, I., & Aharoni, A. Rhizosphere microbiome mediates systemic root metabolite exudation by root-to-root signaling. https://doi.org/10.1073/pnas.1912130117/-/DCSupplemental

34. Lee, J., Kim, D. H., & Hwang, I. (2014). Specific targeting of proteins to outer envelope membranes of endosymbiotic organelles, chloroplasts, and mitochondria. In Frontiers in Plant Science (Vol. 5): Frontiers Research Foundation.

35. Li, M., Yu, G., Cao, C., & Liu, P. (2021). Metabolism, signaling, and transport of jasmonates. In Plant communications (Vol. 2, pp. 100231-100231): NLM (Medline).

36. Lim, G. H., Shine, M. B., De Lorenzo, L., Yu, K., Cui, W., Navarre, D., Hunt, A. G., Lee, J. Y., Kachroo, A., & Kachroo, P. (2016). Plasmodesmata Localizing Proteins Regulate Transport and Signaling during Systemic Acquired Immunity in Plants. Cell Host and Microbe, 19(4), 541-549. https://doi.org/10.1016/j.chom.2016.03.006

37. Lindsey, B. E., Rivero, L., Calhoun, C. S., Grotewold, E., & Brkljacic, J. (2017). Standardized method for high-throughput sterilization of Arabidopsis seeds. Journal of Visualized Experiments, 2017(128). https://doi.org/10.3791/56587

38. Liu, W., Xie, X., Ma, X., Li, J., Chen, J., & Liu, Y. G. (2015). DSDecode: A web-based tool for decoding of sequencing chromatograms for genotyping of targeted mutations. In Molecular Plant (Vol. 8, pp. 1431-1433): Cell Press.

39. Lu, X., Shi, H., Ou, Y., Cui, Y., Chang, J., Peng, L., Gou, X., He, K., & Li, J. (2020). RGF1-RGI1, a Peptide-Receptor Complex, Regulates Arabidopsis Root Meristem Development via a MAPK Signaling Cascade. Molecular Plant, 13(11), 1594-1607. https://doi.org/10.1016/j.molp.2020.09.005

40. Ma, X., Zhu, Q., Chen, Y., & Liu, Y. G. (2016). CRISPR/Cas9 Platforms for Genome Editing in Plants: Developments and Applications. In Molecular Plant (Vol. 9, pp. 961-974): Cell Press.

41. Malinina, L., Patel, D. J., & Brown, R. E. (2017). How α-helical motifs form functionally diverse lipid-binding compartments. Annual Review of Biochemistry, 86, 609-636. https://doi.org/10.1146/annurev-biochem-061516-044445

42. Martínez, E., & Campos-Gómez, J. (2016). Oxylipins produced by Pseudomonas aeruginosa promote biofilm formation and virulence. Nature Communications, 7. https://doi.org/10.1038/ncomms13823

43. Maynard, D., Chibani, K., Schmidtpott, S., Seidel, T., Spross, J., Viehhauser, A., & Dietz, K. J. (2021). Biochemical characterization of 13-lipoxygenases of arabidopsis thaliana. International Journal of Molecular Sciences, 22(19). https://doi.org/10.3390/ijms221910237

44. McLaughlin, H. M., Ang, A. C. H., & Østergaard, L. (2021). Noncanonical Auxin Signaling. In Cold Spring Harbor perspectives in biology (Vol. 13): NLM (Medline).

45. Mohr, P. G., & Cahill, D. M. (2007). Suppression by ABA of salicylic acid and lignin accumulation and the expression of multiple genes, in Arabidopsis infected with Pseudomonas syringae pv. tomato. Functional and Integrative Genomics, 7(3), 181-191. https://doi.org/10.1007/s10142-006-0041-4

46. Mosblech, A., Feussner, I., & Heilmann, I. (2009). Oxylipins: Structurally diverse metabolites from fatty acid oxidation. In Plant Physiology and Biochemistry (Vol. 47, pp. 511-517).

47. Návarová, H., Bernsdorff, F., Döring, A. C., & Zeier, J. (2013). Pipecolic acid, an endogenous mediator of defense amplification and priming, is a critical regulator of inducible plant immunity. Plant Cell, 24(12), 5123-5141. https://doi.org/10.1105/tpc.112.103564

48. Niu, D.-D., Liu, H.-X., Jiang, C.-H., Wang, Y.-P., Wang, Q.-Y., Jin, H.-L., & Guo, J.-H. (2011). The Plant Growth-Promoting Rhizobacterium Bacillus cereus AR156 Induces Systemic Resistance in Arabidopsis thaliana by Simultaneously Activating Salicylate-and Jasmonate/Ethylene-Dependent Signaling Pathways. / 533 MPMI, 24(5), 533-542. https://doi.org/10.1094/MPMI

49. Park, S.-W., Kaimoyo, E., Kumar, D., Mosher, S., & Klessig, D. F. Methyl Salicylate Is a Critical Mobile Signal for Plant Systemic Acquired Resistance. https://www.science.org

50. Pérez-Sancho, J., Tilsner, J., Samuels, A. L., Botella, M. A., Bayer, E. M., & Rosado, A. (2016). Stitching Organelles: Organization and Function of Specialized Membrane Contact Sites in Plants. In Trends in Cell Biology (Vol. 26, pp. 705-717): Elsevier Ltd.

51. Petricka, J. J., Winter, C. M., & Benfey, P. N. (2012). Control of arabidopsis root development. In Annual Review of Plant Biology (Vol. 63, pp. 563-590).

52. Pieterse, C. M. J., Van Wees, S. C. M., Van Pelt, J. A., Knoester, M., Laan, R., Gerrits, H., Weisbeek, P. J., & Van Loon, L. C. (1998). A novel signaling pathway controlling induced systemic resistance in arabidopsis. Plant Cell, 10(9), 1571-1580. https://doi.org/10.1105/tpc.10.9.1571

53. Pitzschke, A., Datta, S., & Persak, H. (2014). Salt Stress in arabidopsis: Lipid transfer protein AZI1 and its control by mitogen-activated protein Kinase MPK3. Molecular Plant, 7(4), 722-738. https://doi.org/10.1093/mp/sst157

54. Pozo, M. J., Van Der Ent, S., Van Loon, L. C., & Pieterse, C. M. J. (2008). Transcription factor MYC2 is involved in priming for enhanced defense during rhizobacteria-induced systemic resistance in Arabidopsis thaliana. New Phytologist, 180(2), 511-523. https://doi.org/10.1111/j.1469-8137.2008.02578.x

55. Qutob, D., Kemmerling, B., Brunner, F., Küfner, I., Engelhardt, S., Gust, A. A., Luberacki, B., Seitz, H. U., Stahl, D., Rauhut, T., Glawischnig, E., Schween, G., Lacombe, B., Watanabe, N., Lam, E., Schlichting, R., Scheel, D., Nau, K., Dodt, G., . . . Nürnberger, T. (2006). Phytotoxicity and innate immune responses induced by Nep1-like proteins. Plant Cell, 18(12), 3721-3744. https://doi.org/10.1105/tpc.106.044180

56. Saradadevi, G. P., Das, D., Mangrauthia, S. K., Mohapatra, S., Chikkaputtaiah, C., Roorkiwal, M., Solanki, M., Sundaram, R. M., Chirravuri, N. N., Sakhare, A. S., Kota, S., Varshney, R. K., & Mohannath, G. (2021). Genetic, epigenetic, genomic and microbial approaches to enhance salt tolerance of plants: A comprehensive review. In Biology (Vol. 10): MDPI.

57. Savchenko, T. V., Zastrijnaja, O. M., & Klimov, V. V. (2014). Oxylipins and plant abiotic stress resistance. In Biochemistry (Moscow) (Vol. 79, pp. 362-375): Maik Nauka Publishing / Springer SBM.

58. Shao, Y., Yu, X., Xu, X., Li, Y., Yuan, W., Xu, Y., Mao, C., Zhang, S., & Xu, J. (2020). The YDA-MKK4/MKK5-MPK3/MPK6 Cascade Functions Downstream of the RGF1-RGI Ligand–Receptor Pair in Regulating Mitotic Activity in Root Apical Meristem. Molecular Plant, 13(11), 1608-1623. https://doi.org/10.1016/j.molp.2020.09.004

59. Sopeña-Torres, S., Jordá, L., Sánchez-Rodríguez, C., Miedes, E., Escudero, V., Swami, S., López, G., Piślewska-Bednarek, M., Lassowskat, I., Lee, J., Gu, Y., Haigis, S., Alexander, D., Pattathil, S., Muñoz-Barrios, A., Bednarek, P., Somerville, S., Schulze-Lefert, P., Hahn, M. G., . . . Molina, A. (2018). YODA MAP3K kinase regulates plant immune responses conferring broad-spectrum disease resistance. New Phytologist, 218(2), 661-680. https://doi.org/10.1111/nph.15007

60. Stringlis, I. A., Proietti, S., Hickman, R., Van Verk, M. C., Zamioudis, C., & Pieterse, C. M. J. (2018). Root transcriptional dynamics induced by beneficial rhizobacteria and microbial immune elicitors reveal signatures of adaptation to mutualists. Plant Journal, 93(1), 166-180. https://doi.org/10.1111/tpj.13741

61. Sun, T., & Zhang, Y. (2022). MAP kinase cascades in plant development and immune signaling. EMBO reports, 23(2). https://doi.org/10.15252/embr.202153817

62. Tateda, C., Zhang, Z., Shrestha, J., Jelenska, J., Chinchilla, D., & Greenberg, J. T. (2014). Salicylic acid regulates Arabidopsis microbial pattern receptor kinase levels and signaling. Plant Cell, 26(10), 4171-4187. https://doi.org/10.1105/tpc.114.131938

63. Truman, W. M., Bennett, M. H., Turnbull, C. G. N., & Grant, M. R. (2010). Arabidopsis auxin mutants are compromised in systemic acquired resistance and exhibit aberrant accumulation of various indolic compounds. Plant Physiology, 152(3), 1562-1573. https://doi.org/10.1104/pp.109.152173

64. Vicente, J., Cascón, T., Vicedo, B., García-Agustín, P., Hamberg, M., & Castresana, C. (2012). Role of 9-lipoxygenase and α-dioxygenase oxylipin pathways as modulators of local and systemic defense. Molecular Plant, 5(4), 914-928. https://doi.org/10.1093/mp/ssr105

65. Wang, G., Hu, C., Zhou, J., Liu, Y., Cai, J., Pan, C., Wang, Y., Wu, X., Shi, K., Xia, X., Zhou, Y., Foyer, C. H., & Yu, J. (2019). Systemic Root-Shoot Signaling Drives Jasmonate-Based Root Defense against Nematodes. Current Biology, 29(20), 3430-3438.e3434. https://doi.org/10.1016/j.cub.2019.08.049

66. Weyman, P. D., Pan, Z., Feng, Q., Gilchrist, D. G., & Bostock, R. M. (2006). DEA1, a circadian- and cold-regulated tomato gene, protects yeast cells from freezing death. Plant Molecular Biology, 62(4-5), 547-559. https://doi.org/10.1007/s11103-006-9039-5

67. Xu, J., & Zhang, S. (2015). Mitogen-activated protein kinase cascades in signaling plant growth and development. In Trends in Plant Science (Vol. 20, pp. 56-64): Elsevier Ltd.

68. Yan, Z., Wang, J., Wang, F., Xie, C., Lv, B., Yu, Z., Dai, S., Liu, X., Xia, G., Tian, H., Li, C., & Ding, Z. (2021). MPK3/6-induced degradation of ARR1/10/12 promotes salt tolerance in Arabidopsis. EMBO reports, 22(10). https://doi.org/10.15252/embr.202152457

69. Zamioudis, C., Hanson, J., & Pieterse, C. M. J. (2014). ß-Glucosidase BGLU42 is a MYB72-dependent key regulator of rhizobacteria-induced systemic resistance and modulates iron deficiency responses in Arabidopsis roots. New Phytologist, 204(2), 368-379. https://doi.org/10.1111/nph.12980

70. Zhang, T. Y., Li, Z. Q., Zhao, Y. D., Shen, W. J., Chen, M. S., Gao, H. Q., Ge, X. M., Wang, H. Q., Li, X., & He, J. M. (2021). Ethylene-induced stomatal closure is mediated via MKK1/3–MPK3/6 cascade to EIN2 and EIN3. Journal of Integrative Plant Biology, 63(7), 1324-1340. https://doi.org/10.1111/jipb.13083

71. Zhang, Z., Shrestha, J., Tateda, C., & Greenberg, J. T. (2014). Salicylic acid signaling controls the maturation and localization of the arabidopsis defense protein ACCELERATED CELL DEATH6. Molecular Plant, 7(8), 1365-1383. https://doi.org/10.1093/mp/ssu072

72. Zhou, W., Lozano-Torres, J. L., Blilou, I., Zhang, X., Zhai, Q., Smant, G., Li, C., & Scheres, B. (2019). A Jasmonate Signaling Network Activates Root Stem Cells and Promotes Regeneration. Cell, 177(4), 942-956.e914. https://doi.org/10.1016/j.cell.2019.03.006

73. Zhu, Q., Shao, Y., Ge, S., Zhang, M., Zhang, T., Hu, X., Liu, Y., Walker, J., Zhang, S., & Xu, J. (2019). A MAPK cascade downstream of IDA–HAE/HSL2 ligand–receptor pair in lateral root emergence. Nature Plants, 5(4), 414-423. https://doi.org/10.1038/s41477-019-0396-x

74. Zoeller, M., Stingl, N., Krischke, M., Fekete, A., Waller, F., Berger, S., & Mueller, M. J. (2012). Lipid profiling of the Arabidopsis hypersensitive response reveals specific lipid peroxidation and fragmentation processes: Biogenesis of pimelic and azelaic acid. Plant Physiology, 160(1), 365-378. https://doi.org/10.1104/pp.112.202846